

# **Sustainable Synthesis of $\gamma$ -Valerolactone**

Zur Erlangung des akademischen Grades eines

**DOKTORS DER NATURWISSENSCHAFTEN**

(Dr. rer. nat.)

Fakultät für Chemie und Biowissenschaften

Karlsruher Institut für Technologie (KIT) - Universitätsbereich

genehmigte

DISSERTATION

von

Dipl.-Chem. Konstantin Hengst

aus

Münster (Westfalen)

Dekan: Prof. Dr. Peter Roesky

Referent: Prof. Dr. Jan-Dierk Grunwaldt

Korreferent: Prof. Dr. Olaf Deutschmann

Tag der mündlichen Prüfung: 17. July 2015



*"It doesn't matter what you do,  
it matters Why you do it."*

**Simon Sinek**



## Preface and acknowledgements

This thesis is submitted as partial fulfillment of the PhD degree at the Karlsruhe Institute of Technology (KIT). This work was carried out between December 2011 and May 2015 at the Institute for Chemical Technology and Polymer Chemistry (ITCP) and Institute of Catalysis Research and Technology (IKFT) at KIT. Between January 2014 and June 2014 the continuous flow experiments were performed at the Institute for Inorganic Materials Chemistry (SMK) at Eindhoven University of Technology (TU/e).

First I would particularly like to thank Prof. Dr. Jan-Dierk Grunwaldt for providing the interesting topic, the excellent working conditions and the freedom of research. His expert advice and encouragement were essential for the success of this work and are highly appreciated.

I wish to thank PD Dr. Wolfgang Kleist for the constant support and illuminating discussions.

I am grateful to Prof. Dr. Emiel Hensen for his constructive advice and support as well as the possibility to spend my KIC InnoEnergy mobility stay in his Institute at the Eindhoven University of Technology, where I felt very welcome.

Thanks to Prof. Dr. Olaf Deutschmann for the kind willingness to be my co-supervisor.

I would also like to thank Angela Beilmann (physisorption), Sonja Habicht (HPLC), Sina Baier (STEM), Kathrin Schäfer (chemisorption), Christin Wagner (TPR), Hermann Köhler (ICP-OES), Arno van Hoof (TEM), Dr. Michel Ligthart (chemisorption) and Dr. Stefan Mangold (XAS) for performing the measurements or their help and support associated with the measurements.

I greatly benefited from Dr. Martin Schubert who contributed many ideas and strategies to the book chapter, from Dr. Hudson Carvalho and Dr. Dmitry Doronkin who analyzed the XAS data as well as from Dr. Changbo Lu who carried out preliminary tests to hydrogenate levulinic acid. Thank you.

I want to thank the students I co-supervised, Christoph and Oliver, for their sound and dedicated work.

I would like to offer my special thanks to my colleagues in Karlsruhe and Eindhoven, in particular to the CN crew Karin, Chiara, Martin und Benjamin. I have been lucky to meet so many nice and inspiring people who helped and supported me both professionally and personally.

I would like to express my gratitude to my parents and siblings who always encouraged me. Thank you for being there for me.

I owe my deepest gratitude to Kathi and Emilia, without your support and love, this thesis would not have been possible.

## Abstract

The utilization of biomass for the production of fuels, fuel additives and chemicals has been intensively investigated in recent years. Levulinic acid is one of the important platform molecules that can be obtained in high purity from lignocellulosic feedstock. Most importantly, unlike for other top-platform molecules, only de- and rehydration reactions as well as a deformylation step (5-hydroxymethylfurfural to levulinic acid) are needed to produce levulinic acid. Levulinic acid is industrially used as a polymer plasticizer and since it shows two functional groups, it serves a platform for a wide range of products. The most important derivative of levulinic acid is  $\gamma$ -valerolactone which can be directly used as a fragrance, green solvent, monomer for the production of plastics or as a gasoline blending compound. In addition, several bio-based fuels and fuel additives can be produced from  $\gamma$ -valerolactone.  $\gamma$ -Valerolactone can be synthesized either by hydrogenation of levulinic acid to  $\gamma$ -hydroxyvaleric acid, which spontaneously condensates to  $\gamma$ -valerolactone, or by dehydration of levulinic acid to angelica lactone, which is subsequently hydrogenated to  $\gamma$ -valerolactone. A promising approach for a more sustainable synthesis route is the use of formic acid as hydrogen source, because formic acid is a stoichiometric side-product in the conversion of glucose or 5-hydroxymethylfurfural into levulinic acid. Alternatively, the hydrogen used in the levulinic acid hydrogenation could be generated via water electrolysis using excess electricity. Various noble metal based catalysts have been developed for the production of  $\gamma$ -valerolactone and Ru based catalysts showed the highest catalytic activity leading to quantitative levulinic acid conversion. The main disadvantage of noble metal catalysts concerns their high costs and therefore the development of non-noble metal based catalysts is desirable.

The aim of this work was the sustainable synthesis of  $\gamma$ -valerolactone over non-noble metal catalysts in batch autoclave (screening) and a continuous flow set-up. In order to further develop an environmentally benign process, formic acid which is generated as a by-product, was considered directly as hydrogen source. For this

purpose decomposition of formic acid towards H<sub>2</sub> and CO<sub>2</sub> as well as LA hydrogenation by formic acid using such decomposition catalysts was studied.

Different 15 wt.% Ni/Al<sub>2</sub>O<sub>3</sub> catalysts were synthesized for the synthesis of  $\gamma$ -valerolactone in batch autoclaves, using wet impregnation, incipient wetness impregnation, precipitation with NaOH and flame spray pyrolysis. The catalysts were thoroughly characterized (temperature programmed reduction, X-ray diffraction, linear combination analysis of X-ray absorption near edge spectra and extended X-ray absorption fine structure) and the results indicated the formation of larger Ni particles during precipitation using NaOH, incorporated Ni particles during flame spray pyrolysis and smaller Ni particles using wet impregnation. The Ni/Al<sub>2</sub>O<sub>3</sub> catalysts were tested in the hydrogenation of levulinic acid and the influence of different solvents (monovalent alcohols and water) as well as solvent free reaction conditions were screened. Whereas alcohols as solvent led to a number of side reactions (mainly the corresponding levulinic acid ester) which could partly be suppressed in the presence of high hydrogen pressures (>20 bar), water as solvent resulted in a  $\gamma$ -valerolactone selectivity of 100 % and  $\gamma$ -valerolactone yields of up to 57 %. Further improvement was achieved without any solvent, whereby the  $\gamma$ -valerolactone yield increased to 92 % at 100 % levulinic acid conversion under optimized reaction conditions (reaction temperature = 200 °C, H<sub>2</sub> pressure = 50 bar). Reuse of the Ni catalysts resulted in a significant drop in activity. Smaller Ni particles (wet impregnated catalyst) showed a better catalytic performance for the  $\gamma$ -valerolactone synthesis, while Ni<sup>2+</sup> species incorporated into the Al<sub>2</sub>O<sub>3</sub> lattice as present in the flame-derived catalyst were less active.

Aiming at the development of an economic and environmental friendly process for  $\gamma$ -valerolactone production, various Ni/Al<sub>2</sub>O<sub>3</sub> catalysts were subsequently tested in the continuous liquid phase hydrogenation of levulinic acid in a trickle-bed reactor using water as solvent. For this purpose and for optimizing the catalysts various synthesis methods (wet impregnation, precipitation with NaOH, precipitation with urea and flame spray synthesis) were used. This additionally allowed to prepare the Ni based catalysts with defined and varying Ni particle sizes. Catalyst characterization (X-ray diffraction, temperature-programmed reduction, scanning transmission electron microscopy, hydrogen chemisorption and X-ray absorption



spectroscopy) showed that a slow and controlled precipitation using urea for a pH controlled deposition resulted in the best Ni dispersion among the synthesis methods applied. Alternatively, the dispersion increased at lower Ni loading. Also under continuous reaction conditions, smaller Ni particles showed a beneficial catalytic performance for the synthesis of  $\gamma$ -valerolactone. 5 wt.% Ni/Al<sub>2</sub>O<sub>3</sub> prepared by wet impregnation showed the highest specific activity for the hydrogenation of levulinic acid to  $\gamma$ -valerolactone (90 % levulinic acid conversion and 75 %  $\gamma$ -valerolactone yields) under optimized reaction conditions (reaction temperature = 200 °C, H<sub>2</sub> pressure = 50 bar) featuring an average Ni particle size of 6 nm. Slight deactivation of the catalysts was observed due to sintering of the Ni particles after transformation of  $\gamma$ -Al<sub>2</sub>O<sub>3</sub> to boehmite but it demonstrates the potential of non-noble metal based catalysts in the hydrogenation of levulinic acid.

Finally, the use of formic acid as hydrogen donor in a cascade reaction was investigated. In a first step, different noble metal catalysts were synthesized and tested in the formic acid decomposition. The H<sub>2</sub>/CO<sub>2</sub> selectivity of the formic acid decomposition (dehydrogenation reaction) could be increased by a higher dilution of formic acid with water. ZrO<sub>2</sub> as catalyst support increased both the conversion of formic acid and the H<sub>2</sub>/CO<sub>2</sub> selectivity compared to SiO<sub>2</sub>. 1 wt.% Pd/ZrO<sub>2</sub> was the most active catalyst for the formic acid decomposition (100 % formic acid conversion and 95 % H<sub>2</sub>/CO<sub>2</sub> selectivity) under optimized reaction conditions (200 °C, 4 h). No deactivation of the catalyst was observed after four cycles. Other Pd and Pd/Au based catalysts showed similar formic acid conversions and H<sub>2</sub>/CO<sub>2</sub> selectivity compared to 1 wt.% Pd/ZrO<sub>2</sub>. The most suitable decomposition catalysts were subsequently studied in the levulinic acid hydrogenation using external hydrogen and finally examined in the cascade reaction of levulinic acid and formic acid towards  $\gamma$ -valerolactone. 5 wt.% Pd/ZrO<sub>2</sub> and 2.5 wt.% Pd + 2.5 wt.% Au/ZrO<sub>2</sub> were the most active catalysts for the  $\gamma$ -valerolactone synthesis using external hydrogen (100 % levulinic acid conversion and > 90 %  $\gamma$ -valerolactone yields). However, no catalytic activity towards  $\gamma$ -valerolactone was observed using formic acid as hydrogen donor. Small amounts of CO, which are formed during the formic acid decomposition, were identified as possible catalyst poison. Tests using 5 % CO/H<sub>2</sub> as external hydrogen

source revealed that CO may be the origin of the lower activity and poisoned the catalysts. Only Au based catalysts were found efficient in this cascade reaction.

## Kurzfassung

Die Nutzung von Biomasse für die Herstellung von Kraftstoffen, Kraftstoffadditiven und Chemikalien als Alternative zu fossilen Rohstoffen wird seit einigen Jahren intensiv erforscht. Lävulinsäure ist eine vielversprechende Plattformchemikalie, die in hoher Reinheit direkt aus lignocellulose-reicher Biomasse gewonnen werden kann. Der Vorteil von Lävulinsäure im Gegensatz zu anderen Plattformchemikalien besteht darin, dass nur De- und Rehydratisierungsreaktionen sowie ein Deformylierungsschritt für die Synthese notwendig sind. Industriell wird Lävulinsäure als Weichmacher verwendet und ist darüber hinaus aufgrund seiner zwei funktionellen Gruppen ein vielseitiges Edukt für ein breites Produktspektrum. Das wichtigste Produkt von Lävulinsäure ist  $\gamma$ -Valerolacton, welches direkt als Duftstoff, „grünes Lösungsmittel“, Monomer für die Kunststoffherstellung und Benzin-Additiv verwendet wird. Darüber hinaus können verschiedene biomassebasierte Kraftstoffe und Kraftstoffadditive aus  $\gamma$ -Valerolacton hergestellt werden. Die Synthese von  $\gamma$ -Valerolacton kann über zwei unterschiedliche Mechanismen erfolgen. Einerseits kann die Ketogruppe von Lävulinsäure hydriert werden, worauf die entstandene  $\gamma$ -Hydroxyvaleriansäure in der Folge spontan zu  $\gamma$ -Valerolacton kondensiert. Alternativ kann Lävulinsäure zu Angelicalacton dehydratisiert werden, das nachfolgend zu  $\gamma$ -Valerolacton hydriert wird. Der benötigte Wasserstoff für die Hydrierung wird derzeit hauptsächlich aus fossilen Rohstoffen gewonnen und könnte durch die Nutzung von Ameisensäure als Wasserstoffquelle ersetzt werden. Ameisensäure wird bei der Synthese von Lävulinsäure aus Glukose oder 5-Hydroxymethylfurfural als stöchiometrisches Nebenprodukt gebildet und die Verwendung von Ameisensäure als Wasserstoffquelle würde die Nachhaltigkeit der  $\gamma$ -Valerolacton Herstellung deutlich verbessern. Alternativ könnte der benötigte Wasserstoff auch durch die Elektrolyse von Wasser mit Überschussstrom nachhaltig bereitgestellt werden. Verschiedene Edelmetallkatalysatoren wurden für die Synthese von  $\gamma$ -Valerolacton bislang untersucht. In den meisten Fällen zeigte Ru als Aktivkomponente die höchste katalytische Aktivität (quantitative Lävulinsäureumsätze). Unedle

Metallkatalysatoren sind jedoch deutlich günstiger als Edelmetallkatalysatoren, weswegen ihre Entwicklung besonders erstrebenswert ist.

Ziel dieser Arbeit war die Synthese von  $\gamma$ -Valerolacton an nickelbasierten Katalysatoren in satzweiser und kontinuierlicher Reaktionsführung. Darüber hinaus wurde das Potenzial von Ameisensäure als Wasserstoffquelle für die Hydrierung von Lävulinsäure zu  $\gamma$ -Valerolacton untersucht.

Für die diskontinuierliche Synthese von  $\gamma$ -Valerolacton wurden verschiedene 15 Gew.% Ni/Al<sub>2</sub>O<sub>3</sub> Katalysatoren mittels Trockenimprägnierung, Nassimprägnierung, Fällung mit NaOH und Flammensprühydrylyse (FSP) hergestellt. Die Katalysatoren wurden eingehend mittels (temperaturprogrammierte Reduktion, Röntgendiffraktion, Röntgenabsorptionsspektroskopie (XANES und EXAFS)) charakterisiert, wobei sich zeigte, dass mit Nassimprägnierung die kleinsten Nickelpartikel erhalten wurden. Die Hydrierung von Lävulinsäure zu  $\gamma$ -Valerolacton wurde zunächst in unterschiedlichen Lösungsmitteln (einwertige Alkohole und Wasser) sowie lösungsmittelfrei in Autoklaven durchgeführt. Bei Versuchen in unterschiedlichen Alkoholen wurden Nebenreaktionen zu den entsprechenden Lävulinsäureestern beobachtet, welche nur durch einen höheren Wasserstoffdruck (>20 bar) unterbunden werden konnten. Mit Wasser als Lösungsmittel wurden Selektivitäten von 100 % zu  $\gamma$ -Valerolacton erreicht und die  $\gamma$ -Valerolacton Ausbeute konnte mit steigendem Reaktionsdruck (50 bar) auf bis zu 57 % gesteigert werden. Die lösungsmittelfreie Hydrierung von Lävulinsäure zu  $\gamma$ -Valerolacton lieferte unter optimierten Reaktionsbedingungen die höchste Ausbeute an  $\gamma$ -Valerolacton (92 %) bei 100 % Selektivität. Recyclingexperimente mit den Nickelkatalysatoren zeigten eine deutlich verschlechterte katalytische Aktivität im Bezug auf die Lävulinsäureumsätze. Kleinere Nickelpartikel (Nassimprägnierung) weisen eine höhere katalytische Aktivität hinsichtlich der Lävulinsäurehydrierung auf, während Ni<sup>2+</sup>, welches bei der Flammensprühydrylyse in das Al<sub>2</sub>O<sub>3</sub>-Gitter eingebaut wird, weniger katalytisch aktiv ist.

Im Hinblick auf zukünftige industrielle Anwendungen sind unter dem Aspekt der Nachhaltigkeit besonders eine kontinuierliche Reaktionsführung und Wasser als „grünes Lösungsmittel“ von Interesse. Daher wurden im Anschluss die aktivsten Ni/Al<sub>2</sub>O<sub>3</sub>-Katalysatoren in der kontinuierlichen Lävulinsäurehydrierung mit Wasser

als Lösungsmittel in einem Rieselbettreaktor getestet. Verschiedene Präparationsmethoden wurden für die Katalysatorsynthese verwendet und die erhaltenen Ni/Al<sub>2</sub>O<sub>3</sub> Katalysatoren unterschieden sich im Wesentlichen in den Nickelpartikelgrößen, welche mittels temperaturprogrammierten Reduktion, Röntgendiffraktion, Röntgenabsorptionsspektroskopie (XANES und EXAFS), Wasserstoffchemisorption und Elektronenmikroskopie untersucht wurde. Dabei zeigte sich, dass eine langsame Fällung von Nickel auf Al<sub>2</sub>O<sub>3</sub> mit Harnstoff die Dispersion erhöht. Alternativ kann die Dispersion durch eine niedrigere Nickelbeladung erhöht werden. Der Einfluss der verschiedenen Nickelpartikelgrößen auf die katalytische Aktivität wurde untersucht und kleine Nickelpartikel zeigten eine höhere Aktivität hinsichtlich der Hydrierung von Lävulinsäure zu  $\gamma$ -Valerolacton als große Nickelpartikel. Die höchste spezifische Aktivität bezüglich der  $\gamma$ -Valerolacton Synthese zeigte 5 Gew.% Ni/Al<sub>2</sub>O<sub>3</sub> (90 % Lävulinsäureumsatz und 75 %  $\gamma$ -Valerolacton Selektivität) mit einer durchschnittlichen Nickelpartikelgröße von 6 nm. Mit längerer Reaktionszeit nimmt die Aktivität der Katalysatoren ab. Sintern der Nickelpartikel kann ein Grund für die Katalysatordeaktivierung sein, welches durch die Phasenumwandlung von  $\gamma$ -Al<sub>2</sub>O<sub>3</sub> in Böhmit unter den hydrothermalen Reaktionsbedingungen begünstigt wird.

Die Verwendung des meist fossil gewonnenen externem Wasserstoff in der  $\gamma$ -Valerolacton Synthese verringert dessen Nachhaltigkeit, so dass in der Folge die Nutzung von Ameisensäure als Wasserstoffquelle untersucht wurde. Zunächst wurden Vorversuche zur Zersetzung von Ameisensäure zu H<sub>2</sub> und CO<sub>2</sub> an verschiedenen Edelmetallkatalysatoren durchgeführt. Die Selektivität der Ameisensäurezersetzung zu H<sub>2</sub> und CO<sub>2</sub> konnte durch die Verdünnung von Ameisensäure mit Wasser deutlich verbessert werden und die Verwendung von ZrO<sub>2</sub> als Katalysatorträger erhöhte sowohl die Ameisensäureumsätze als auch die Selektivität zu H<sub>2</sub> und CO<sub>2</sub> gegenüber SiO<sub>2</sub> als Trägermaterial. Unter optimierten Reaktionsbedingungen (200 °C, 4 h) zeigte 1 Gew.% Pd/ZrO<sub>2</sub> die höchste katalytische Aktivität hinsichtlich der Ameisensäurezersetzung (100 % Ameisensäureumsatz und 95 % H<sub>2</sub>/CO<sub>2</sub> Selektivität). Auch nach drei Recyclingversuchen wurde keine Abnahme der katalytischen Aktivität beobachtet. Die aktivsten Zersetzungskatalysatoren wurden anschließend in der Hydrierung von

Lävulinsäure zu  $\gamma$ -Valerolacton sowohl mit externem als auch mit *in situ* gebildetem Wasserstoff aus der Ameisensäurezersetzung getestet. Für die Hydrierung mit externem Wasserstoff waren 5 Gew.% Pd/ZrO<sub>2</sub> and 2.5 Gew.% Pd + 2.5 Gew.% Au/ZrO<sub>2</sub> am besten geeignet. Lävulinsäure wurde nahezu quantitativ zu  $\gamma$ -Valerolacton umgesetzt. In der Synthese von  $\gamma$ -Valerolacton mit Ameisensäure als Wasserstoffquelle wurde bei hohen Ameisensäureumsätzen (> 90 %) außer mit Gold-Katalysatoren kaum  $\gamma$ -Valerolacton erhalten. Möglicherweise tritt eine Vergiftung der Katalysatoren durch CO auf, da in Hydrierversuchen von Lävulinsäure mit 5 % CO/H<sub>2</sub> ebenfalls kein  $\gamma$ -Valerolacton gebildet wurde.

## Table of Contents

<b>Preface and acknowledgements</b>	I
<b>Abstract</b>	III
<b>Kurzfassung</b>	VII
<b>Table of Contents</b>	XI
<b>1. Introduction</b>	1
1.1. Utilization of biomass for fuels and chemicals	2
1.2. Effective H/C ratio and its importance	6
1.3. Hydrogenation of levulinic acid to $\gamma$ -valerolactone	9
1.3.1. LA hydrogenation using molecular hydrogen	11
1.3.1.1. Heterogeneous noble metal based catalysts in batch autoclaves	11
1.3.1.2. Heterogeneous non-noble metal catalysts in batch autoclaves	12
1.3.1.3. Continuous hydrogenation of LA to GVL	13
1.3.2. LA hydrogenation using formic acid as a hydrogen source	13
1.3.2.1. Formic acid decomposition	15
1.3.3. Alcohols as hydrogen donor for the hydrogenation of LA and LA esters to GVL via Meerwein-Ponndorf-Verley reaction	18
1.4. Motivation	18
<b>2. Materials and Methods</b>	20
2.1. Catalyst preparation	20
2.1.1. Wet impregnation	20
2.1.2. Incipient wetness impregnation	21
2.1.3. Precipitation	22
2.1.4. Flame spray pyrolysis	22
2.2. Catalyst characterization	23

2.2.1.	Physisorption	23
2.2.2.	Temperature-programmed reduction (TPR)	23
2.2.3.	X-ray diffraction	24
2.2.4.	Inductively coupled plasma-optical emission spectrometry	24
2.2.5.	Chemisorption	25
2.2.6.	Electron microscopy	25
2.2.7.	X-ray absorption spectroscopy	26
2.3.	Catalyst testing	27
2.3.1.	Custom made batch autoclaves	27
2.3.2.	<i>Parr</i> batch autoclave	28
2.3.3.	Trickle-bed reactor	28
2.4.	Product analysis	31
2.4.1.	High pressure liquid chromatography	31
2.4.2.	Gas chromatography	31
2.4.3.	Nuclear magnetic resonance spectroscopy	31
<b>3.</b>	<b>Results of catalyst characterization</b>	<b>32</b>
3.1.	Nickel based catalysts	32
3.1.1.	Elemental composition, BET surface area and reducibility	32
3.1.2.	Determination of catalyst structure and Ni particle size	34
3.1.2.1.	X-ray diffraction	34
3.1.2.2.	<i>Ex situ</i> X-ray absorption spectroscopy	38
3.1.2.3.	<i>In situ</i> X-ray absorption spectroscopy	44
3.1.2.4.	Electron microscopy	49
3.1.2.5.	Hydrogen chemisorption	53
3.2.	Noble metal based catalysts	54
3.2.1.	Metal content	55



3.2.2.	BET surface area	56
3.2.3.	X-ray diffraction	56
3.2.4.	CO chemisorption	56
<b>4.</b>	<b>Synthesis of <math>\gamma</math>-valerolactone in batch autoclaves over Nickel catalysts</b>	<b>57</b>
4.1.	Introduction	57
4.2.	Results and discussion of catalytic tests	57
4.2.1.	Conversion of LA to GVL in different solvents	57
4.2.2.	Solvent free conversion of LA to GVL	62
4.3.	Conclusion	68
<b>5.</b>	<b>Continuous synthesis of <math>\gamma</math>-valerolactone in a trickle-bed reactor</b>	<b>70</b>
5.1.	Introduction	70
5.2.	Results and discussion of catalytic tests	70
5.2.1.	Catalyst screening in batch autoclaves	70
5.2.2.	Catalytic tests in a trickle-bed reactor	72
5.2.2.1.	Influence of reaction temperature and H <sub>2</sub> pressure	72
5.2.2.2.	Effect of the preparation route and Ni particle size	74
5.2.2.3.	Comparison of Ni/Al <sub>2</sub> O <sub>3</sub> and Ru/C catalysts	77
5.2.2.4.	Catalyst stability	78
5.3.	Conclusion	79
<b>6.</b>	<b>Formic acid as hydrogen donor for the <math>\gamma</math>-valerolactone synthesis</b>	<b>81</b>
6.1.	Introduction	81
6.2.	Results and discussion of catalytic tests	81
6.2.1.	Formic acid decomposition	81
6.2.1.1.	Blank tests	81
6.2.1.2.	Catalyst screening	83

6.2.1.3.	Influence of catalyst support, reaction temperature and catalyst amount	84
6.2.1.4.	Catalyst stability	87
6.2.2.	Hydrogenation of levulinic acid to $\gamma$ -valerolactone using formic acid as hydrogen donor	88
6.2.2.1.	Screening of noble metal catalysts using external hydrogen	88
6.2.2.2.	Catalytic tests using formic acid as H <sub>2</sub> donor	89
6.3.	Conclusion	92
<b>7.</b>	<b>Final remarks and outlook</b>	<b>93</b>
	<b>Literature</b>	<b>97</b>
	<b>List of Abbreviations</b>	<b>i</b>
	<b>List of Symbols</b>	<b>iv</b>
	<b>Curriculum Vitae</b>	<b>v</b>
	<b>List of Publications</b>	<b>vi</b>

## 1. Introduction

Crude oil, natural gas and coal (fossil resources) have always been the most important carbon sources for the chemical and fuel industry and they have triggered the technological evolution in the last century.[1, 2] 87 % of global energy demand (13 billion tons of oil equivalents, Figure 1) is provided by crude oil, natural gas and coal and the global consumption increased by 2.3 % in 2013 (10 years average: 2.5 %).[3]

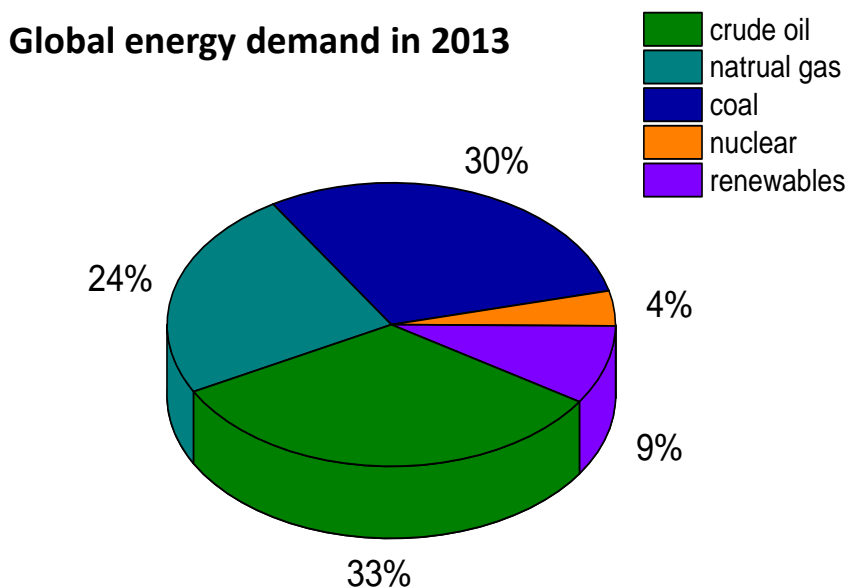


**Figure 1:** Global energy demand in 2013. Figure adapted from [3].

In Germany, 81 % of the primary energy demand (0.33 million tons of oil equivalents) is covered by crude oil (33.6 %), natural gas (22.9 %) and coal (24.7 %). 15 % of these fossil resources are used as transportation fuels and 4 % are used in the chemical industry, which corresponds to 59 % and 14 %, respectively, of the annual crude oil consumption.[4]

## Introduction

However, the amount of fossil energy sources is limited and the demand for energy sources is increasing due to the increasing world population and rising economies (China, India, Brazil). Furthermore, most of the fossil oil and gas deposits are located in regions which are difficult to access and politically instable. The consequence of this are continuously rising prices for energy sources, especially for crude oil and political and economical dependence on petroleum exporting countries.[3, 5]

Since the first oil crisis in the 1970s, alternative fuel productions and renewable chemicals were sought to guarantee sustainability in mobility and the chemical value chain. Different processes for the production of fuels or hydrocarbons, which are not based on crude oil, have been developed (e.g. coal-to-liquid (CtL)[6, 7] or gas-to-liquid (GtL) processes)[8]. However, the raw materials of these processes are also not renewable and therefore limited.

Biomass, including plants and animal or human organic materials, is the only renewable carbon source for fuels and the chemical industry. Therefore, biomass is the major alternative for fossil based crude oil. Key benefit is the cheap and easy production and that biomass is considered to be carbon-neutral.[9] The most important biogenic raw materials used in the chemical industry are oils (37 %), cellulose (15 %), starch (10 %) and lipids (7 %).[10] Consequently, the substitution of fossil based crude oil by biomass is a main issue which is investigated intensively worldwide. Note that only biomass which does not compete with the human food chain should be used for the production of fuels and chemicals. Nowadays, 6 % of the primary energy demand is provided by solid or liquid biomass. That means that more biomass (in terms of oil equivalent) is provided per year, than needed in the chemical industry and that the chemical industry could, even today, operate independently from fossil resources.

### **1.1. Utilization of biomass for fuels and chemicals**

Two main routes have been established for the utilization of plant biomass in chemical processes.[11-13] In the first route, biomass is gasified at high temperatures and its complex carbon backbone is decomposed into synthesis gas (CO and H<sub>2</sub>, Figure 2).[11, 14] Gasification of biomass has been examined on pilot to industrial scale, e.g. the Bioliq process [15], Chemrec's gasification [16], or the

Carboma/Haldor Topsøe gasification plant [17]. An advantage is that the whole biomass is used and clean fuels can be obtained. A fundamental disadvantage of the gasification process is that synthetic fuels or chemicals have to be built up from the bottom (e.g. via Fischer-Tropsch, methanol or dimethyl ether syntheses). Consequently, insertion of functional groups is quite elaborate within this approach since they need to be reintroduced into the hydrocarbon backbone. In the second route, a structural use of plant biomass is achieved by thermochemical treatment (e.g. flash pyrolysis), selective chemical conversion or fermentation performed in the liquid phase at lower temperatures. These processes are carried out at lower temperatures than gasification processes (Figure 2).[12, 18, 19]

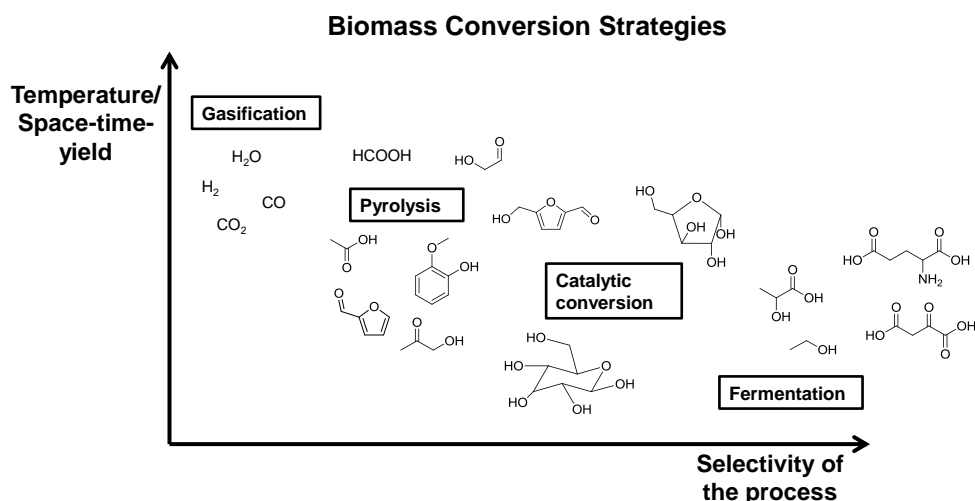


**Figure 2:** Approaches for the utilization of plant biomass and platform (bio)chemicals. [20] – Reproduced by permission of The Royal Society of Chemistry.

Whereas flash pyrolysis results in a bio-oil that needs to be upgraded by hydrodeoxygenation and fractionated [21, 22], the selective defunctionalization of biomass is an important pathway to pave the way for tailor-made biofuels and chemicals. This route has been exploited by many research consortia, e.g. "Tailor-Made Fuels from Biomass" (Aachen/Germany) [23], CatchBio in the Netherlands [24], or CASE in Denmark [25] and several other initiatives worldwide.

## Introduction

The selective structural use of biomass is currently present in several industrial processes for the large-scale production of many platform chemicals (e.g. bioethanol, citric acid, lactic acid, etc.). It is noteworthy that the space-time yield of the enzymatic and fermentative processes is rather low compared to chemical processes performed either in gas or liquid phase. Accordingly, chemical and thermochemical conversions of biomass may still offer more attractive alternatives for large-scale operations.[21, 22] Prior to the chemical conversion of lignocellulose, the fractionation of its major components - cellulose, hemicellulose and lignin – is required for the efficient catalytic conversion into desired products (Figure 3).[11, 13, 26] Alternatively, the biomass is pyrolyzed and converted by hydrodeoxygenation, forming a less-complex reaction mixture that can be fractionized similarly to crude oil.

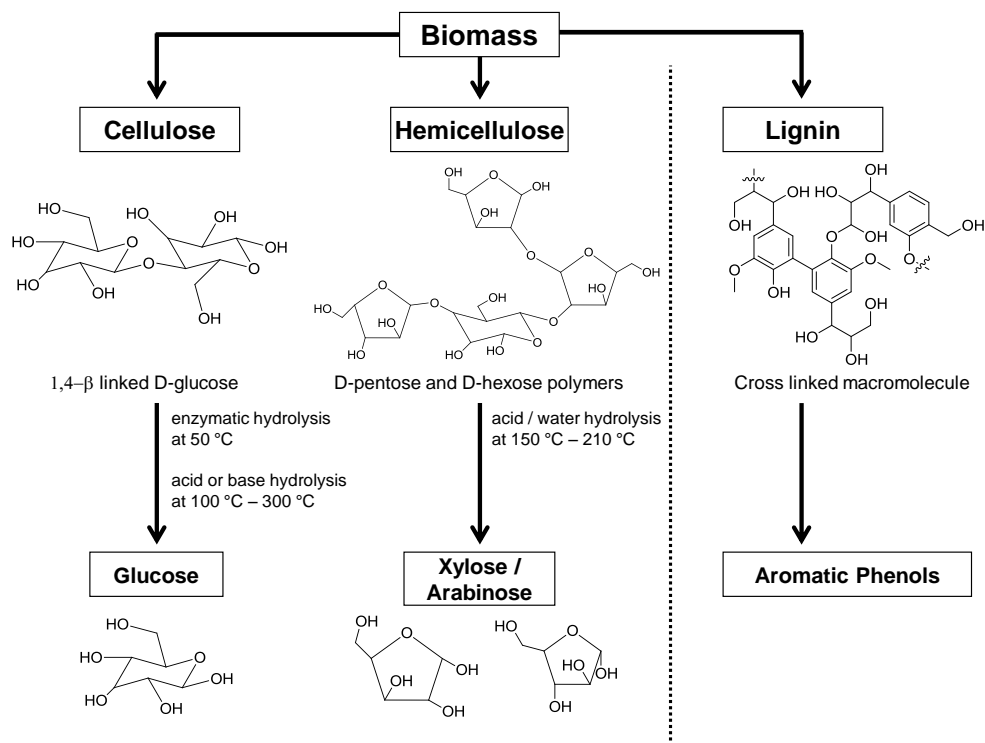


**Figure 3:** Components of lignocellulose. [20] – Reproduced by permission of The Royal Society of Chemistry.

Hydrolysis of lignocellulose leads first to sugars, which can subsequently be transferred into a number of platform molecules. Some of these chemicals have been outlined in a report by the *National Renewable Energy Laboratory* (NREL)[26] and are depicted in Figure 4. These platform chemicals show high oxygen-contents and structural similarity to compounds that are found in the pyrolysis oil after thermal treatment. Therefore, a selective removal of the oxygen functionalities by decarboxylation, dehydration, ketonization or hydrodeoxygenation reactions is crucial for the synthesis of various commodity chemicals or, in case of pyrolysis oil, to receive a less complex mixture.

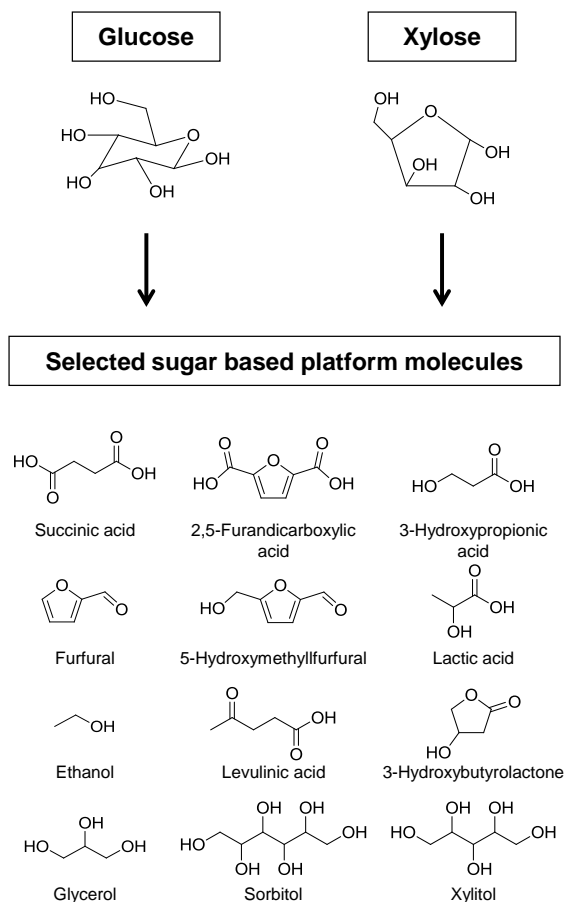


**Figure 4:** Biomass platform molecules from sugars as examples discussed in ref. [26]. [20] – Reproduced by permission of The Royal Society of Chemistry.

## Introduction

The present thesis focuses on the hydrodeoxygenation of levulinic acid (LA) as a biomass-derived platform molecule to  $\gamma$ -valerolactone (GVL) (cf. section 1.3). LA can be obtained in relatively high purity from lignocellulosic feedstocks. Most importantly, unlike other top-platform molecules, only de- and rehydration reactions as well as a deformylation step (5-hydroxymethylfurfural to LA) are needed to produce LA. Accordingly, no molecular hydrogen is needed for the deoxygenation of cellulose and hemicellulose rendering LA. This fact is important at the current industrial development since molecular hydrogen is still mostly obtained from non-renewable resources (e.g. natural gas).[27] In addition, LA may be considered also as a representative for organic ketones or acids that are typical constituents of pyrolysis oils produced via pyrolysis processes of biomass degradation processes.[28, 29]

### 1.2. Effective H/C ratio and its importance

Typically, platform chemicals and fuels derived from biomass are much more functionalized than hydrocarbons. This fact accounts for the lower energy density of first generation biofuels compared to petroleum-based fuels. The degree of functionalization of a molecule can be compared by its 'mean oxidation number of organic carbon' (MOC) or by the 'effective H/C ratio' (i.e., effective H/C ratio = - MOC), which is defined as:

$$\text{MOC} = \frac{\sum_{i=1}^n \text{OC}_i}{n} \quad (1)$$

where  $\text{OC}_i$  is the formal oxidation state of the  $i$ th carbon atom in the organic molecule, and  $n$  corresponds to the number of carbon atoms in the molecule. Since the MOC concept does not differentiate between different heteroatoms, several compounds may be classified by the same MOC value.[30] A more convenient manner to classify different feedstock and biofuels is by using their effective H/C ratios, as proposed by Vennestrøm *et al.* [31].

Considering the transformation of plant biomass into biofuels, a high effective H/C ratio is related to a high energy content per carbon (i.e. heating value or combustion enthalpy). For example, the combustion enthalpies per carbon atom for methane and octane are -890.4 and -683.8 kJ/mol, respectively, compared to -485.4 kJ/mol for LA



and -463.5 kJ/mol for 5-hydroxymethylfurfural (HMF). In comparison, the effective H/C ratio decreases in the same order found for the combustion enthalpies (*i.e.* the effective H/C ratio is 4 for methane, 2.25 for octane, 0.4 for LA, and zero for HMF). Transportation fuels exhibit effective H/C ratios in the range from 1 to 2.3 (cf. Figure 5).[31] While the use of effective H/C ratios is a good descriptor to group several compounds regarding their overall functionalization, any generalization always shows some limitations. Although carbohydrates show a much lower energy content than high-ranking coals, the classification by effective H/C ratio clusters carbohydrates close to high-ranking coals.

The concept of the effective H/C ratio underlines that subsequent deoxygenation of the biomass streams is mandatory for the production of biofuels. In practice, biomass streams are subject to catalytic hydrodeoxygenation (HDO) in order to increase their effective H/C ratio, and consequently their energy content. Moreover, deoxygenation of fast pyrolysis bio-oil does not only increase its energy content but also its chemical stability.

Figure 5 classifies resources, platform and intermediates, and target chemicals according to their effective H/C ratios, and reveals another important aspect of the analysis based on the effective H/C ratio. The horizontal axis represents the degree of processing. The second vertical axis semiquantitatively correlates the effective H/C ratio of the respective substances with the energy content per carbon atom. This correlation is helpful when discussing upgrading of biomass platform molecules via hydrodeoxygenation for the production of biofuels. A large difference between the effective H/C ratio of a resource and a target chemical is, in most cases, accompanied by a need of complex processing.[31] Moreover, this implies that substantial amounts of energy (and most likely losses of energy and/or product) would be observed throughout the process chain. In this context, carbohydrates have effective H/C ratios comparable to many highly functionalized platform or target chemicals. In some scenarios, plant biomass should be a more suitable feedstock than conventional resources (*e.g.* natural gas, oil or coal), because fewer, or even no, hydrodeoxygenation steps may be necessary. Conversely, a process initiated from conventional resources may need many steps in order to introduce the desired functionalities.[31] The effective H/C ratio is continuously increasing for the

## Introduction

hydrodeoxygenation of carbohydrates (H/C: 0) to LA (H/C: 0.4) and further to GVL (H/C: 0.8).

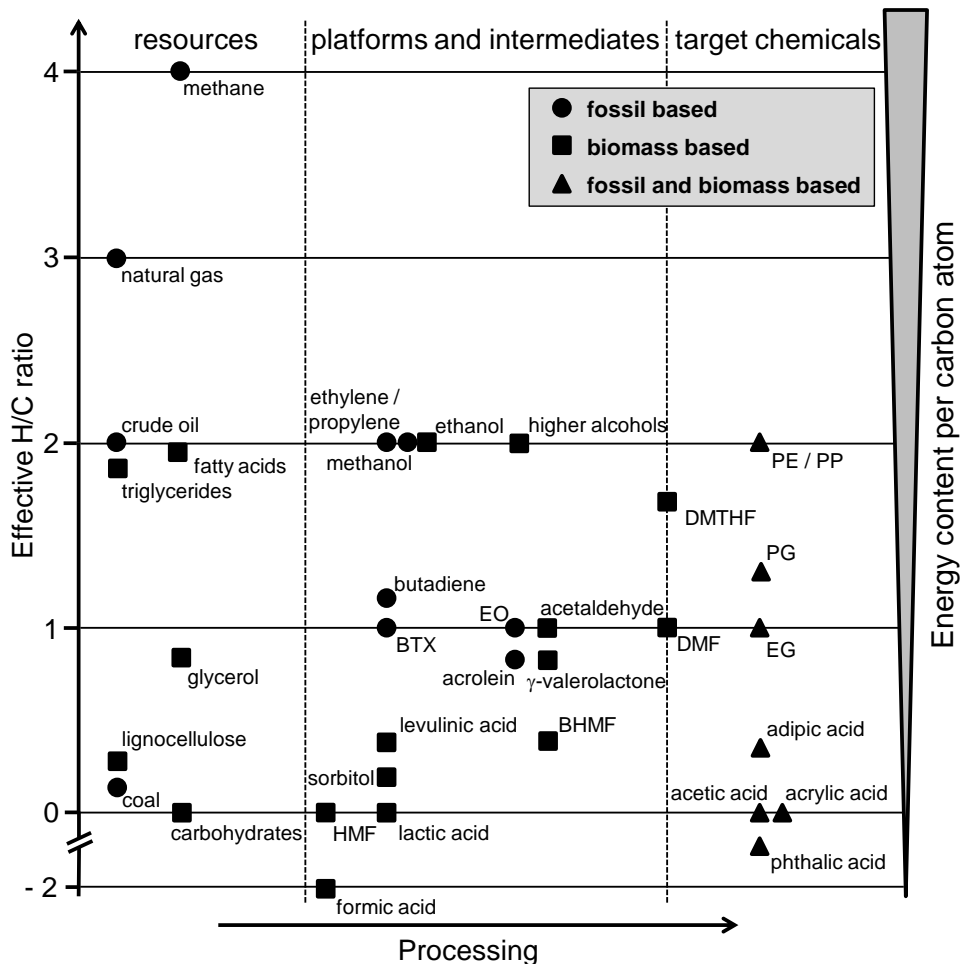
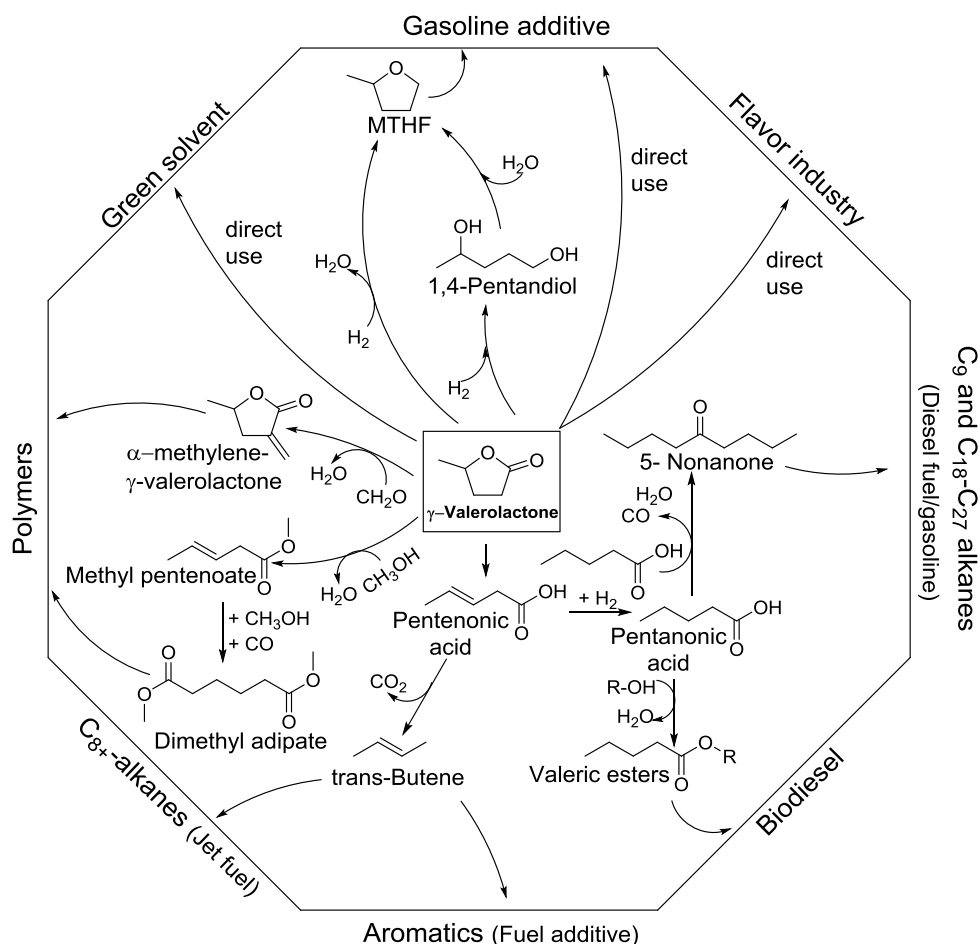


**Figure 5:** Effective H/C ratio versus degree of processing. Abbreviations: HMF – 5-hydroxymethylfurfural, BTX – benzene, toluene, xylene, EO – ethylene oxide, BHMF – 2,5-bis-(hydroxymethyl)furfural, 2,5DMF – 2,5-dimethylfuran, DMTHF – 2,5-dimethyltetrahydrofuran, EG – ethylene glycol, PG – propylene glycol, PE – polyethylene, PP – polypropylene. [20] – Reproduced by permission of The Royal Society of Chemistry.

### 1.3. Hydrogenation of levulinic acid to $\gamma$ -valerolactone

Levulinic acid (LA) is a C<sub>5</sub>-keto acid and one of the top-twelve sugar-based platform molecules.[26] LA is soluble in water and industrially used as a polymer plasticizer. Since LA shows two functional groups, it serves as a platform for the production of a wide range of products. Important chemicals derived from the upgrading of LA are  $\gamma$ -valerolactone, 1,4-pentanediol, levulinic acid esters and diphenolic acid.[26]  $\gamma$ -Valerolactone (GVL) is the most important derivative of LA. It serves as a platform for several specialty chemicals as well as synthetic fuels, as depicted in Scheme 1. Due to its herbaceous odor, GVL is used by the perfume and flavor industry.

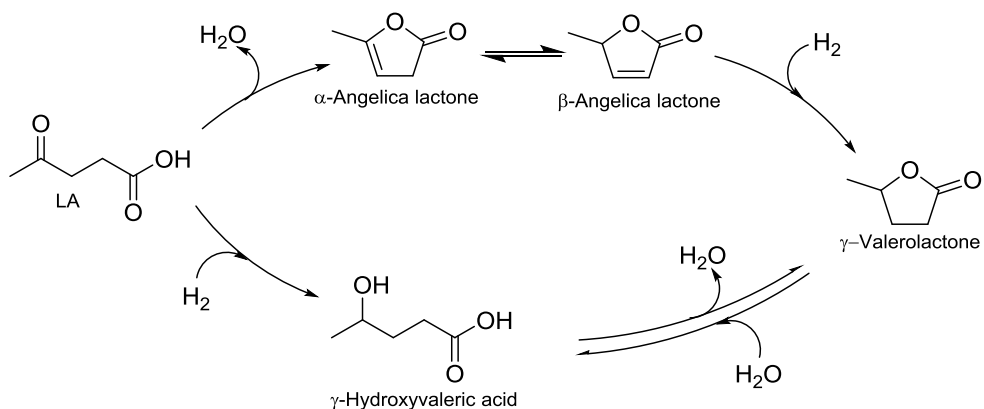


**Scheme 1:** Use of GVL and its derivatives. [20] – Reproduced by permission of The Royal Society of Chemistry.

## Introduction

Furthermore, GVL can be converted into  $\alpha$ -methylene- $\gamma$ -valerolactone or dimethyl adipate, which are monomers in the plastic industry.[32] GVL also shows interesting solvent properties, and is hence proposed as a green solvent or even as a precursor for other green solvents.[33] Moreover, GVL holds promise as a synthetic biofuel or fuel additive. Alternatively, GVL is proposed as a platform for the production of jet fuels ( $C_{8+}$  alkanes) or diesel fuels ( $C_9$ - $C_{18}$  alkanes).[34-36]

Different reaction pathways have been reported to produce GVL from LA (Scheme 2). A possible reaction route is the hydrogenation to  $\gamma$ -hydroxyvaleric acid, an unstable intermediate, which undergoes spontaneous lactonization rendering  $\gamma$ -valerolactone.[37] In an alternative pathway, LA is dehydrated to  $\alpha$ -angelica lactone (which occurs in equilibrium with  $\beta$ -angelica lactone), and is then hydrogenated. This reaction pathway is limited to systems, in which acidic functionalities in the catalyst and water are present. As a result, the yields of GVL are lower due to coke formation during the synthesis of angelica lactones.[37] In both pathways, deoxygenation is achieved by releasing water. A third possibility is the esterification of LA, followed by a hydrogenation and transesterification of the obtained levulinic acid esters (LA ester) to GVL.[38, 39]



**Scheme 2:** Reaction pathways for the hydrogenation of LA to GVL. [20] – Reproduced by permission of The Royal Society of Chemistry.

### 1.3.1. LA hydrogenation using molecular hydrogen

Various transition metal based catalysts, both homogeneous and heterogeneous, have been examined in the hydrogenation of LA. Already in 1909, the hydrogenation of LA to GVL was reported by Sabatier and Mailhe [40] using a Raney-nickel catalyst in the gas phase at 250 °C. Also Christian *et al.* [41] used a Raney-nickel catalyst at 220 °C for the hydrogenation of LA to GVL (GVL yields of 94 %) and Schütte and Thomas [42] investigated the GVL synthesis using platinum oxide as catalyst and diethyl ether as solvent (GVL yields of 87 %).

#### 1.3.1.1. Heterogeneous noble metal based catalysts in batch autoclaves

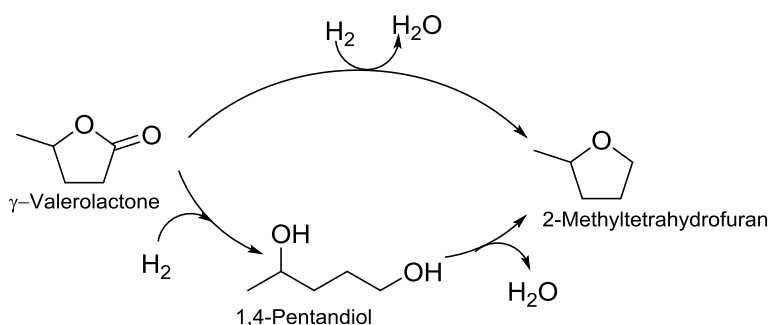
Since 2000, the hydrogenation of LA to GVL has received renewed attention using supported Ru, Pd and Pt based catalysts in both continuous and discontinuous reaction modes at reaction temperatures between 25 °C and 220 °C and hydrogen pressures up to 55 bar. In most studies, various alcohols, water or different ethers were used as solvents and only a few investigations on solvent free hydrogenation of LA to GVL have been reported.[37, 43-53] For instance, Al-Shaal *et al.* [45] tested 5 wt.% Ru supported on activated carbon, Al<sub>2</sub>O<sub>3</sub>, TiO<sub>2</sub> and SiO<sub>2</sub> as catalysts for the GVL synthesis. The reactions were conducted in autoclaves using different solvents. Nearly quantitative conversion of LA to GVL was achieved after 2.5 h using 1-butanol as solvent, a hydrogen pressure of 20 bar and a reaction temperature of 130 °C. The effect of Ru particle size, catalyst support and potassium doping on Ru activity for the LA hydrogenation (6 h, 220 °C, 14 bar H<sub>2</sub>) was investigated by Cao *et al.*[48] using 1,4-dioxane as solvent. A Ru particle size of about 1.5 nm was found to be the optimum for the LA hydrogenation and Ru supported on activated carbon showed a higher catalytic activity compared to Ru on alumina. Doping the catalyst with potassium further increased the activity of the Ru catalysts for both activated carbon and alumina as support. The enhanced activity resulted by electron donation from K to Ru. Deactivation (up to 58 %) of all catalysts was observed, which was more pronounced for K-doped ones. Sintering of Ru nanoparticles and leaching of K were responsible for the loss in activity.

The catalyst stability, especially in the case of Ru systems, could be enhanced by using bimetallic systems. Yang *et al.* [54] investigated Ru-Ni/OMC (ordered mesoporous carbon) and no loss of its catalytic performance was observed after 15

## Introduction

recycles. Also Ru/TiO<sub>2</sub> catalysts tested by Luo *et al.* [55] (200 °C, 40 bar H<sub>2</sub>, 1,4-dioxane as solvent) showed sintering of Ru particles after the first catalytic run. Using bimetallic Ru-Pd/TiO<sub>2</sub> alloys for the catalytic tests, no growth of particle size was observed and the activity was the same for at least 3 cycles.

Pd or Pt based catalysts often show high catalytic activity for the hydrogenation of LA. However, they can also catalyze the hydrogenation of GVL to 2-methyltetrahydrofuran (MTHF) or 1,4-pentanediol, hence decreasing the selectivity to GVL (Scheme 3).[44, 56-59] MTHF is a promising gasoline additive (cf. Scheme 1) because less NO<sub>x</sub> and soot is formed during the combustion. Bi-functional catalysts (Ru-Re/C, Pd-Re/C, Pt-Re/C) led to an increased activity for the GVL hydrogenation to 1,4-pentanediol and MTHF (160 °C, 150 bar H<sub>2</sub>).[56]



**Scheme 3:** Reaction pathways for the hydrogenation of GVL to MTHF. [20] – Reproduced by permission of The Royal Society of Chemistry.

In addition to a variety of organic solvents, water or even solvent-free conditions, supercritical CO<sub>2</sub> (scCO<sub>2</sub>) was tested by Manzer and Hutcherson [60] (Ru/Al<sub>2</sub>O<sub>3</sub>) and the group of Poliakoff [61] (Ru/SiO<sub>2</sub>). Full conversion of LA and yields up to 100 %  $\gamma$ -valerolactone were obtained using a continuous flow (200 °C and 100 bar) and batch reactor (200 °C and 250 bar) set-up, respectively. [60, 61]

### 1.3.1.2. Heterogeneous non-noble metal catalysts in batch autoclaves

The main disadvantage of noble metal catalysts concerns their high costs and therefore the development of non-noble metal based catalysts is desirable. Recently, Ni and Cu based catalysts have been studied for LA hydrogenation to GVL.[39, 62-

[68] Manzer [43] investigated 5 % Ni supported on carbon in 1,4-dioxane as solvent (150 °C, reaction time: 2 h, 55 bar H<sub>2</sub>). Compared to other metals (Ir, Rh, Pd, Ru, Pt, Re), which were tested under the same conditions, Ni showed both the lowest conversion of LA (5 %) and the lowest GVL selectivity (20 %). Bimetallic Ni-MoO<sub>x</sub>/C [63] and Ni-Cu/Al<sub>2</sub>O<sub>3</sub> [66] catalysts were tested at high reaction temperatures (250 °C) and H<sub>2</sub> pressures (50 to 60 bar) and with both catalysts GVL yields of over 90 % were obtained. Furthermore, Shimizu *et al.* tested Ni on different supports for LA hydrogenation at much milder conditions (T = 140 °C and P<sub>H<sub>2</sub></sub> = 8 bar) and found a maximum LA conversion (X<sub>LA</sub>) of 38 % with a 100 % selectivity to GVL.[63]

### 1.3.1.3. Continuous hydrogenation of LA to GVL

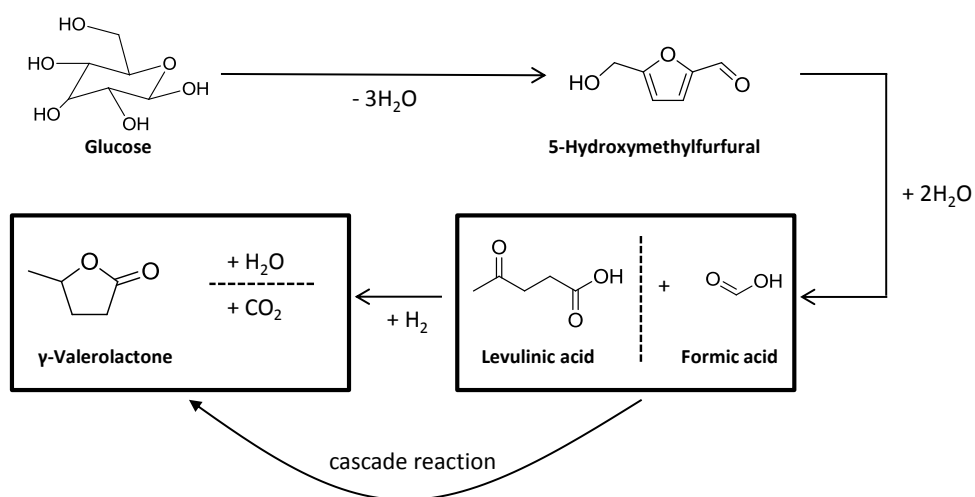
With a view on industrial applications of bio-based LA, continuous production of GVL has many advantages compared to batch processes. Up to now, only a few studies focused on the continuous hydrogenation of LA to GVL.[44, 61, 64, 65, 67, 68] Beside Poliakoff's group, who tested the reaction at T = 200 °C and P = 100 bar in supercritical CO<sub>2</sub> over 5 wt.% Ru/SiO<sub>2</sub> in a continuous flow set-up (quantitative LA conversion to GVL) [61], Tukaca *et al.* [67] tested Ru/C, Pd/C and Raney-Ni catalysts at T = 100 °C and P<sub>H<sub>2</sub></sub> = 100 bar. The addition of a phosphine ligand had a positive effect on X<sub>LA</sub> (from 83 % to 98 %) for Ru/C. The groups of Chang [44] (Ru/C, Pd/C, Pt/C), Chary [68] (Cu/Al<sub>2</sub>O<sub>3</sub>) and Rao [64, 65] (Ni on different supports) as well as Dunlop and Madden [69] (CuO/Cr<sub>2</sub>O<sub>3</sub>) investigated the vapour phase hydrocyclization of LA to GVL at reaction temperatures above 250 °C. Ru/C turned to be the most active and stable catalyst, but the sustainability of those studies was limited due to the use of 1,4-dioxane as solvent. [44] Also catalyst stability is an important issue concerning the LA hydrogenation, especially for non-noble metal catalysts using a continuous set-up. Deactivation of the catalysts was observed by Putrakumar *et al.* [68] (Cu/Al<sub>2</sub>O<sub>3</sub>) and Mohan *et al.* [65] (Ni/H-ZSM5) and must be inhibited if such catalysts should be applied in industrial processes.

### 1.3.2. LA hydrogenation using formic acid as a hydrogen source

The use of formic acid as hydrogen source was investigated for the synthesis of GVL from LA. This process option is interesting because formic acid is a stoichiometric side-product in the conversion of glucose / HMF into LA (Scheme 4). Therefore, the

## Introduction

use of formic acid as a hydrogen source could hold the key for a more sustainable, hydrogen-efficient production of GVL (cascade reaction). Two reaction mechanisms are proposed for the hydrogenation using formic acid as the hydrogen source.[70-72] In the first mechanism, formic acid is catalytically decomposed on metallic particles to  $\text{CO}_2$  and  $\text{H}_2$ . [72] Molecular hydrogen remains adsorbed resulting in two M-H sites, where the hydrogenation of LA takes place following the classical hydrogenation mechanism.[70, 72] In the second mechanism, LA is hydrogenated by a transfer hydrogenation of formic acid adsorbed on metal surfaces.[71]



**Scheme 4:** Reaction pathway of glucose to GVL using formic acid as hydrogen donor in a cascade reaction.

Mainly noble metals catalysts have been studied for the LA hydrogenation in the presence of formic acid as hydrogen source, since these metals also catalyze the decomposition of formic acid.[72-78] GVL yields > 90 % were obtained using homogeneous Ru complexes ( $[\text{Ru}(\text{PPh}_3)_3]$  [78] or Shvo catalyst [77]). Also heterogeneous catalysts were studied, and a quantitative yield of GVL was reported for experiments performed in the presence of a 1 mol% Au/ZrO<sub>2</sub> catalyst (150 °C, 5 bar N<sub>2</sub> pressure, water as a solvent).[72] Under similar reaction conditions, Pd- and Pt based catalysts produced only traces of GVL. Also 1 mol% Au supported on activated carbon, SiO<sub>2</sub> and TiO<sub>2</sub> was tested and Au/TiO<sub>2</sub> achieved 55 % LA rendering



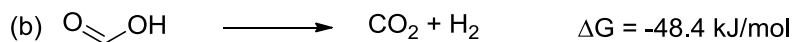
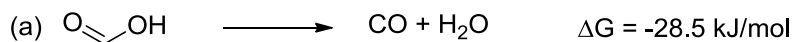
a 55 % GVL yield. Au on activated carbon or SiO<sub>2</sub> was virtually inactive for the production of GVL. This fact is ascribed to the low stability of these catalysts in the presence of formic acid.[72] Beside supported noble metals as catalysts for the LA hydrogenation using FA as H<sub>2</sub>-donor Cu supported on ZrO<sub>2</sub> was investigated.[79] Quantitative LA conversion to GVL was achieved after 5 h at 200 °C and 10 bar N<sub>2</sub> pressure.

In addition to LA and FA as starting reactants more crude materials (HMF, fructose, glucose, giant reed) were applied for the GVL production.[80-83] GVL yields of 52 mol% were obtained for the dehydration and transfer hydrogenation of D-fructose in combination with trifluoroacetic acid (TFA) and FA over Ru supported on activated carbon.[83]

In fact, most of the supported metal catalysts often suffer from low stability issues due to leaching of the active phase.[72] Therefore, the improvement of the catalyst stability in the presence of substantial amounts of formic acid is essential for the replacement of externally supplied molecular hydrogen by formic acid. Catalyst poisoning (mainly of Ru) by chlorine or sulfur is a main issue if cellulose or sugars are applied as starting reactants because HCl or H<sub>2</sub>SO<sub>4</sub> are often used as catalysts for the dehydration reactions to LA and FA.

### 1.3.2.1. Formic acid decomposition

Formic acid decomposes at temperatures above 100 °C and two possible decomposition reactions exist. FA can be dehydrated (Scheme 5a) to CO and water or dehydrogenated (Scheme 5b) to CO<sub>2</sub> and hydrogen.



**Scheme 5:** Decomposition of FA with free enthalpy at 25 °C; (a) dehydration, (b) dehydrogenation.

## Introduction

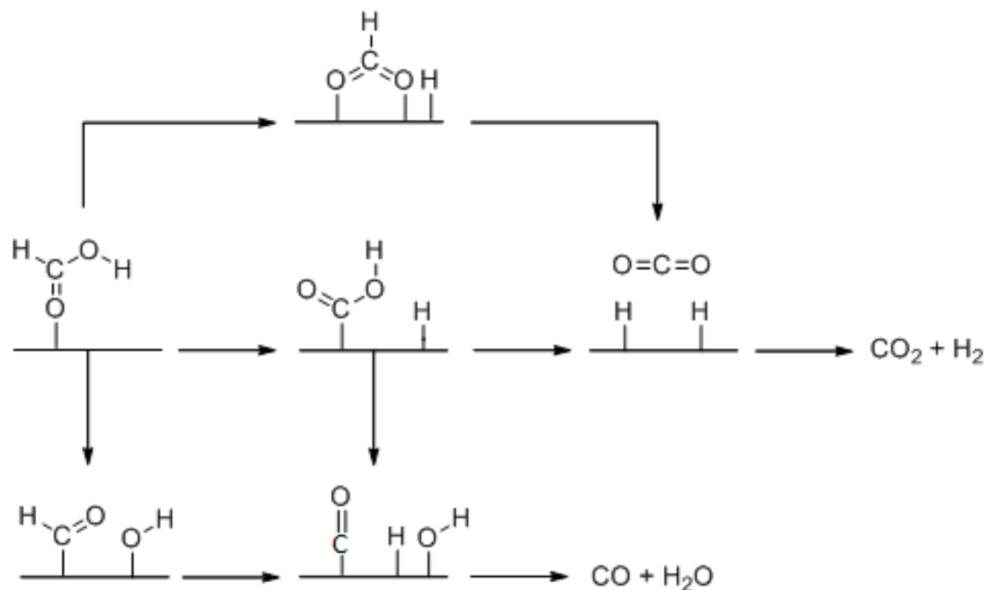
The dehydrogenation of FA is thermodynamically favored (up to 200 °C) but at low temperatures kinetically controlled.[84] Therefore, CO and water are formed at temperatures >200 °C and also in the presence of acid functionalities. In the past few years various homogeneous and heterogeneous catalysts for the FA decomposition have been developed because FA has been regarded as a sustainable hydrogen storage material (e.g. for fuel cells)[85]. FA is also a major by-product during biomass processing and an *in situ* harvesting of H<sub>2</sub> would lead to more sustainable processes (e.g. LA hydrogenation to GVL)[86]. A high FA decomposition selectivity towards CO<sub>2</sub> and H<sub>2</sub> is required for applications in fuel cells, because CO can poison the frequently used Pt based catalysts.

Homogeneous noble and non-noble metal complexes showed high FA conversion and H<sub>2</sub>/CO<sub>2</sub> selectivity for the FA decomposition even at low temperatures (25 °C to 60 °C). The group of *Beller* [87, 88] investigated [RuCl<sub>2</sub>(PPh<sub>3</sub>)<sub>3</sub>] complexes as well as [Fe<sub>3</sub>(CO)<sub>12</sub>] complexes in the presence of phosphine, pyridine and amide groups for the FA decomposition and they achieved FA conversions above 90 % and nearly CO free products, which can be used directly in fuel cells. Also [Ru(TPPTS)<sub>2</sub>] complexes were studied for the H<sub>2</sub> production from FA and showed high FA conversion at low temperature (25 °C to 120 °C).[89]

Considering the cascade reaction of LA and FA to GVL (Scheme 4) heterogeneous catalysts would be more suitable for the FA decomposition. Mainly platinum-group metals on different supports as well as alloys of platinum-group metals were reported for the heterogeneously catalyzed FA decomposition both in continuous [84, 90-95] and batch [93, 96-102] reaction mode. The rate of adsorption of FA is optimal on platinum-group metals (volcano plot) at relatively low temperatures. The rate limiting steps are for Au the too low adsorption of FA and for non-noble metals (Ni, Fe, Co) the too low desorption of the decomposition products.[103] The FA conversion and H<sub>2</sub>/CO<sub>2</sub> selectivity is higher for reactions in continuous flow and could be further increased at elevated pressure [104] and by dilution of FA with water [84].

Furthermore, the mechanism of FA decomposition was studied by density functional theory (DFT) calculations [105] as well as microkinetic modeling and reaction kinetic experiments [86]. Singh *et al.* [86] considered three different FA decomposition

pathways (Scheme 6) for their calculations on different Au surface sites (Au(111), Au(100), Au(211)).

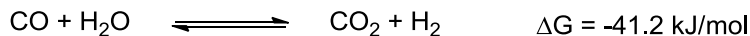


**Scheme 6:** Reaction mechanisms of FA decomposition over noble metal surfaces. Scheme adapted from [86].

DFT calculations, kinetic modeling and kinetic experiments revealed that the FA decomposition using Au catalysts comprised the following elementary steps:

First, FA is adsorbed on the metal surface (HCOOH\*), followed by splitting of one hydrogen atom (adsorbed on the metal, (HCOO\*\* 1H\*). Afterwards, CO<sub>2</sub> is formed and the second hydrogen atom remains on the metal (HCOO\*\* → CO<sub>2</sub>\* + 1H\*). Finally, the two H atoms are bonding to H<sub>2</sub> and desorbs as well as CO<sub>2</sub>. [86] No CO was formed under any experimental conditions, which is in accordance with the theoretical data.

In addition, the undesired products of FA dehydration, CO and H<sub>2</sub>O, can be converted to CO<sub>2</sub> and H<sub>2</sub> via the water-gas shift (WGS) reaction (Scheme 7), especially at higher temperature.



**Scheme 7:** Water-gas shift reaction with free enthalpy at 25 °C.[106]

The platinum-group metal based catalysts used for FA conversion are also catalytically active for the WGS reaction and the selectivity of FA decomposition could be further increased.[94] The following trend in the catalytic activity of the different metals was observed for the WGS reaction [106, 107]:

Cu > Co > Ru > Ni > Pt > Au > Fe > Pd > Rh > Ir

### 1.3.3. Alcohols as hydrogen donor for the hydrogenation of LA and LA esters to GVL via Meerwein-Ponndorf-Verley reaction

Recently, the conversion of LA and its esters to GVL via transfer hydrogenation was described by Chia and Dumesic [38] as an alternative for the classical hydrogenation reaction. The GVL production through Meerwein-Ponndorf-Verley reduction is beneficial because inexpensive metal oxides or zeolites can be used as catalysts.[38, 108, 109] ZrO<sub>2</sub> was the most active metal oxide for the transfer hydrogenation (GVL yields up to 85 % using 2-butanol, butyllevulinate, 150 °C for 16 h)[38] and nearly quantitative GVL yields (98 %) were obtained using Zr-beta zeolite (levulinic acid, 2-butanol, 120 °C, 11 h)[109]. Quantitative GVL yields were achieved starting from ethyllevulinate using Raney-Ni at 25 °C for 9 h and 2-propanol as solvent.[62]

## 1.4. Motivation

The utilization of biomass for the production of fuels, fuel additives and chemicals was intensively investigated in recent years. Especially the use of raw materials which not compete with the human food chain is desirable and so called “second generation biofuels and fuel additives” as well as “green chemicals” are obtained. Different biomass conversion strategies exist (Figure 2) and both sugars and platform molecules can be produced with relatively high selectivities and reasonable space-time-yields using the catalytic conversion strategy. Levulinic acid (LA) can be

obtained at high purity degree from lignocellulosic feedstocks. Most importantly, unlike other top-platform molecules, only de- and rehydration reactions as well as a deformylation step are needed to produce LA.  $\gamma$ -Valerolactone (GVL) is the most important derivative of LA and serves as a platform for several specialty chemicals as well as synthetic fuels and additives (Scheme 1). Various transition metal based catalysts, both homogeneous and heterogeneous, have been examined in the hydrogenation of LA. Ru based catalysts supported on activated carbon showed the highest catalytic activity in batch reaction mode. Up to now, only a few studies focused on the continuous GVL synthesis which would be beneficial for further industrial applications. From an economic perspective, the use of non-expensive base catalysts in a continuous reaction mode is advantageous over their noble metal counterparts. Unfortunately, the required reaction temperatures for quantitative GVL yields using base metal catalysts are much higher (e.g. Ni/Al<sub>2</sub>O<sub>3</sub>, T > 190 °C) than that for noble metal catalysts (e.g. Ru/C, T < 130 °C). Therefore, the catalytic activity of base metal catalysts has to be improved at low temperatures.

A promising approach for a more sustainable synthesis route for GVL is the use of FA as hydrogen source, because FA is a stoichiometric side-product in the conversion of glucose / HMF into LA (Scheme 4).

The aim of this work was the sustainable synthesis of GVL over non-noble metal catalysts both in batch autoclave (section 4) and continuous flow set-ups (section 5). The hydrogen used in the hydrogenation of levulinic acid to  $\gamma$ -valerolactone is often fossil generated and the sustainability of  $\gamma$ -valerolactone production would increase if formic acid is used as hydrogen source. For this approach, FA can be decomposed towards H<sub>2</sub> and CO<sub>2</sub> (conventional hydrogenation using *in situ* formed H<sub>2</sub>) or LA could be hydrogenated via transfer hydrogenation (section 6). In this work, various Ni based catalysts were prepared, thoroughly characterized and tested for the LA hydrogenation to GVL both in batch and continuous operation mode. The effects of Ni particle size, different solvents as well as catalyst stability were studied under optimized reaction conditions. Furthermore, different noble and non-noble metal catalysts were synthesized and tested in the FA decomposition. The most promising catalysts were afterwards applied in the cascade reaction of LA and FA to GVL.

## 2. Materials and Methods

This chapter describes the general catalyst preparation and characterization procedures as well as the experimental set-ups, the procedure of the catalytic tests and the product analysis. All chemicals used were of analytical grade and applied as received without further purification.

### 2.1. Catalyst preparation

Different noble and non-noble metal based catalysts were prepared using wet impregnation (WI). SiO<sub>2</sub> (Alfa Aesar), ZrO<sub>2</sub> (Alfa Aesar), activated carbon (C, Fluka) and  $\gamma$ -Al<sub>2</sub>O<sub>3</sub> (Merk) were used as catalyst supports. 15 wt.% Ni/Al<sub>2</sub>O<sub>3</sub> was also prepared by incipient wetness impregnation (IWI), precipitation with urea (urea), precipitation with NaOH (P) and flame spray pyrolysis (FSP). The catalysts prepared by impregnation or precipitation were dried for 1 h at 110 °C after the preparation. Both, the non-noble metal based and the noble metal based catalysts were typically calcined at 600 °C and 350 °C, respectively, for 5 h. All catalysts were pre-reduced in a 10 % H<sub>2</sub>/N<sub>2</sub> flow (20 L/h) at 600 °C (non-noble metal catalysts) or 350 °C (noble metal catalysts) for 2 h (5 °C/min) in a tube furnace prior to the catalytic tests in the batch autoclave or the continuous trickle-bed reactor. The catalysts are denoted xNi/Al<sub>2</sub>O<sub>3</sub>\_m with x being the metal loading and m the synthesis method, i.e. 5Ni/Al<sub>2</sub>O<sub>3</sub>\_wi for the 5 wt.% catalyst prepared by wet impregnation.

#### 2.1.1. Wet impregnation

The catalyst support (typically between 2 g and 10 g) was suspended in an aqueous metal precursor solution (typically between 10 mL and 30 mL) and the excess water was removed using a rotary evaporator. For bimetallic catalysts, both metal precursors were dissolved at the same time. The amounts of catalyst support and metal precursor are depicted in Table 1.

**Table 1:** Amount of catalyst support and metal precursor for the catalysts prepared via wet impregnation.

Catalyst	amount catalyst support [g]	amount metal precursor [g]	metal precursor
5Ni/Al <sub>2</sub> O <sub>3</sub>	8.5	7.427	Ni(NO <sub>3</sub> ) <sub>2</sub> ·6H <sub>2</sub> O
15Ni/Al <sub>2</sub> O <sub>3</sub>	9.5	2.491	Ni(NO <sub>3</sub> ) <sub>2</sub> ·6H <sub>2</sub> O
1Ru/SiO <sub>2</sub>	2	0.78	Ru(acac) <sub>3</sub>
1Ru/ZrO <sub>2</sub>	2	0.78	Ru(acac) <sub>3</sub>
1Ru/C	4.95	0.199	Ru(acac) <sub>3</sub>
1Pd/SiO <sub>2</sub>	2	0.043	Pd(NO <sub>3</sub> ) <sub>2</sub>
1Pd/ZrO <sub>2</sub>	4.95	0.124	Pd(NH <sub>3</sub> ) <sub>4</sub> Cl <sub>2</sub> ·H <sub>2</sub> O
5Pd/ZrO <sub>2</sub>	2.375	0.31	Pd(NH <sub>3</sub> ) <sub>4</sub> Cl <sub>2</sub> ·H <sub>2</sub> O
0.75Pd+15Ni/ZrO <sub>2</sub>	4.21	0.092 + 3.716	Pd(NH <sub>3</sub> ) <sub>4</sub> Cl <sub>2</sub> ·H <sub>2</sub> O + Ni(NO <sub>3</sub> ) <sub>2</sub> ·6H <sub>2</sub> O
2.5Pd+2.5Au/ZrO <sub>2</sub>	2.375	0.155 + 0.13	Pd(NH <sub>3</sub> ) <sub>4</sub> Cl <sub>2</sub> ·H <sub>2</sub> O + HAuCl <sub>4</sub>
1Au/SiO <sub>2</sub>	2	0.34	HAuCl <sub>4</sub>
1Pt/SiO <sub>2</sub>	2	0.033	Pt(NO <sub>3</sub> ) <sub>2</sub>
1Ir/SiO <sub>2</sub>	1.3	0.02	IrCl <sub>3</sub>

### 2.1.2. Incipient wetness impregnation

The 15Ni/Al<sub>2</sub>O<sub>3</sub>\_iwi catalyst was prepared by treating 8.5 g of the uncalcined  $\gamma$ -Al<sub>2</sub>O<sub>3</sub> with 8.5 mL of an aqueous Ni(II) nitrate solution (7.427 g Ni(II) nitrate·6H<sub>2</sub>O). The volume of the aqueous Ni(II) nitrate solution was equal to the pore volume of the  $\gamma$ -Al<sub>2</sub>O<sub>3</sub> (pore volume 1 cm<sup>3</sup>/g). Note that 15Ni/Al<sub>2</sub>O<sub>3</sub>\_iwi was calcined and reduced at 450 °C after the impregnation.

### 2.1.3. Precipitation

For precipitation of Ni on Al<sub>2</sub>O<sub>3</sub> two different methods were used. 15Ni/Al<sub>2</sub>O<sub>3</sub>\_p was prepared by suspending 8.5 g  $\gamma$ -Al<sub>2</sub>O<sub>3</sub> in a 100 mL aqueous solution containing 7.427 g Ni(NO<sub>3</sub>)<sub>2</sub>·6H<sub>2</sub>O and stir for 1 h. Subsequently, 465 mL 0.1 M NaOH solution were added to the mixture at room temperature until a pH of 9 was reached. For 15Ni/Al<sub>2</sub>O<sub>3</sub>\_urea, 4.25 g  $\gamma$ -Al<sub>2</sub>O<sub>3</sub> was suspended in a 30 mL aqueous solution containing 3.714 g Ni(NO<sub>3</sub>)<sub>2</sub>·6H<sub>2</sub>O and a 50 mL aqueous solution with 4.93 g urea (molar ratio urea/precursor = 6.3). The mixture was diluted with demineralized H<sub>2</sub>O to a total volume of 550 mL, the pH was adjusted to 2 by adding nitric acid, and thereafter gradually heated to 90 °C for 18 h. The pH of the solution increased to about 9 after 18 h. After precipitation, the sample was filtered off and washed with demineralized water until the pH of the filtrate was 7. The 15Ni+0.75Pt/Al<sub>2</sub>O<sub>3</sub>\_urea catalyst was prepared similarly by adding 0.0744 g of tetraammineplatinum(II) nitrate to the Ni(II) nitrate solution.

### 2.1.4. Flame spray pyrolysis

Flame spray pyrolysis is a novel one-step method for preparation of non-porous nanoparticles.[110] Materials derived by flame spray pyrolysis are very interesting for the use as heterogeneous catalysts, due to their high surface area and homogeneity of their particles.[111] In addition, the synthesis of multi-component catalysts is much faster using this one-step process compared to traditional impregnation or precipitation methods.[112]

For 15Ni/Al<sub>2</sub>O<sub>3</sub>\_fsp, 2.975 g nickel(II) nitrate and 24.995 g aluminum nitrate were dissolved in 120 mL methanol. This mixture was pumped with a 50 mL syringe at a flowrate of 5 mL/min into the center of a 45 % CH<sub>4</sub>/O<sub>2</sub> supporting flame and dispersed with 5 L/min O<sub>2</sub> to form a fine spray. This sample was collected on a water chilled filter ( $\varnothing$  240 mm, Whatman GF6) 30 cm above the flame by means of a vacuum pump. After scraping the fine powder from the filter, the catalyst was calcined. The set-up used for FSP (Figure 6) has been described in previous work.[113] Note that particle production and collection on the filter must be performed in a closed fume hood under appropriate safety measures.



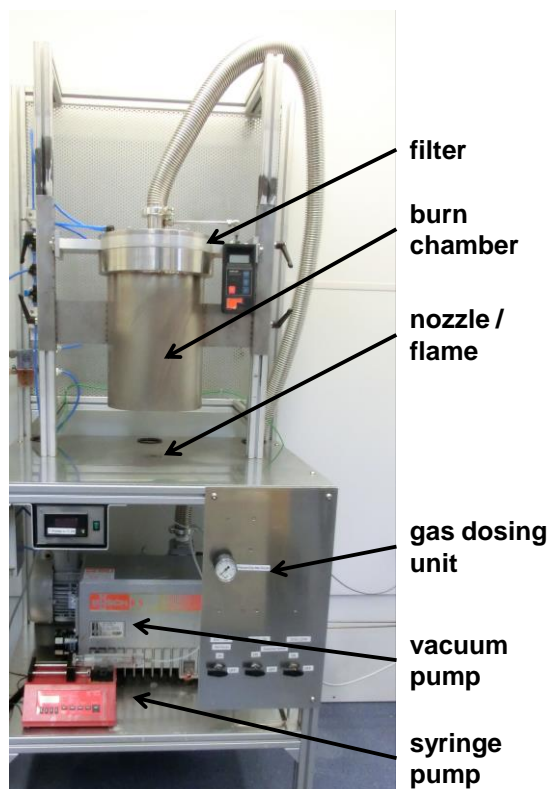


**Figure 6:** Picture of the flame spray pyrolysis set-up at the Institute for Chemical Technology and Polymer Chemistry (ITCP, KIT). The whole set-up is placed in a fume hood.

## 2.2. Catalyst characterization

### 2.2.1. Physisorption

The surface area of the catalysts was determined by N<sub>2</sub> physisorption (Belsorp II mini, BEL Japan Inc.) at -196 °C. All samples were outgassed at 300 °C for 2 h prior to the adsorption measurements. The BET surface area was determined using 10 points in the range of  $P/P_0 = 0.05 - 0.3$ .

### 2.2.2. Temperature-programmed reduction (TPR)

The reduction behavior of the catalysts was investigated by TPR using a ChemBET TPR/TPD analyzer (Quantachrome). The calcined catalyst (100 mg) was loaded into a quartz reactor, placed into the tube furnace and heated to 900 °C (5 °C/min) in a 5 % H<sub>2</sub>/Ar mixture at a total flow of 73 mL/min. The H<sub>2</sub> concentration of the influent

## Materials and Methods

and effluent gas was measured with a thermal conductivity detector (TCD) and the H<sub>2</sub> consumption was plotted against the temperature.

### 2.2.3. X-ray diffraction

Powder X-ray diffraction (XRD) patterns were collected with a PANalytical X'Pert PRO diffractometer with Cu K<sub>α</sub> radiation (Cu K<sub>α1</sub> = 1.54060 Å and Cu K<sub>α2</sub> = 1.54443 Å and Ni filter). The scan was recorded in a 2θ range of 20 – 80° with a 0.017° step width and an acquisition time of 0.51 s per point. Crystalline phases were determined using the Cambridge Structural Database (CSD) of the Cambridge Crystallographic Data Center (CCDC). The Scherrer equation (2) was used to estimate the mean crystalline diameter (d) of the Ni particles (average of all Ni reflexes) and a LaB<sub>6</sub> crystal was used as a standard to correct the instrumental line broadening. Subsequently, for convenience the crystalline diameter estimated with the Scherrer equation is named the Ni particle size (XRD). K is the shape factor and was set to 0.9 (spherical nanoparticles), λ is the X-ray wavelength, β is the line broadening at FWHM and cosθ is the Bragg angle.[114] The X-ray diffraction pattern were fitted and β was determined using X'Pert Highscore software of PANalytical.

$$d = \frac{K \cdot \lambda}{\beta \cdot \cos\theta} \quad (2)$$

*In situ* X-ray diffraction patterns were recorded using a Bruker D8 Advance with Cu K<sub>α</sub> radiation (Cu K<sub>α1</sub> = 1.5406 Å and Cu K<sub>α2</sub> = 1.5444 Å). The calcined catalyst (50 mg) was loaded in an *in situ* XRD cell (*Anton Paar, XRK900*) and afterwards heated stepwise in 50 °C steps to 650 °C in 5 % H<sub>2</sub>/N<sub>2</sub> with a total flow of 100 mL/min. At each temperature a scan was recorded in a 2θ range of 20 – 80° (0.016 ° step width, 1 s data acquisition time, total 1 hour). For analysis of the crystalline phase, the reflections were assigned using references from the International Centre for Diffraction Data (ICDD).

### 2.2.4. Inductively coupled plasma-optical emission spectrometry

The metal content of the catalysts was validated by inductively coupled plasma optical emission spectrometry (ICP-OES) using an Agilent 720/725-ES spectrometer. The catalysts were dissolved in a 5 M H<sub>2</sub>SO<sub>4</sub> solution (Ni/Al<sub>2</sub>O<sub>3</sub>

catalysts) or in aqua regia (noble metal catalyst) in a microwave at 600 W for 2 h, afterwards diluted with demineralized water and finally injected into the plasma.

### 2.2.5. Chemisorption

Hydrogen chemisorption of the Ni based catalysts was carried out at 40 °C using a Micromeritics ASAP 2020C setup. The sample (100 mg) was first reduced at 600 °C (5 °C/min) for 2 h and evacuated for 4.5 h. The double isotherm method with an intermediate vacuum treatment of 1 h was employed. An adsorption stoichiometry of one H per surface Ni atom was assumed.[115]

CO chemisorption of the Pd based catalyst was carried out in an in-house built setup.[116] The sample was first oxidized (synthetic air) at 500 °C (5 °C/min) for 20 min and afterwards reduced at 400 °C (5 % H<sub>2</sub>/N<sub>2</sub>) for 1 h. After flushing the setup for 1 h with 1 % CO/N<sub>2</sub> (25 °C) the adsorbed CO was desorbed by heating the sample to 500 °C under N<sub>2</sub> (5 °C/min). An adsorption stoichiometry of one CO molecule per surface Pd atom was assumed.[117]

### 2.2.6. Electron microscopy

Transmission electron microscopy (TEM) was conducted on a FEI Tecnai 20 electron microscope at an acceleration voltage of 200 kV with a LaB<sub>6</sub> filament. Typically, a small amount of sample was ground and suspended in ethanol, sonicated and dispersed over a Cu grid with a carbon film.

For scanning transmission electron microscopy (STEM), a powdered sample was ultrasonically dispersed in ethanol and one drop of the suspension was dried on a gold grid covered with holey carbon film. The catalyst specimens were examined in a FEI Titan 80-300 aberration corrected electron microscope operated at 300 kV. Scanning transmission electron microscopy (STEM) images were acquired by a Fischione model 3000 HAADF STEM detector and energy dispersive X-ray spectra (EDX) were acquired by an EDAX SUTW EDX detector. The particle size was determined by counting / marking particles (ellipsoids mode) using ImageJ program.

### 2.2.7. X-ray absorption spectroscopy

The local structure of Ni was characterized using X-ray absorption spectroscopy (XAS) at the Ni K edge (8333 eV). X-ray absorption spectra (X-ray absorption near edge spectra, XANES, and extended X-ray absorption fine structure, EXAFS) were recorded at the XAS beamline of the ANKA synchrotron (Karlsruhe, Germany) using a Si (111) double crystal monochromator in transmission and fluorescence modes. Typically, the catalyst (pressed and sieved to 100-200  $\mu\text{m}$  grains, ca. 5 mg) was placed in an *in situ* microreactor (quartz capillary, 1 mm diameter, 20  $\mu\text{m}$  wall thickness) [118] and heated by a hot air blower (Gas Blower GSB-1300, FMB Oxford) similar to [119]. Catalysts containing 15 wt% Ni were diluted (1:1 by weight) with  $\gamma\text{-Al}_2\text{O}_3$  prior to pressing and sieving to reduce the total absorption by the packed bed. *Ex situ* measurements were recorded on pelletized catalyst samples which were pressed after dilution with cellulose. The beam size was kept at 5 mm x 0.75 mm. During the TPR-XANES measurement the catalyst was heated in a 5 %  $\text{H}_2/\text{He}$  flow (50 mL/min) to 600 °C (5 °C/min). After 30 min it was cooled down to 25 °C in 5 %  $\text{H}_2/\text{He}$  flow and EXAFS spectra at the Ni K edge (8333 keV) were recorded. The spectra were energy-calibrated, background subtracted and normalized using the ATHENA program of the IFFEFIT package [120]. A linear combination analysis (LCA) of the TPR-XANES spectra was performed using Ni foil, NiO, and  $\text{NiAl}_2\text{O}_4$  spinel reference spectra in the range of 8325 - 8360 eV. For analysis of the extended X-ray absorption fine structure (EXAFS) only the single scattering paths were considered. The corresponding theoretical backscattering amplitudes and phases were calculated by the FEFF 6.0 code.[121, 122] The theoretical single scattering paths were adjusted to the experimental ones by a least square method in R-space to obtain the coordination number (N), bond distances (R), and mean square deviation of interatomic distances ( $\sigma^2$ ). The amplitude reduction factor ( $S_0$ ) was obtained by refining a Ni reference foil and used for the other samples. The absolute misfit between theory and experiment is expressed by the  $\rho$  factor (cf. ref. [123]).

## 2.3. Catalyst testing

### 2.3.1. Custom made batch autoclaves

Custom made batch autoclaves ( $T_{\max}$ : 350 °C,  $P_{\max}$ : 200 bar,  $V$  = 65 mL, (Figure 7)) were used for the catalytic tests. The batch autoclaves were configured and constructed together with the work shop at the Institute of Catalysis research and Technology (IKFT), KIT. For the catalytic tests, the reactor was usually charged with 10 mL of the reaction mixture and the pre-reduced catalyst (stored under air). The reactor was purged with  $N_2$  and pressurized with  $H_2$ . The magnetically stirred autoclave was heated with a heating sleeve and plate. The starting point of the reaction was defined as the time, when the desired temperature was reached (usually after 20 to 30 min). After the desired reaction time (usually 4 h) the reactor was quenched in ice water, depressurized, flushed with nitrogen and finally the product was separated from the catalyst by filtration. The custom made batch autoclaves were applied for the LA hydrogenation in water and solvent free, as well as for all reactions concerning FA.

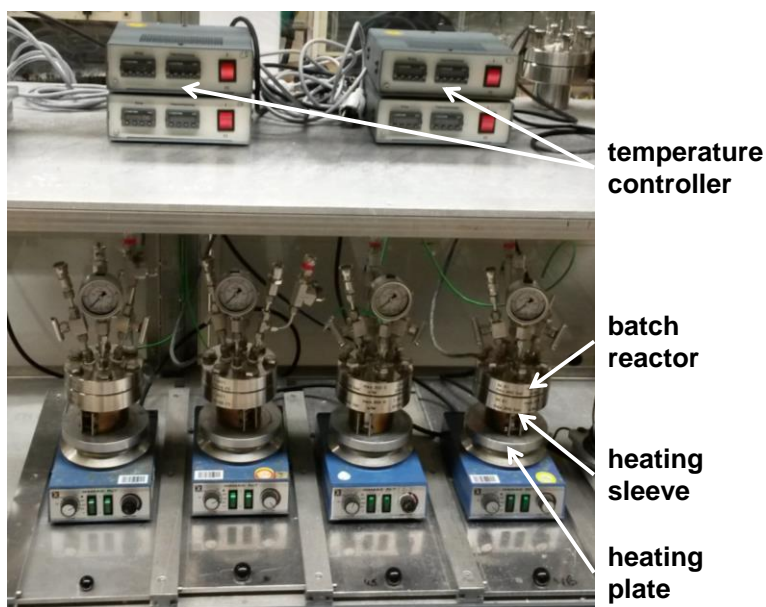


**Figure 7:** Picture of custom made batch autoclaves at the Institute of Catalysis Research and Technology (IKFT, KIT).  $T_{\max}$ : 350 °C,  $P_{\max}$ : 200 bar,  $V$  = 65 mL.

### 2.3.2. *Parr* batch autoclave

The *Parr* batch autoclave ( $T_{\max}$ : 500 °C,  $P_{\max}$ : 350 bar,  $V$  = 100 mL, (Figure 8) was applied for the LA hydrogenation using different monovalent alcohols, DMF and acetic acid as solvent. Charging of the reactor was similar, but the *Parr* batch autoclave was mechanically stirred and heated with a tube furnace. The reactor was also quenched in ice water, depressurized, flushed with nitrogen and finally the product was separated from the catalyst by filtration after the reaction.

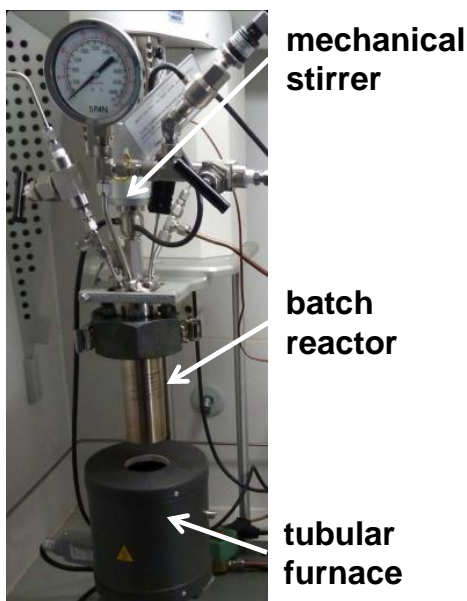


**Figure 8:** *Parr* batch autoclave at ITCP, KIT.  $T_{\max}$ : 500 °C,  $P_{\max}$ : 350 bar,  $V$  = 100 mL.

### 2.3.3. Trickle-bed reactor

The continuous flow experiments were conducted in a trickle-bed-reactor (Figure 9). The reactor was a vertically placed stainless-steel tube with an inner diameter of 4 mm and a length of 200 mm. It is heated by a tube furnace. The liquid feed was regulated by a high pressure piston pump (Hewlett Packard series 1050). Gases were delivered by thermal mass flow controllers (Bronkhorst). Usually, 0.5 g catalyst was loaded into the reactor. Prior to reaction, the set-up was flushed with  $N_2$  followed by reduction of the catalyst at 600 °C (10 °C/min) in a 250 mL/min  $H_2$  flow for 1 h.

After cooling the reactor to the desired reaction temperature, the gas flow was changed to a 50 mL/min H<sub>2</sub> flow. The reaction pressure was set using a back pressure controller (Tescom). The liquid flow consisting of 10 wt.% levulinic acid in water was set at 5 g/h. The typical reaction conditions are T = 200 °C and P<sub>H<sub>2</sub></sub> = 50 bar. Effluent products were collected every 60 min for analysis.

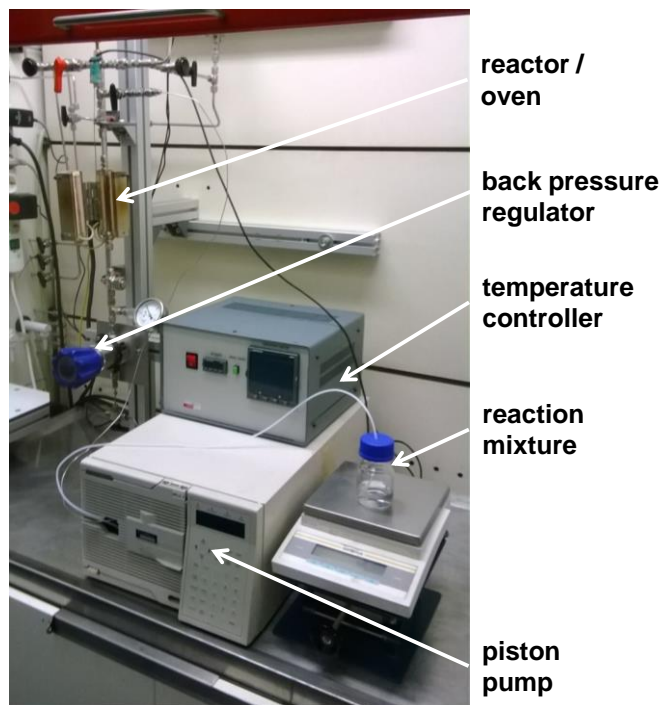


**Figure 9:** Continuous set-up at Institute for Inorganic Materials Chemistry (SMK, Eindhoven University of Technology (TU/e)). T<sub>max</sub>: 700 °C, P<sub>max</sub>: 100 bar.

The weight hourly space velocities (WHSV) were varied by adjusting the amount of catalyst.

$$\text{WHSV} = \frac{m_{LA}/h}{m_{catalyst}} \quad (3)$$

## Materials and Methods

The turnover frequency (TOF) was calculated from mol LA ( $n_{LA}$ ), percent LA conversion ( $X_{LA}$ ), mol metal ( $n_{metal}$ ) and metal dispersion ( $D$ ):

$$TOF = \frac{n_{LA} \cdot (X_{LA}/100)}{D \cdot n_{metal} \cdot time} \quad (4)$$

The turnover number (TON) was calculated from mol LA ( $n_{LA}$ ), percent LA conversion ( $X_{LA}$ ) and mol metal ( $n_{metal}$ ).

$$TON = \frac{n_{LA} \cdot (X_{LA}/100)}{n_{metal}} \quad (5)$$

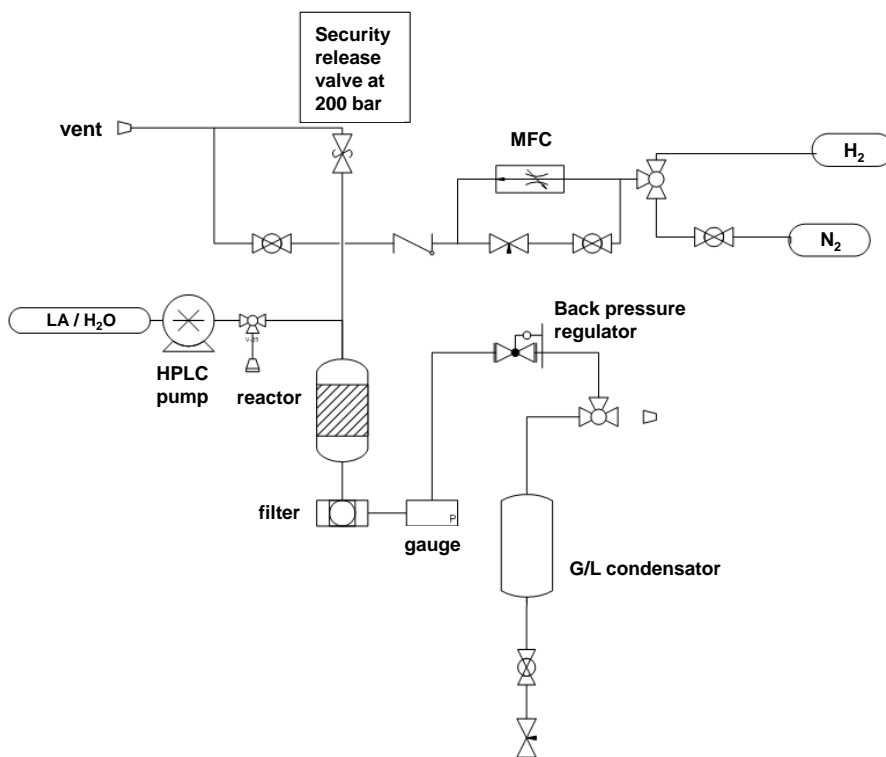


**Figure 10:** Flow diagram of the continuous set-up at SMK (Eindhoven University of Technology).



## 2.4. Product analysis

### 2.4.1. High pressure liquid chromatography

Product mixtures were diluted with demineralized water and then analyzed by high performance liquid chromatography (HPLC, Merck-Hitachi) containing a BioRad organic acid column (Aminex HPX 87H), a refraction index detector and a UV detector (wavelength: 254 nm). A 0.004 M H<sub>2</sub>SO<sub>4</sub> solution was used as the mobile phase with a 0.5 mL/min flowrate. The column was operated at 50 °C and 50 bar. Product concentrations were calculated using calibration curves using mixtures of LA, GVL and FA (all from Sigma-Aldrich, analytical grade).

### 2.4.2. Gas chromatography

The product mixtures of the catalytic tests with organic solvents were analyzed using gas chromatography (Shimadzu GC2010 plus; polar Restek column (Rxi®-624Sil)) and tetradecane (TD) as internal standard to calculate the LA and GVL concentrations.

The gaseous products of the FA decomposition were analyzed using gas chromatography (7890 Agilent Technology; Molsieve 5A and Porapak PLOT Q columns).

### 2.4.3. Nuclear magnetic resonance spectroscopy

In case of GVL selectivity <100 %, the product mixture (100 mg) was also analyzed by nuclear magnetic resonance spectroscopy (250 Hz NMR, Bruker) using D<sub>2</sub>O (900 mg) as solvent in order to quantify intermediate products, such as 4-hydroxypentanoic acid or angelica lactone.

### **3. Results of catalyst characterization**

This chapter focuses on the characterization results of the Ni based catalysts applied in the LA hydrogenation to GVL both in batch and continuous reaction mode. In addition, the characterization results of the noble metal based catalysts investigated in the FA decomposition and LA hydrogenation using FA as H<sub>2</sub> donor are reported.

#### **3.1. Nickel based catalysts**

##### **3.1.1. Elemental composition, BET surface area and reducibility**

The Ni contents, the BET surface areas, the reducibility and the crystalline phases of the catalysts were investigated and the results are summarized in Table 2. All synthesis routes led to the expected Ni content for the fresh catalysts, except for the precipitation with urea. With this method a metal loading of only 11.1 % Ni was obtained, instead of expected 15 %. Nevertheless, the Ni loading for the bimetallic 15Ni+0.75Pt/Al<sub>2</sub>O<sub>3</sub>\_urea catalyst was in accordance with the expected Ni amount. However, the precipitation of Pt with urea on 15Ni+0.75Pt/Al<sub>2</sub>O<sub>3</sub>\_urea was only partially successful. Only 10% of the expected Pt was found, which may be caused by a too high pH-value during Pt precipitation on  $\gamma$ -Al<sub>2</sub>O<sub>3</sub>.

The surface areas of the Ni/Al<sub>2</sub>O<sub>3</sub> catalysts were moderately lower than pure Al<sub>2</sub>O<sub>3</sub> (145 m<sup>2</sup>/g). 15Ni/Al<sub>2</sub>O<sub>3</sub>\_fsp exhibited a much lower surface area, which is often linked to nickel aluminates.[124] The surface area of 15Ni/Siral70\_wi (242 m<sup>2</sup>/g) was also substantially lower than pure Siral70 (400 m<sup>2</sup>/g).

**Table 2:** Analysis of the Ni catalyst by ICP-OES, BET surface area, TPR and XRD.

Ni content [wt.%]		BET surface area [m <sup>2</sup> /g] <sup>c</sup>	Reduction peak maximum [°C]	Crystal phase [XRD]
Fresh catalyst	Catalyst after continuous reaction			
4.7	4.8	108	700	Ni
14.0	13.4	96	380 and 700	Ni
14.0	12.9	122	380	Ni
14.8	n.d.	98	530	Ni, NiO
11.1	9.7	127	380 <sup>d</sup> and 700	Ni
13.4	n.d.	31	800	no Ni phases
15.5 (0.05 Pt)	13.2	115	700 <sup>e</sup>	N
14.1	n.d.	242	650	Ni

a = reduced at 600 °C; b = reduced at 450 °C; c = after reduction; d = main peak at 380 °C; e = starts at 450 °C; n.d. not determined.

## Results of catalyst characterization

The reduction behavior of the catalysts was investigated by TPR (Figure 11). The profiles of 15Ni/Al<sub>2</sub>O<sub>3</sub>\_wi, and 15Ni/Al<sub>2</sub>O<sub>3</sub>\_urea were rather similar. Reduction started at 300 °C with a broad feature at 380 °C. A second H<sub>2</sub> consumption peak observed at 700 °C was less pronounced for 15Ni/Al<sub>2</sub>O<sub>3</sub>\_urea. The two peaks of H<sub>2</sub> consumption indicate an inhomogeneous Ni particle size distribution. Large NiO particles are typically reduced at temperatures in the 300 °C – 400 °C range, while higher temperatures (600 °C – 750 °C) are necessary for the reduction of small NiO particles [125] and nickel alumina spinel [126, 127]. The TPR profile of 15Ni/Al<sub>2</sub>O<sub>3</sub>\_p and 15Ni/Al<sub>2</sub>O<sub>3</sub>\_iwi (not shown) showed only a broad H<sub>2</sub> consumption peak with maxima at 380 °C and 530 °C, respectively, hinting to the presence of large NiO particles. The TPR profiles of 5Ni/Al<sub>2</sub>O<sub>3</sub>\_wi, 15Ni+0.75Pt/Al<sub>2</sub>O<sub>3</sub>\_urea and 15Ni/Al<sub>2</sub>O<sub>3</sub>\_fsp are not that different as they feature one broad H<sub>2</sub> consumption peak with a maximum at 600, 700 and 800 °C, respectively. Former two suggest the presence of small NiO particles and a fairly homogeneous particle size distribution as a result of the low Ni content (5Ni/Al<sub>2</sub>O<sub>3</sub>\_wi) or Pt doping (15Ni+0.75Pt/Al<sub>2</sub>O<sub>3</sub>\_urea). The high reduction temperature of 15Ni/Al<sub>2</sub>O<sub>3</sub>\_fsp was related to the high temperature (> 900 °C) reached during the flame spray pyrolysis method. This corresponds to NiAl<sub>2</sub>O<sub>4</sub> spinel or NiO, embedded in alumina, which was more difficult to reduce. In fact, the TPR profile of the FSP catalyst was similar to those reported for Ni aluminium spinels.[126, 127]

### 3.1.2. Determination of catalyst structure and Ni particle size

The structure of the catalysts and the Ni particle size were investigated by powder X-ray diffraction, X-ray absorption spectroscopy, electron microscopy and chemisorption.

#### 3.1.2.1. X-ray diffraction

Figure 12 (i) show the XRD patterns of the reduced Ni/Al<sub>2</sub>O<sub>3</sub> catalysts (as well as the catalysts after continuous reaction, cf. section 5.2.2.2). The XRD patterns of the 15Ni/Al<sub>2</sub>O<sub>3</sub> catalysts prepared by wet impregnation, incipient wetness impregnation and precipitation showed a NiO phase for the calcined catalysts without any reflections of metallic Ni. For the calcined and reduced 15Ni/Al<sub>2</sub>O<sub>3</sub>\_fsp only reflections from  $\gamma$ -Al<sub>2</sub>O<sub>3</sub> were observed. No metallic Ni was found and also a possible

nickel aluminum spinel formation as indicated by TPR could not be identified. 15Ni/Al<sub>2</sub>O<sub>3</sub>\_wi was reduced at 450 °C and the NiO phase was still found after the reduction (Figure 12 (i)). The XRD patterns of the reduced 5Ni/Al<sub>2</sub>O<sub>3</sub>\_wi, 15Ni/Al<sub>2</sub>O<sub>3</sub>\_wi, 15Ni/Al<sub>2</sub>O<sub>3</sub>\_p, 15Ni/Al<sub>2</sub>O<sub>3</sub>\_urea and 15Ni+0.75Pt/Al<sub>2</sub>O<sub>3</sub>\_urea catalysts showed, in addition to  $\gamma$ -Al<sub>2</sub>O<sub>3</sub>, characteristic reflections of metallic Ni with differences in intensity and FWHM. The Ni (NiO) particle sizes were estimated using the Scherrer equation (Table 3).

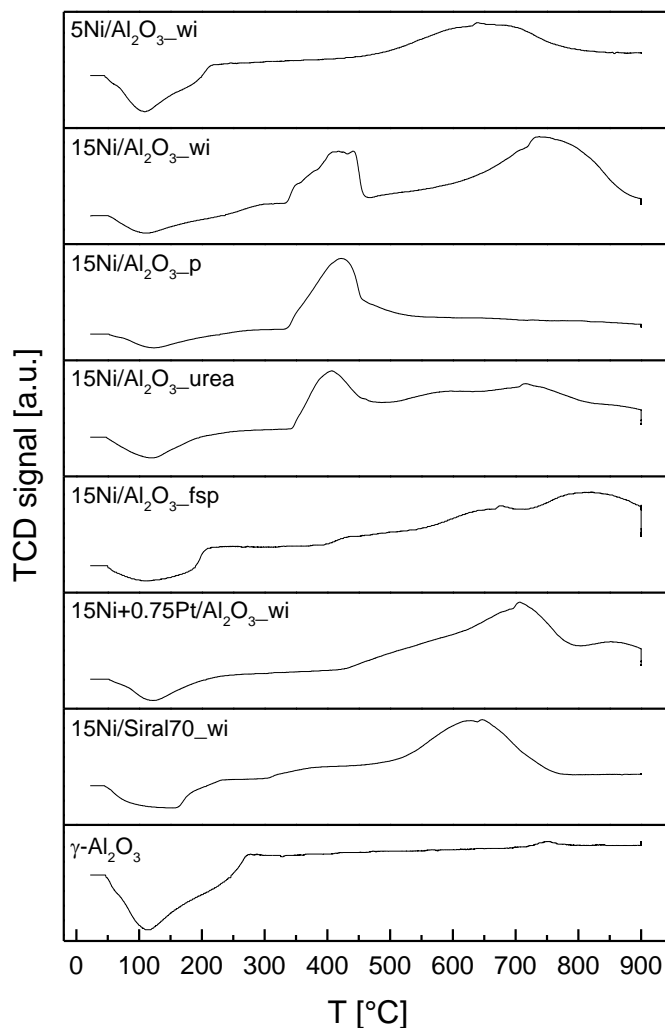


**Figure 11:** TPR-profiles of the different Ni catalysts and pure  $\gamma$ -Al<sub>2</sub>O<sub>3</sub>; conditions: 25 °C – 900 °C (5 °C/min) in a 5 % H<sub>2</sub>/Ar flow (73 mL/min).

## Results of catalyst characterization

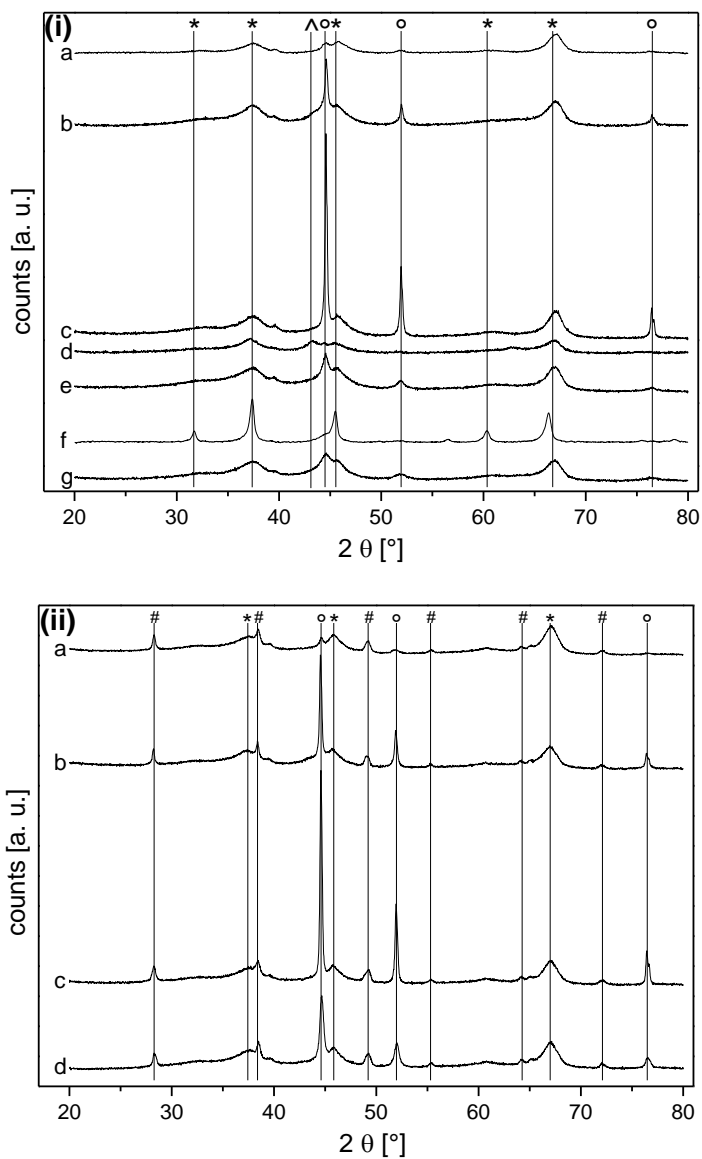


**Figure 12:** XRD patterns of the Ni/Al<sub>2</sub>O<sub>3</sub> catalysts after reduction (i) and after continuous reaction (ii); a = 5Ni/Al<sub>2</sub>O<sub>3\_wi</sub>; b = 15Ni/Al<sub>2</sub>O<sub>3\_wi</sub>; c = 15Ni/Al<sub>2</sub>O<sub>3\_p</sub>; d = 15Ni/Al<sub>2</sub>O<sub>3\_iwi</sub>; e = 15Ni/Al<sub>2</sub>O<sub>3\_urea</sub>; f = 15Ni/Al<sub>2</sub>O<sub>3\_fsp</sub>; g = 15Ni+0.75Pt/Al<sub>2</sub>O<sub>3\_urea</sub>; o = Ni; \* =  $\gamma$ -Al<sub>2</sub>O<sub>3</sub>; ^ = NiO; # = boehmite.

**Table 3:** Ni dispersion and Ni particle size of the different pre-reduced and used catalysts estimated by H<sub>2</sub> chemisorption, XRD and STEM.

Catalyst	Dispersion [%]	d <sub>Ni</sub> [nm]	d <sub>Ni</sub> [nm]	d <sub>Ni</sub> [nm]	d <sub>Ni</sub> [nm]
	(Chemisorp.)	(Chemisorp.)	(XRD)	(XRD) <sup>a</sup>	(STEM)
5Ni/Al <sub>2</sub> O <sub>3</sub> _wi	0.9 <sup>b</sup>	(117)	12	13	6
15Ni/Al <sub>2</sub> O <sub>3</sub> _wi	2.7 <sup>b</sup>	(38)	37	52	11 <sup>c</sup>
15Ni/Al <sub>2</sub> O <sub>3</sub> _p	1.3	79	65	83	n.d.
15Ni/Al <sub>2</sub> O <sub>3</sub> _iwi <sup>d</sup>	n.d.	n.d.	7 (NiO)	n.d.	n.d.
15Ni/Al <sub>2</sub> O <sub>3</sub> _urea	2.8	36	15	19	7 <sup>c</sup>
15Ni/Al <sub>2</sub> O <sub>3</sub> _fsp	0.7 <sup>b</sup>	(154)	n.d.	n.d.	n.d.
15Ni+0.75Pt/ Al <sub>2</sub> O <sub>3</sub> _urea	6.9	15	10	36	n.d.
15Ni/Siral70_wi	3	34	8	n.d.	n.d.

a = after continuous reaction; b = not all Ni was reduced at 600 °C due to the formation of NiAl<sub>2</sub>O<sub>4</sub>; (*italic*) = minimum of dispersion due to lower degree of reduction (spinel formation); c = only Ni particles smaller than 20 nm were counted; d = reduced at 450 °C; n.d. = not determined.

*In situ* XRD patterns were acquired during the reduction of the 15Ni/Al<sub>2</sub>O<sub>3</sub>\_wi to determine its optimal reduction temperature. Similar to the TPR results reduction of NiO to Ni started at 300 °C. The XRD pattern collected at 300 °C showed reflections of both NiO and minor contributions of metallic Ni. The broad temperature range of reduction obtained with TPR could be proven by the *in situ* collected XRD patterns. All XRD patterns between 300 °C and 550 °C showed reflections of NiO and metallic Ni (Figure 13). At 600 °C the XRD pattern featured only a metallic Ni phase indicating

## Results of catalyst characterization

the complete reduced of the catalyst. Ni particles which are too small to be detected by XRD are not considered in this case and could still be oxidized.

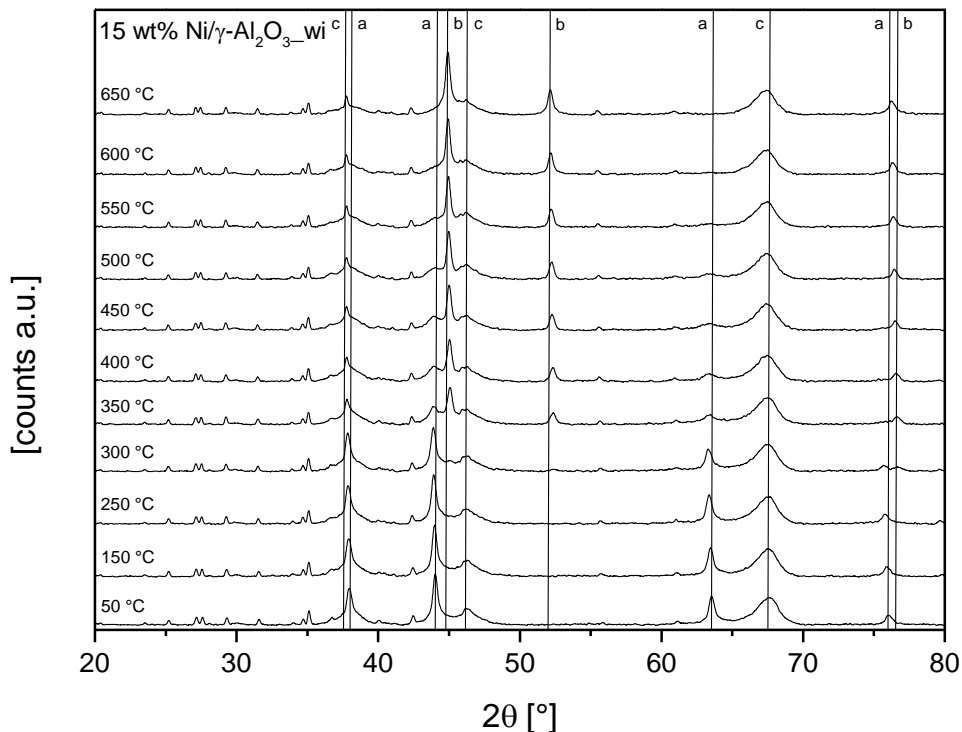


**Figure 13:** *In situ* XRD patterns of the 15Ni/Al<sub>2</sub>O<sub>3</sub>\_wi catalyst during the reduction in 5% H<sub>2</sub>/N<sub>2</sub> and a total flow of 100 mL/min (ramp rate: 5 K/min); a = NiO; b = Ni; c = Al<sub>2</sub>O<sub>3</sub>.

### 3.1.2.2. *Ex situ* X-ray absorption spectroscopy

Figure 14a shows the near edge X-ray absorption spectra at the Ni K edge for the 15Ni/Al<sub>2</sub>O<sub>3</sub>\_wi, 15Ni/Al<sub>2</sub>O<sub>3</sub>\_p and 15Ni/Al<sub>2</sub>O<sub>3</sub>\_fsp catalysts after reduction at 600 °C in H<sub>2</sub>. According to XRD analysis (Figure 13) this treatment led to a completely reduced 15Ni/Al<sub>2</sub>O<sub>3</sub>\_wi catalyst. Due to the similar structural data the same is expected for 15Ni/Al<sub>2</sub>O<sub>3</sub>\_p. XANES data (Figure 14a) offers more information about the oxidation state. As expected the spectra for 15Ni/Al<sub>2</sub>O<sub>3</sub>\_wi and 15Ni/Al<sub>2</sub>O<sub>3</sub>\_p are very similar. However, the white line of 15Ni/Al<sub>2</sub>O<sub>3</sub>\_fsp catalyst was significantly more pronounced and the spectrum was shifted to higher energy, indicating a higher



oxidation state. This *ex situ* XAS analysis reflected the state of the catalysts as they were loaded in the batch reactor. Re-oxidation may partially occur for the 15Ni/Al<sub>2</sub>O<sub>3</sub>\_fsp after the reduction procedure as well.

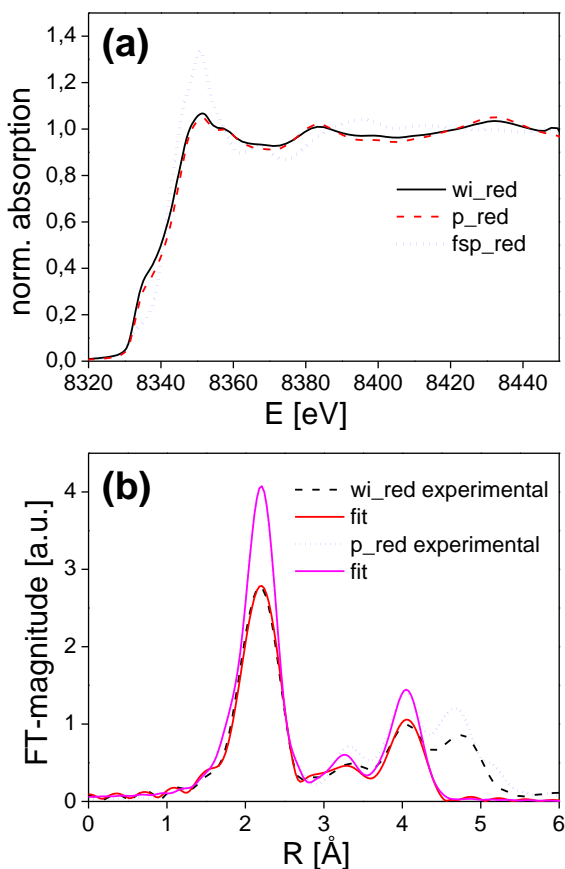


**Figure 14:** (a) X-ray absorption near edge spectra of the reduced 15Ni/Al<sub>2</sub>O<sub>3</sub>\_wi, 15Ni/Al<sub>2</sub>O<sub>3</sub>\_p and 15Ni/Al<sub>2</sub>O<sub>3</sub>\_fsp catalysts at the Ni K edge; (b) Experimental and refined Fourier transformed  $k^2$  weighted EXAFS spectra.

The refinement of EXAFS data provided further information on the local chemical environment of the Ni atoms. Figure 14b shows the experimental and refined Fourier transformed  $k^2$  weighted EXAFS spectra of 15Ni/Al<sub>2</sub>O<sub>3</sub>\_wi and 15Ni/Al<sub>2</sub>O<sub>3</sub>\_p. The backscattering contributions of the oxygen and Ni neighbours of the 15Ni/Al<sub>2</sub>O<sub>3</sub>\_p

## Results of catalyst characterization

catalyst is higher than those of 15Ni/Al<sub>2</sub>O<sub>3</sub>\_wi. This is also reflected by the lower coordination numbers (Table 4) and confirms that Ni/Al<sub>2</sub>O<sub>3</sub>\_wi features smaller particles than Ni/Al<sub>2</sub>O<sub>3</sub>\_p (Table 3). According to the fit results in Table 4 15Ni/Al<sub>2</sub>O<sub>3</sub>\_wi and 15Ni/Al<sub>2</sub>O<sub>3</sub>\_p contain mainly metallic species, although some oxygen neighbours were found around Ni, meaning that these catalysts were partially oxidized after air exposure. More details on the refinement and individual scattering paths are depicted in Figure 15.

**Table 4:** Structural parameters of the Ni absorber extracted from the EXAFS spectra of the calcined and activated 15Ni/Al<sub>2</sub>O<sub>3</sub> catalyst.

Sample	Shell	Atom	<i>N</i>	<i>R</i> [Å]	$\sigma^2 \times 10^{-3}$ [Å <sup>2</sup> ]	$\Delta E_0$ [eV]	$\rho$ [%]
<b>15Ni/Al<sub>2</sub>O<sub>3</sub>_wi</b>	1 <sup>st</sup>	O	1.2 ± 0.4 <sup>a</sup>	2.04 ± 0.04 <sup>a</sup>	6.2 ± 1.6 <sup>a</sup>	7.9 ± 1.0	2.5
	2 <sup>nd</sup>	Ni	8.0 ± 0.9 <sup>a</sup>	2.49 <sup>§a</sup>	6.7 ± 0.9 <sup>a</sup>		
	3 <sup>rd</sup>	Ni	4.0 ± 0.4 <sup>c</sup>	3.49 ± 0.02 <sup>a</sup>	9.2 ± 2.7 <sup>a</sup>		
	4 <sup>th</sup>	Ni	17.5 ± 6.1 <sup>a</sup>	4.34 ± 0.01 <sup>a</sup>	9.6 ± 2.8 <sup>a</sup>		
<b>15Ni/Al<sub>2</sub>O<sub>3</sub>_p</b>	1 <sup>st</sup>	O	1.0 ± 0.4 <sup>a</sup>	2.02 ± 0.03 <sup>a</sup>	6.0 ± 3.5 <sup>a</sup>	7.5±0.7	2.7
	2 <sup>nd</sup>	Ni	10.0 ± 0.7 <sup>a</sup>	2.49 <sup>§a</sup>	6.4 ± 0.5 <sup>a</sup>		
	3 <sup>rd</sup>	Ni	5.0 ± 0.4 <sup>c</sup>	3.49 ± 0.02 <sup>a</sup>	8.7 ± 1.8 <sup>a</sup>		
	4 <sup>th</sup>	Ni	20.0 ± 2.0 <sup>c</sup>	4.34 ± 0.01 <sup>a</sup>	8.5 ± 0.9 <sup>a</sup>		
<b>15Ni/Al<sub>2</sub>O<sub>3</sub>_fsp</b>	1 <sup>st</sup>	O	3.8 <sup>f</sup>	2.02 ± 0.03 <sup>a</sup>	5.1 ± 2.1 <sup>a</sup>	-1.6±4.1	2.1
	2 <sup>nd</sup>	Ni	6.2 ± 0.6 <sup>a</sup>	2.49 <sup>§a</sup>	6.4 ± 0.5 <sup>a</sup>		
	3 <sup>rd</sup>	Al	3 <sup>f</sup>	2.80 ± 0.03 <sup>a</sup>	16.1 ± 5.9 <sup>a</sup>		
	4 <sup>th</sup>	Al	3 <sup>f</sup>	3.29 ± 0.02 <sup>a</sup>	3.6 ± 2.1 <sup>a</sup>		
	5 <sup>th</sup>	Al	6 <sup>f</sup>	3.70±0.02 <sup>a</sup>	9.2± 3.2 <sup>a</sup>		
<b>Ni foil</b>	1 <sup>st</sup>	Ni	12 <sup>f</sup>	2.48 <sup>§a</sup>	5.9± 0.1 <sup>a</sup>	6.7±0.3	1.5
<b>NiO</b>	1 <sup>st</sup>	O	6 <sup>f</sup>	2.08 ± 0.01 <sup>a</sup>	3.8 ± 1.5 <sup>a</sup>	-0.7±0.9	1.2

$S_0^2=0.80$ , §= fitted uncertainty lower than 1%, a= fitted, f=fixed and c=constraint (3<sup>rd</sup> shell=2<sup>nd</sup> shell/2 and 4<sup>th</sup> shell=2<sup>nd</sup> shell x 2). Structural parameters: N=number of neighboring atoms, r= interatomic distance,  $\sigma^2$ = mean square deviation of interatomic distances,  $\rho$ = misfit between the experimental data and the theory.

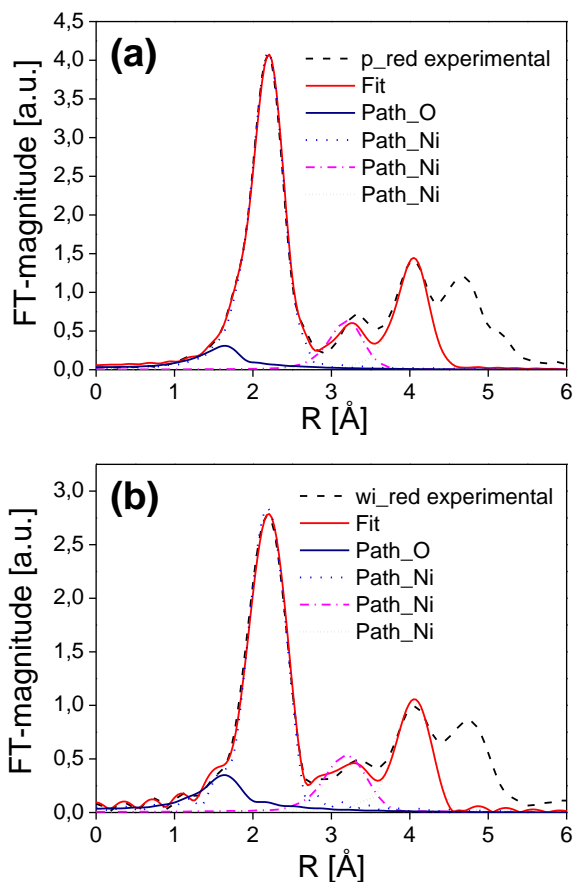


**Figure 15:** Experimental and refined Fourier transformed  $k^2$  weighted EXAFS spectra and individual refined paths of (a) 15Ni/Al<sub>2</sub>O<sub>3</sub>\_p catalyst and (b) 15Ni/Al<sub>2</sub>O<sub>3</sub>\_wi catalyst.

In order to shed more insight into the structure of the partially reduced FSP catalyst, linear combination fitting of the Ni K edge XANES spectrum with the reduced 15Ni/Al<sub>2</sub>O<sub>3</sub>\_wi catalyst (mainly small metallic particles), a NiAl<sub>2</sub>O<sub>4</sub> reference and NiO was conducted (Figure 16).

The linear combination analysis revealed that the Ni/Al<sub>2</sub>O<sub>3</sub>\_fsp catalyst could be described best as a combination of 47% NiAl<sub>2</sub>O<sub>4</sub> and air exposed Ni particles (fraction of 53 %, reduced 15Ni/Al<sub>2</sub>O<sub>3</sub>\_wi catalyst). Linear combinations based on a combination of NiO and metallic Ni resulted in poor agreement (Figure 17). Hence

## Results of catalyst characterization

the best description of the FSP-derived catalyst consists of a mixture of Ni in a spinel-like phase and metallic Ni after reduction at 600 °C.

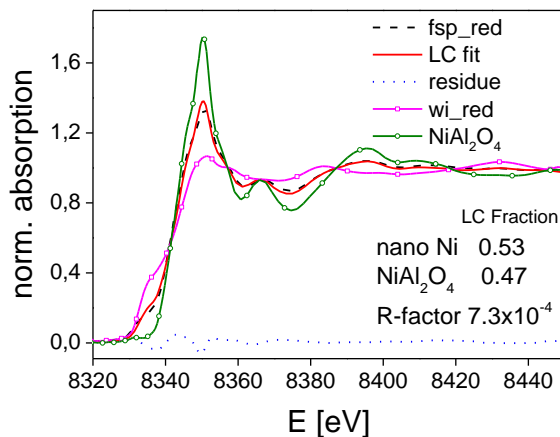


**Figure 16:** X-ray absorption near edge spectra at the Ni K edge and linear combination analysis of 15Ni/Al<sub>2</sub>O<sub>3</sub>\_fsp catalyst after reduction.

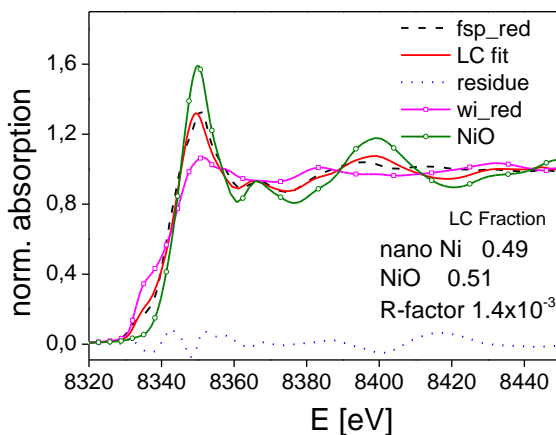


**Figure 17:** X-ray absorption near edge spectra at the Ni K edge and linear combination analysis of 15Ni/Al<sub>2</sub>O<sub>3</sub>\_fsp catalyst after reduction fitted with NiO.

This is in line with previous studies showing that catalysts prepared by flame spray pyrolysis are more difficult to reduce than impregnated ones, since the metal ions

could be within the oxide lattice. [128] According to powder X-ray diffraction results (only the presence of an  $\text{Al}_2\text{O}_3$  phase is visible) Ni is highly dispersed. Hence, a structural model was built to refine the EXAFS data based on the following assumptions: (i) one first coordination shell with Ni in a spinel-like phase in octahedral coordination and the outer shells with Ni in the lattice of  $\text{Al}_2\text{O}_3$  and (ii) a metallic Ni phase. The Fourier transformed EXAFS spectrum and the corresponding refinement are presented in Figure 18. To reduce the fitting parameters the O coordination number was weighted and fixed according to the oxidized fraction obtained by the linear combination of the near edge structure. In the same way the number of Al atoms in the outer shells was also fixed according to the crystal structure of  $\text{Al}_2\text{O}_3$  [129].

The results suggest that at least some of the Ni atoms were incorporated into the  $\text{Al}_2\text{O}_3$  lattice during the preparation. Therefore, the surface Ni may be reduced forming the metallic particles, whereas the incorporated fraction was converted into a spinel-like phase. The spinel-like phase was similar to those reported by Fu *et. al.* [130]. In this study the authors annealed Ni acetate impregnated on  $\gamma\text{-Al}_2\text{O}_3$ . While the sample treated at  $500^\circ\text{C}$  presented mainly NiO features, the spectra for the samples treated at  $750^\circ\text{C}$  and  $950^\circ\text{C}$  were similar to the one obtained for  $15\text{Ni}/\text{Al}_2\text{O}_3\text{\_fsp}$  in the present work. However, their Ni-O spinel-like bond length was around  $1.83 \text{ \AA}$ , whereas in the present study  $2.02 \text{ \AA}$  (Table 4) were found, indicating that only a spinel-like phase was formed in case of  $\text{Ni}/\text{Al}_2\text{O}_3\text{\_fsp}$ .

In summary, the local structure of nickel was strongly influenced by the preparation method, which therefore may play an important role on the catalytic activity (see comparison of catalysts in section 4.2.2). Both precipitation and wet impregnation resulted in small metallic Ni particles covered by oxygen. However, the impregnation method led to smaller particles. On the other hand, the flame made material was composed of a mixture of metallic Ni and Ni in an  $\text{Al}_2\text{O}_3$  matrix. The *ex situ* XAS analysis showed, that besides large Ni particles estimated with Scherrer equation from XRD also small Ni particles (2 – 4 nm) exist for  $15\text{Ni}/\text{Al}_2\text{O}_3\text{\_wi}$  and  $15\text{Ni}/\text{Al}_2\text{O}_3\text{\_p}$ .

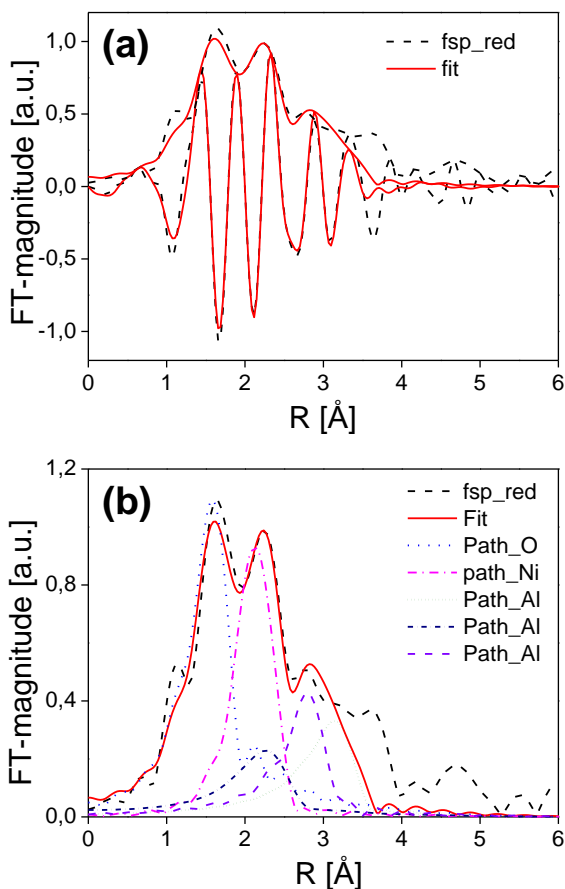


**Figure 18:** (a) experimental and refined  $k^2$  weighted Fourier transformed EXAFS spectra for of 15Ni/Al<sub>2</sub>O<sub>3</sub>\_fsp catalyst after reduction and (b) respective individual refined paths.

### 3.1.2.3. *In situ* X-ray absorption spectroscopy

To investigate the local Ni environment and the reduction behavior in more detail, *in situ* X-ray absorption near edge structure (XANES) spectra before, during and after reduction were recorded for, 15Ni/Al<sub>2</sub>O<sub>3</sub>\_wi and 15Ni/Al<sub>2</sub>O<sub>3</sub>\_urea at the Ni K edge. The XANES spectra of the calcined (i) and reduced (ii) catalysts are shown in Figure 19. The XANES spectra of the calcined Ni/Al<sub>2</sub>O<sub>3</sub>\_wi catalysts featured a higher whiteline intensity and a slight shift to higher energies compared to the NiO reference spectrum (Figure 19), especially for the 5Ni/Al<sub>2</sub>O<sub>3</sub>\_wi catalyst. This reflects a strong interaction with the alumina support and potentially a spinel formation.

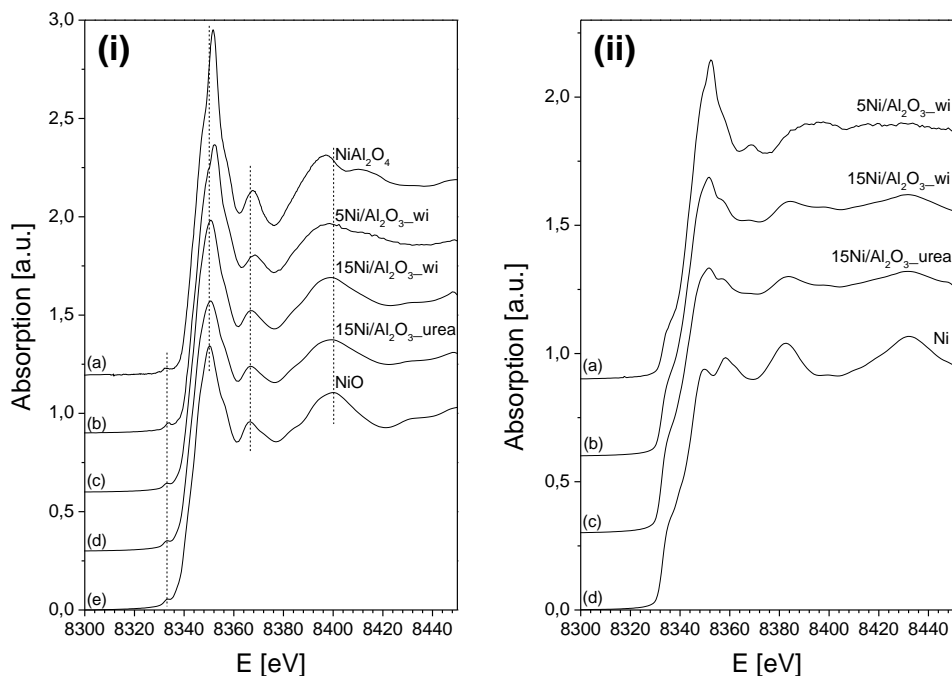


**Figure 19:** XANES spectra at the Ni K edge of (i) calcined 5Ni/Al<sub>2</sub>O<sub>3</sub>\_wi (b), 15Ni/Al<sub>2</sub>O<sub>3</sub>\_wi (c) and 15Ni/Al<sub>2</sub>O<sub>3</sub>\_urea (d) catalysts in comparison with NiO (e) and NiAl<sub>2</sub>O<sub>4</sub> (a) reference spectra and (ii) of 5Ni/Al<sub>2</sub>O<sub>3</sub>\_wi (a), 15 Ni/Al<sub>2</sub>O<sub>3</sub>\_wi (b) and 15 Ni/Al<sub>2</sub>O<sub>3</sub>\_urea (c) catalysts after in situ TPR in comparison with Ni reference spectrum (d).

In fact, from the linear combination analysis we estimated a NiAl<sub>2</sub>O<sub>4</sub> fraction of 60 % for 5Ni/Al<sub>2</sub>O<sub>3</sub>\_wi and 0.26 % for 15Ni/Al<sub>2</sub>O<sub>3</sub>\_wi. Further evidence for spinel formation can be acquired from the comparison of EXAFS spectra of the Ni catalysts with the spectrum of the spinel reference (cf. Figure 20).

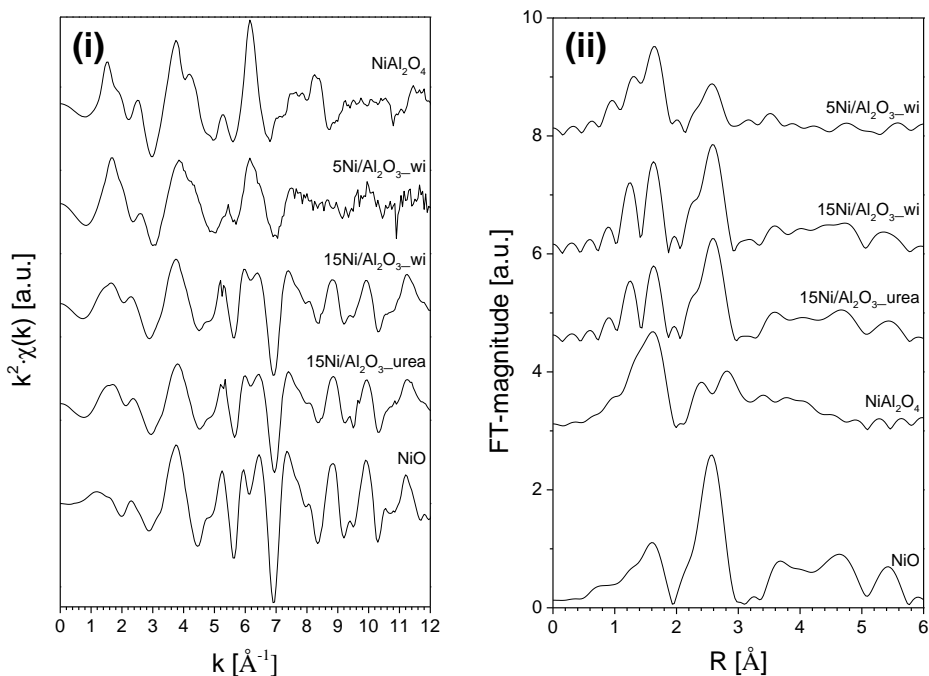


**Figure 20:** (i)  $k^2$ -weighted EXAFS spectra of calcined  $5\text{Ni}/\text{Al}_2\text{O}_3\text{-wi}$ ,  $15\text{Ni}/\text{Al}_2\text{O}_3\text{-wi}$  and  $15\text{Ni}/\text{Al}_2\text{O}_3\text{-urea}$  catalysts in comparison with  $\text{NiO}$  and  $\text{NiAl}_2\text{O}_4$  reference spectra; (ii) Fourier transformed  $k^3$  EXAFS spectra (not corrected for phase shift) of calcined  $5\text{Ni}/\text{Al}_2\text{O}_3\text{-wi}$ ,  $15\text{Ni}/\text{Al}_2\text{O}_3\text{-wi}$  and  $15\text{Ni}/\text{Al}_2\text{O}_3\text{-urea}$  catalysts in comparison with  $\text{NiO}$  and  $\text{NiAl}_2\text{O}_4$  reference spectra.

Next, complementary to the TPR-data (section 3.1.1), the reduction behavior was studied by XANES for three selected catalysts. The results of the LCA of the *in situ* TPR-XANES spectra are shown in Figure 21 (for XANES data, cf. Figure 19(ii) and Figure 22).



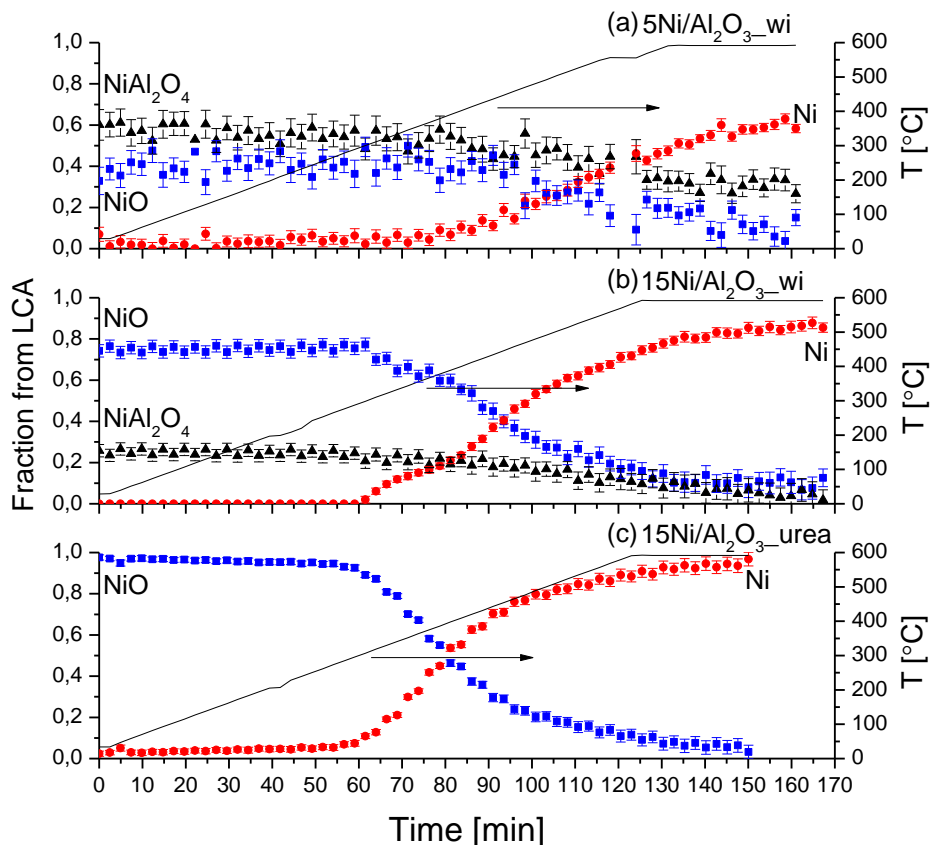


**Figure 21:** Linear combination analysis (LCA) results of *in situ* TPR-XANES spectra at the Ni K-edge of the calcined catalysts 5Ni/Al<sub>2</sub>O<sub>3\_wi</sub> (a), 15Ni/Al<sub>2</sub>O<sub>3\_wi</sub> (b) and 15Ni/Al<sub>2</sub>O<sub>3\_urea</sub> (c) using the spectra of bulk NiO, NiAl<sub>2</sub>O<sub>4</sub> and Ni-metal as references. TPR conditions: 5% H<sub>2</sub>/He, ramp rate of 5 °C/min.

For both Ni/Al<sub>2</sub>O<sub>3\_wi</sub>, the fraction of NiO was not fully reduced at 600 °C possibly due to stabilization in the spinel phase. Note that interpretations of the ratio between NiO and NiAl<sub>2</sub>O<sub>4</sub> phases at high temperature are difficult due to similarities in the spectral features for the XANES data, which results in large error bars. Therefore, taking the different reducibilities of NiO and NiAl<sub>2</sub>O<sub>4</sub> into account the unreduced Ni was mainly connected to the NiAl<sub>2</sub>O<sub>4</sub> phase following: 5Ni/Al<sub>2</sub>O<sub>3\_wi</sub> > 15Ni/Al<sub>2</sub>O<sub>3\_wi</sub> > 15Ni/Al<sub>2</sub>O<sub>3\_urea</sub>, as supported by XANES and EXAFS spectra after *in situ* TPR (cf. Figure 19(ii), Figure 22, Figure 23). The profiles of *in situ* XANES-TPR are in good agreement with conventional TPR (Figure 11).

## Results of catalyst characterization

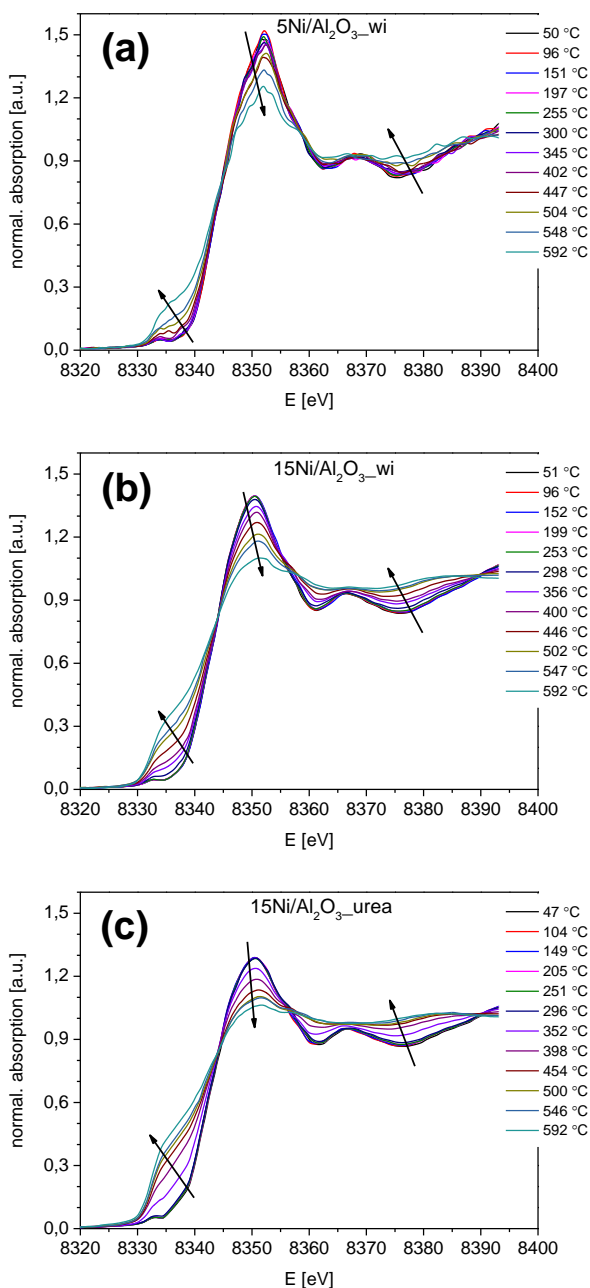


**Figure 22:** Plots of XANES spectra at the Ni K edge of 5Ni/Al<sub>2</sub>O<sub>3</sub>\_wi (a), 15Ni/Al<sub>2</sub>O<sub>3</sub>\_wi (b) and 15Ni/Al<sub>2</sub>O<sub>3</sub>\_urea (c) catalysts during *in situ* TPR measured in a temperature range of 50 – 600 °C.

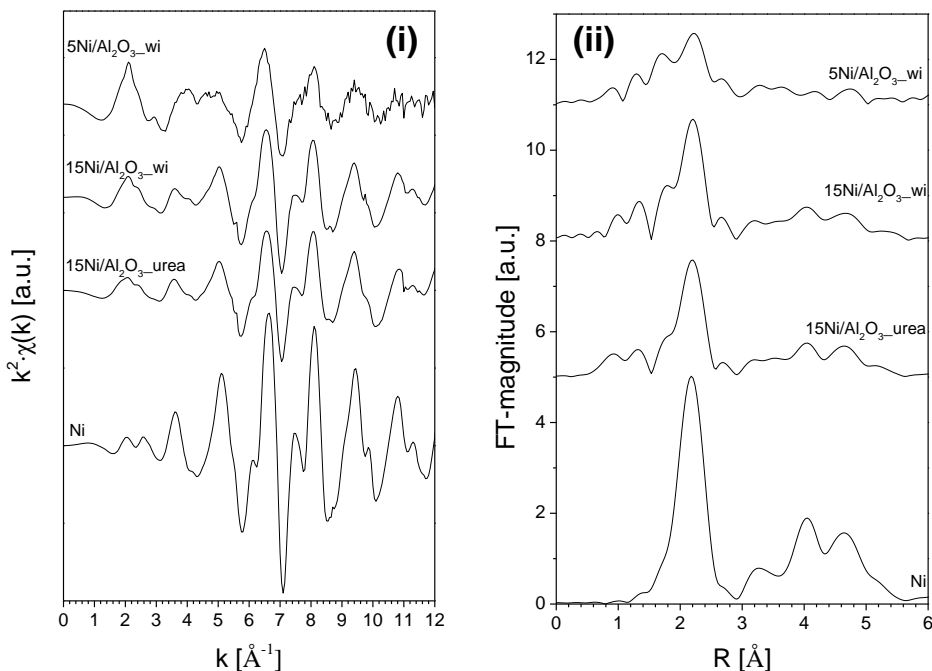


**Figure 23:** (i)  $k^2$ -weighted EXAFS spectra of 5Ni/Al<sub>2</sub>O<sub>3</sub>\_wi, 15Ni/Al<sub>2</sub>O<sub>3</sub>\_wi and 15Ni/Al<sub>2</sub>O<sub>3</sub>\_urea catalysts after in situ TPR in comparison with Ni reference spectrum; (ii) Fourier transformed  $k^3$  EXAFS spectra (not corrected for phase shift) of 5Ni/Al<sub>2</sub>O<sub>3</sub>\_wi, 15 Ni/Al<sub>2</sub>O<sub>3</sub>\_wi and 15 Ni/Al<sub>2</sub>O<sub>3</sub>\_urea catalysts after in situ TPR in comparison with Ni reference spectrum.

The main focus of the catalyst characterization concerned the determination of the Ni particle size. To verify the conclusions derived for the different Ni particle sizes based on the TPR profiles and *ex situ* XAS, H<sub>2</sub> chemisorption was measured, TEM and STEM images were recorded and the Ni particle size was derived from the XRD. The Ni dispersion and Ni particle size from various techniques are collected in Table 3.

#### 3.1.2.4. Electron microscopy

Transmission electron microscopic analysis was conducted for the reduced 15Ni/Al<sub>2</sub>O<sub>3</sub>\_wi and 15Ni/Al<sub>2</sub>O<sub>3</sub>\_p samples to prove the existence of small and large Ni particles as assumed from TPR and *ex situ* XAS analysis (section 3.1.2.2). Also TEM images of the 15Ni/Al<sub>2</sub>O<sub>3</sub>\_fsp catalyst were recorded to reveal the Ni particle size because the Ni phase could not be detected by XRD. XAS analysis suggested small Ni particles. The corresponding TEM images of the three catalysts can be

## Results of catalyst characterization

found in Figure 24. The TEM images confirmed the existence of small and large Ni particles on the 15Ni/Al<sub>2</sub>O<sub>3</sub>\_wi and 15Ni/Al<sub>2</sub>O<sub>3</sub>\_p catalysts. Also small Ni particles on the 15Ni/Al<sub>2</sub>O<sub>3</sub>\_fsp catalyst as assumed from XAS measurements (section 3.1.2.2) could be verified. Only a limited number of images were available and the smaller Ni particles gave a rather bad contrast due to re-oxidation. We did not determine the particle size with the TEM images. For TOF calculation in section 4.2.2 the average particle size determined by XRD was used.

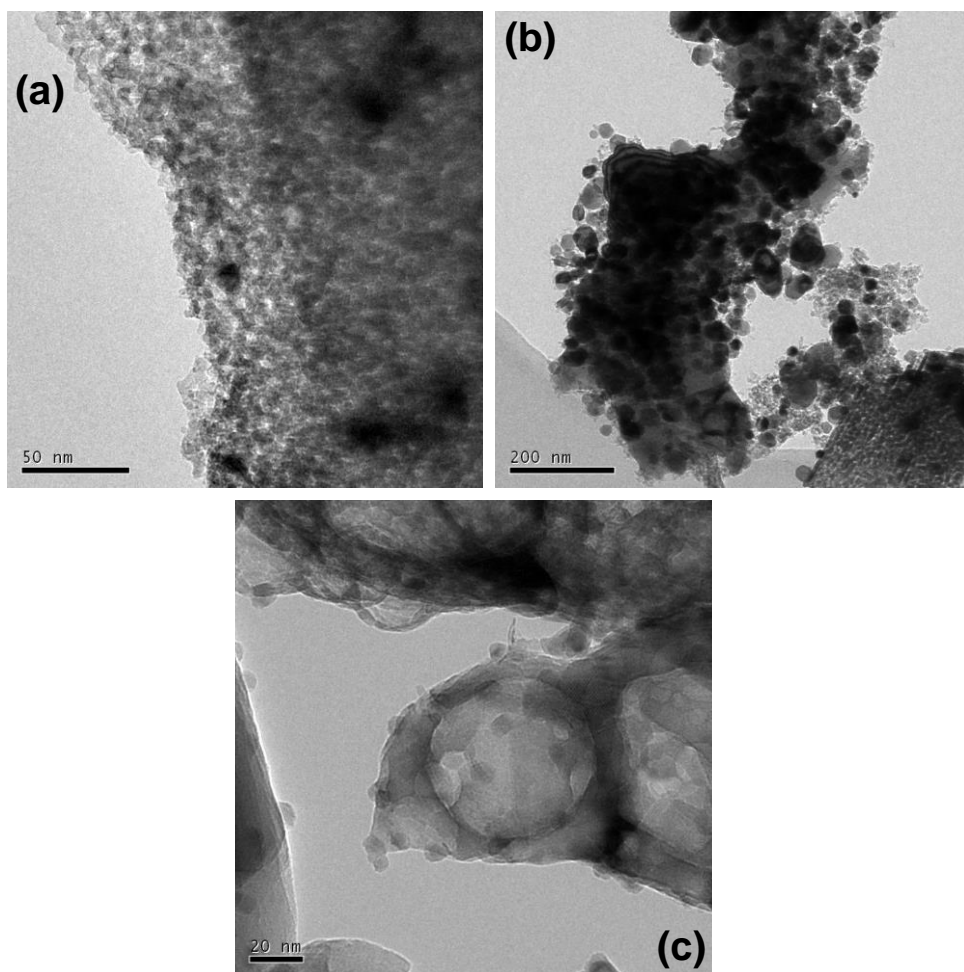


**Figure 24:** Selected TEM images of the reduced 15Ni/Al<sub>2</sub>O<sub>3</sub>\_wi (a), 15Ni/Al<sub>2</sub>O<sub>3</sub>\_p (b) and 15Ni/Al<sub>2</sub>O<sub>3</sub>\_fsp (c) catalysts.

In addition, selected STEM images of the catalysts 5Ni/Al<sub>2</sub>O<sub>3</sub>\_wi, 15Ni/Al<sub>2</sub>O<sub>3</sub>\_wi and 15Ni/Al<sub>2</sub>O<sub>3</sub>\_urea are depicted in Figure 25.

The STEM images and particle size distribution of 5Ni/Al<sub>2</sub>O<sub>3</sub>\_wi showed the presence of on average 6 nm Ni particles (472 counted particles) in a rather narrow particle size range. Those of 15Ni/Al<sub>2</sub>O<sub>3</sub>\_wi are much larger at on average 11 nm (142 counted particles) and a few very large particles (40 – 65 nm) exist. The Ni particles of 15Ni/Al<sub>2</sub>O<sub>3</sub>\_urea are less homogeneously distributed, though their average particle size of 7 nm (644 counted particles), if only <20 nm particles are taken into account, is close the 6 nm of 5Ni/Al<sub>2</sub>O<sub>3</sub>\_wi. The larger Ni particles of 15Ni/Al<sub>2</sub>O<sub>3</sub>\_urea are slightly smaller (35 – 60 nm) than those of 15Ni/Al<sub>2</sub>O<sub>3</sub>\_wi (40 – 65 nm). The histograms of the >20 nm Ni particles of these catalysts are presented in Figure 26. The particle size distributions obtained from STEM images of 5Ni/Al<sub>2</sub>O<sub>3</sub>\_wi, 15Ni/Al<sub>2</sub>O<sub>3</sub>\_wi and 15Ni/Al<sub>2</sub>O<sub>3</sub>\_urea confirmed the conclusions derived from the TPR profiles. Also the assumptions made from *ex situ* XAS spectra and TEM images of 15Ni/Al<sub>2</sub>O<sub>3</sub>\_wi were confirmed. A good agreement between the Ni particle size estimated from XRD using the Scherrer equation and the STEM results was obtained. The XRD particle sizes were slightly larger.

## Results of catalyst characterization

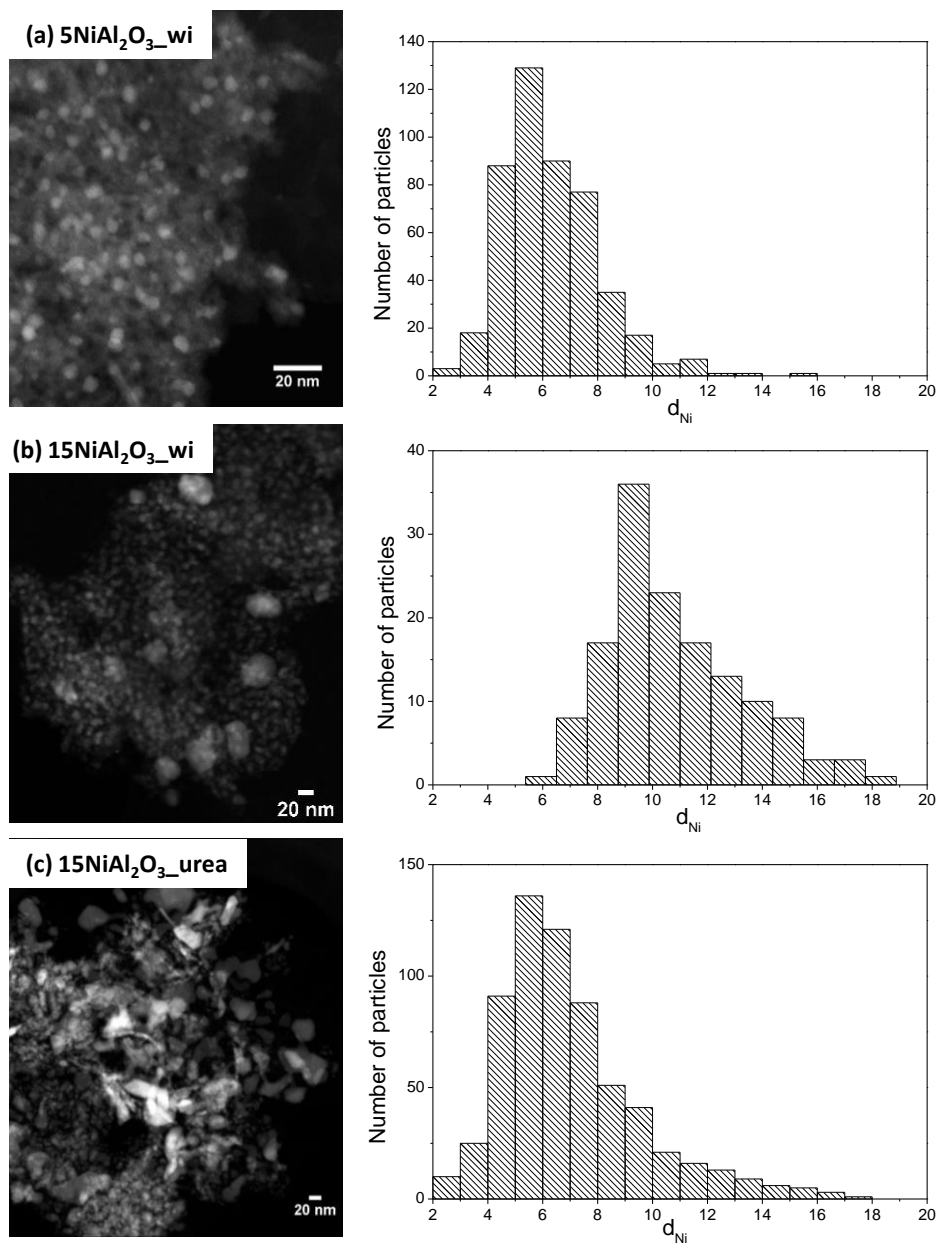


**Figure 25:** Selected STEM images and corresponding histograms of reduced catalysts  $5Ni/Al_2O_3\_wi$  (a),  $15 Ni/Al_2O_3\_wi$  (b) and  $15 Ni/Al_2O_3\_urea$  (c).

### 3.1.2.5. Hydrogen chemisorption

The Ni dispersion determined by H<sub>2</sub> chemisorption indicated that the dispersions for all catalysts were between that of 0.9 % for 5Ni/Al<sub>2</sub>O<sub>3</sub>\_wi and 6.9 % for 15Ni+0.75Pt/Al<sub>2</sub>O<sub>3</sub>\_urea (cf. Table 3). Note that the lower degree of reduction for 5Ni/Al<sub>2</sub>O<sub>3</sub>\_wi, 15Ni/Al<sub>2</sub>O<sub>3</sub>\_wi and 15Ni/Al<sub>2</sub>O<sub>3</sub>\_fsp strongly affected these results. Therefore the real dispersion of those catalysts might be higher due to the fact that Ni was not completely reduced at 600 °C. The Ni particle sizes derived from their dispersion via H<sub>2</sub> chemisorption are however only slightly larger than those from XRD.

The various techniques applied nevertheless clearly reveal the presence of small Ni particles by urea precipitation (15 nm, cf. Table 3) and larger ones when more conventional wet impregnation (37 nm) and precipitation (65 nm) were used. Doping with Pt might have decreased the average Ni particle size (10 nm). A lower Ni loading is also beneficial to obtain smaller particles i.e. 12 nm for 5 wt.% and 37 nm for 15 wt.%. The higher specific surface area of Siral70 (400 m<sup>2</sup>/g) in comparison to Al<sub>2</sub>O<sub>3</sub> (145 m<sup>2</sup>/g) resulted in small Ni particles (8 nm) with a narrow particle size distribution. The particle size of 15Ni/Al<sub>2</sub>O<sub>3</sub>\_fsp could not be accurately determined as no Ni reflections were visible in its diffraction pattern (cf. Figure 12)

## Results of catalyst characterization

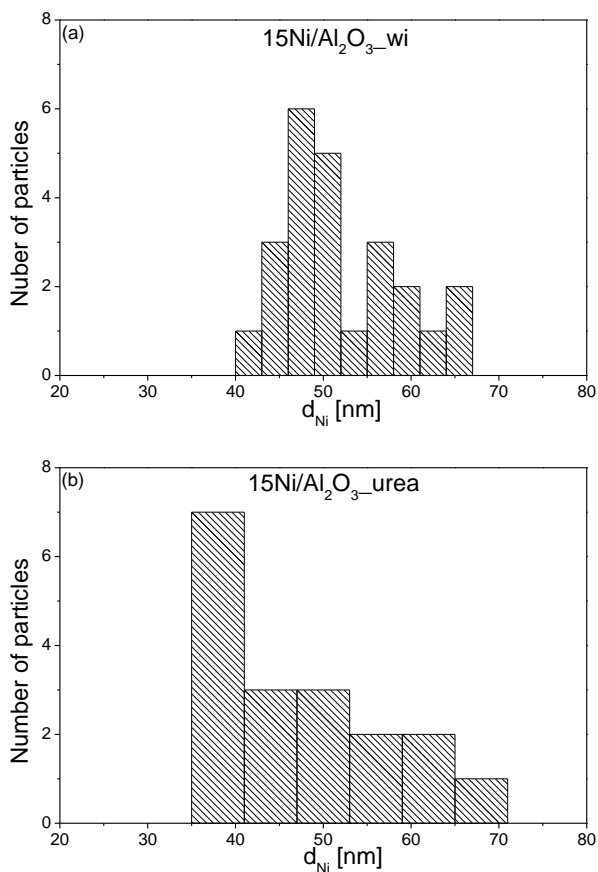


**Figure 26:** STEM derived histograms of Ni particles larger than 20 nm of catalysts 15Ni/Al<sub>2</sub>O<sub>3</sub>\_wi (a) and 15Ni/Al<sub>2</sub>O<sub>3</sub>\_urea (b).

### 3.2. Noble metal based catalysts

The following noble metals catalysts were prepared using wet impregnation as described in section 2.1.1:

1Ru/C, 1Ru/SiO<sub>2</sub>, 1Ru/ZrO<sub>2</sub>, 1Pd/SiO<sub>2</sub>, 1Pd/ZrO<sub>2</sub>, 5Pd/ZrO<sub>2</sub>, 0.75Pd+15Ni/ZrO<sub>2</sub>, 2.5Pd+2.5Au/ZrO<sub>2</sub>, 1Au/SiO<sub>2</sub>, 1Au/ZrO<sub>2</sub>, 1Pt/SiO<sub>2</sub>, 1Pt/ZrO<sub>2</sub> and 1Ir/SiO<sub>2</sub>.

In addition, a 1 mol% Au/ZrO<sub>2</sub> reference catalyst was prepared by precipitation with ammonium hydroxide according to Du *et al.* [72].



### 3.2.1. Metal content

The metal contents of the fresh catalysts are summarized in Table 5.

**Table 5:** Metal content of the noble metal catalysts determined by ICP-OES.

Catalyst	Metal content [wt.%]
1Ru/SiO <sub>2</sub>	(0.4)
1Ru/ZrO <sub>2</sub>	0.7
1Ru/C	n.d.
1Pd/SiO <sub>2</sub>	(0.7)
1Pd/ZrO <sub>2</sub>	0.8
5Pd/ZrO <sub>2</sub>	4.9
0.75Pd+15Ni/ZrO <sub>2</sub>	0.7 Pd + 14.3 Ni
2.5Pd+2.5Au/ZrO <sub>2</sub>	2.2 Pd + 1.9
1Au/SiO <sub>2</sub>	(0.3)
1Pt/SiO <sub>2</sub>	(0.6)
1Ir/SiO <sub>2</sub>	(0.1)

(*italic*): incorrect due to incomplete dissolution of the catalyst sample.

The metal contents of the SiO<sub>2</sub> catalysts were significantly lower than the theoretical values, because dissolution of the catalysts was incomplete. In addition, possible overlapping of Si ICP-OES signals with metal ICP-OES signals could not be ruled out. The metal content (except for Au) of the ZrO<sub>2</sub> catalysts was only slightly lower compared to the theoretical values. The Au content was substantially lower than the theoretical value (approx. 50 %) as a consequence of a higher water content of the Au precursor. The higher water content of the Au precursor led to an incorrect weighted precursor mass before the impregnation.

### 3.2.2. BET surface area

The surface areas of the noble metal catalysts supported on SiO<sub>2</sub> (137 m<sup>2</sup>/g) and ZrO<sub>2</sub> (77 m<sup>2</sup>/g) were identical to the pure supports indicating a high metal dispersion. The surface area of 0.75Pd+15Ni/ZrO<sub>2</sub> was only slightly smaller (51 m<sup>2</sup>/g) than pure ZrO<sub>2</sub> and can be explained with the high Ni amount. Supporting Ru on activated carbon resulted in some decrease of the surface area of 1Ru/C (1336 m<sup>2</sup>/g) compared to bare activated carbon (1820 m<sup>2</sup>/g).

### 3.2.3. X-ray diffraction

All XRD patterns of the calcined noble metal catalysts supported on SiO<sub>2</sub> showed only reflections of the corresponding metal oxides. After reduction only the corresponding metal reflections were observed. No Ru reflections were found for 1Ru/C, which hints to a good dispersion of Ru on activated carbon. No metal reflection could be identified on the XRD pattern when ZrO<sub>2</sub> was used as support due to the high crystallinity of ZrO<sub>2</sub>. The reflections of ZrO<sub>2</sub> overlay the noble metal reflections. Only the XRD pattern of 0.75Pd+15Ni/ZrO<sub>2</sub> showed NiO reflection for the calcined catalysts and Ni reflections after reduction.

### 3.2.4. CO chemisorption

CO chemisorption was measured for the 1Pd/ZrO<sub>2</sub> catalyst and a Pd dispersion of 45 % was obtained. The determined dispersion of 45 % is similar to that of other 1Pd/ZrO<sub>2</sub> catalysts which are reported in literature [131, 132].

## **4. Synthesis of $\gamma$ -valerolactone in batch autoclaves over Nickel catalysts**

### **4.1. Introduction**

15Ni/Al<sub>2</sub>O<sub>3</sub> catalysts were tested for the hydrogenation of levulinic acid (LA) to  $\gamma$ -valerolactone (GVL). Up to now, little attention has been paid to the solvent and the preparation method for non noble metal based catalysts. Hence, we screened different 15Ni/Al<sub>2</sub>O<sub>3</sub> catalysts prepared by wet impregnation, incipient wetness impregnation, precipitation with NaOH and flame spray pyrolysis. In addition, the influence of different solvents (monovalent alcohols and water) as well as solvent free reaction conditions were investigated.

Supported nickel catalysts were brought into focus as cheaper alternative to the expensive noble metals and Raney-nickel. Especially, solvent free conditions or water as solvent would enhance the sustainability of the GVL synthesis.

### **4.2. Results and discussion of catalytic tests**

#### **4.2.1. Conversion of LA to GVL in different solvents**

First, the influence of different solvents on the conversion of LA to GVL was investigated using 15Ni/Al<sub>2</sub>O<sub>3</sub>\_iwi and 15Ni/Al<sub>2</sub>O<sub>3</sub>\_wi as catalysts. Different monovalent alcohols (C<sub>1</sub> – C<sub>5</sub>), acetic acid, N,N-dimethylformamide (DMF) and water were used as solvents. When acetic acid was used only traces of GVL were found in the reaction mixture. In DMF a GVL yield of only 3 % was achieved at a LA conversion of 24 %. Hence, these solvents were not suitable for the hydrogenation of LA to GVL (cf. Table 6).

## Synthesis of $\gamma$ -valerolactone in batch autoclaves over Nickel catalysts

**Table 6:** LA conversion, GVL yield and GVL selectivity using different solvents and 15Ni/Al<sub>2</sub>O<sub>3</sub>-iwi catalyst (reaction conditions: p<sub>H2</sub>: 10 bar, T<sub>reaction</sub>: 150 °C, t<sub>reaction</sub>: 6 hours, n<sub>Ni</sub>/n<sub>LA</sub>: 0.03, m<sub>catalyst</sub>: 0.1 g).

Solvent	LA conversion [%]	GVL yield [%]	GVL selectivity [%]
DMF	24	3	13
acetic acid	<1	<1	100

DMF = N,N-dimethylformamide

Figure 27 shows LA conversion and GVL yield obtained with different alcohols and water as solvent.

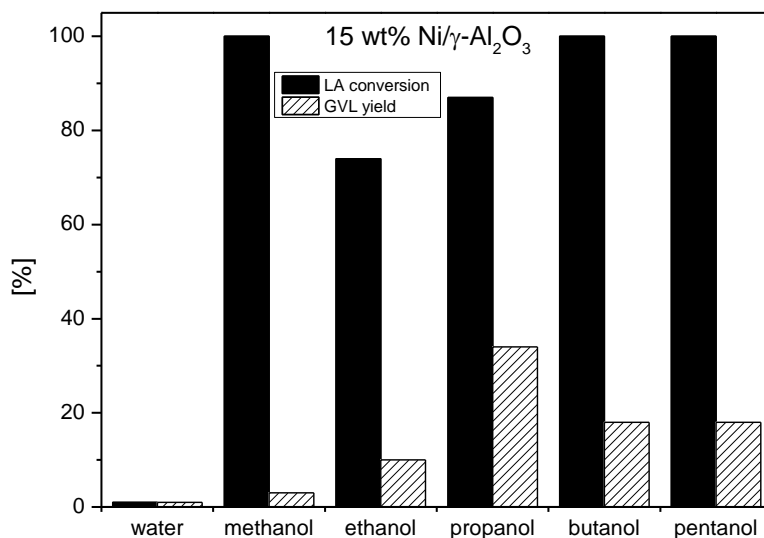


**Figure 27:** LA conversion and GVL yield using different solvents and 15Ni/Al<sub>2</sub>O<sub>3</sub>-iwi catalyst; reaction conditions: p<sub>H2</sub>: 10 bar, T<sub>reaction</sub>: 150 °C, t<sub>reaction</sub>: 6 hours, n<sub>Ni</sub>/n<sub>LA</sub>: 0.03, m<sub>catalyst</sub>: 0.1 g.

Quantitative conversion of LA was obtained using methanol, 1-butanol and 1-pentanol as solvent. The conversions of LA in ethanol and 2-propanol were 75 % and 87 %, respectively, while only 2 % of LA conversion was observed in aqueous medium. In contrast to the high LA conversion, GVL yields were comparatively low in the presence of alcohols. The highest GVL yield of 34 % was achieved with 2-propanol. 1-Butanol and 1-pentanol resulted in a GVL yield of only 19 %. With

## Synthesis of $\gamma$ -valerolactone in batch autoclaves over Nickel catalysts

methanol and ethanol the GVL yield was lower than 10 %. The GVL yield in water was 2 % which is much lower compared to the catalytic tests with alcohols. However, the selectivity was 100 % in the presence of water. A selectivity of 100 % to GVL was also found when Pd [59] Cu-ZrO<sub>2</sub> [39] and Ni-MoO<sub>x</sub> [63] catalysts were used in water, whereas Ru/C as catalyst [45] resulted in a lower GVL selectivity of 86 %. The low selectivity towards GVL in the presents of alcohols can be explained by esterification of LA to the corresponding levulinic acid esters and is in good agreement with the literature.[39] The gas chromatograms (Figure 28) indicate, that the corresponding levulinic acid esters were the main side products.

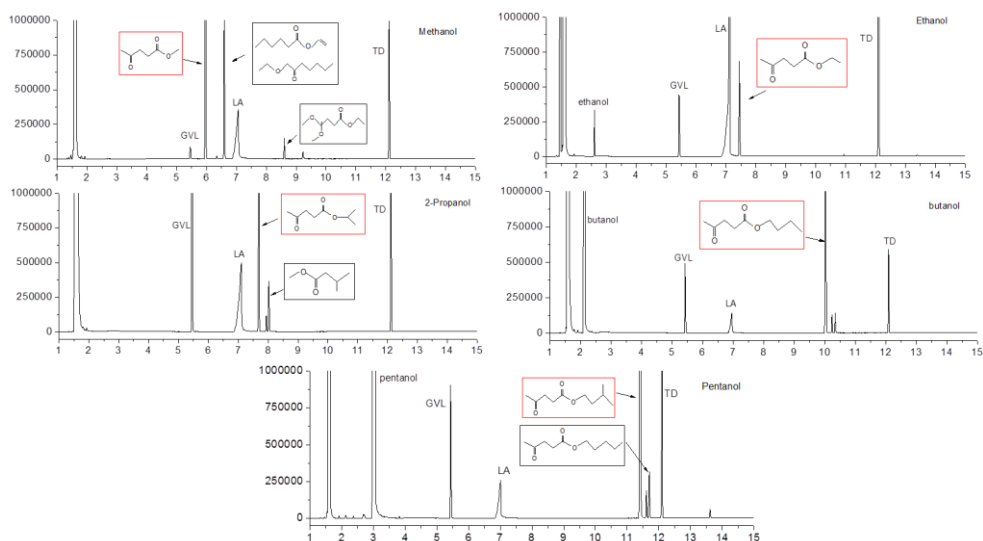


**Figure 28:** Gas chromatograms of the product mixture after conversion of LA to GVL using different solvents.

The levulinic acid ester yields were also estimated with the effective carbon number (ECN) method. The obtained yields prove that the levulinic acid esters are the main side product and the results can be found in Table 7. Palkovits *et al.* [45] also described the formation of levulinic acid esters, thus lowering the GVL yields. Note that formation of the levulinic acid ester decreased the GVL yields significantly more if Ni catalysts were used compared to noble metal based catalysts. This can be

## Synthesis of $\gamma$ -valerolactone in batch autoclaves over Nickel catalysts

ascribed to the fact that noble metal based catalysts also catalyze the GVL formation starting from levulinic acid esters and therefore in those cases alcohols are often used as solvents.[45, 133] A longer reaction time for the hydrogenation of LA to GVL in presence of an alcohol did not increase the GVL yield, not even at 100 % LA conversion. This is surprising, because Ni catalysts (and also  $\gamma$ -Al<sub>2</sub>O<sub>3</sub>) were also reported as catalyst for the hydrogenation of levulinic acid ester via the Meerwein-Ponndorf-Verley reaction.[62, 134] Note that all transfer hydrogenation reactions via MPV-reduction are carried out at ambient pressure and the hydrogen pressure used in our hydrogenation reactions may have suppressed this reaction pathway. Note that no 4-hydroxypentanoic acid was found, either by GC, nor by NMR (not shown).

**Table 7:** Levulinic acid ester yields and C-balance for catalytic tests with different alcohols as solvent.

Solvent	LA (conversion) [%]	GVL (yield) [%]	LA ester (yield) [%]	C-balance [%]	ECN
Methanol	100	2	29	36	3.5
Ethanol	74	9	40	76	4.5
Propanol	87	34	13	56	5.5
Butanol	100	19	63	92	6.5
Pentanol	100	19	77	108	7.5

Note that the effective carbon numbers (ECN) were estimated from literature [135, 136] and therefore the ECNs, LA ester yields and C-balance should be interpreted with caution. The calculation method using the ECNs was applied as described in [135, 136].

The highest selectivity towards GVL over 15Ni/Al<sub>2</sub>O<sub>3</sub> in the presence of an alcohol was obtained for 2-propanol (39 %). Additionally, a possible influence of the H<sub>2</sub> pressure was investigated using 2-propanol and water as solvents. Figure 29 shows LA conversion, GVL yields and selectivities at hydrogen pressures between 5 and 50 bar with 2-propanol as solvent.

## Synthesis of $\gamma$ -valerolactone in batch autoclaves over Nickel catalysts

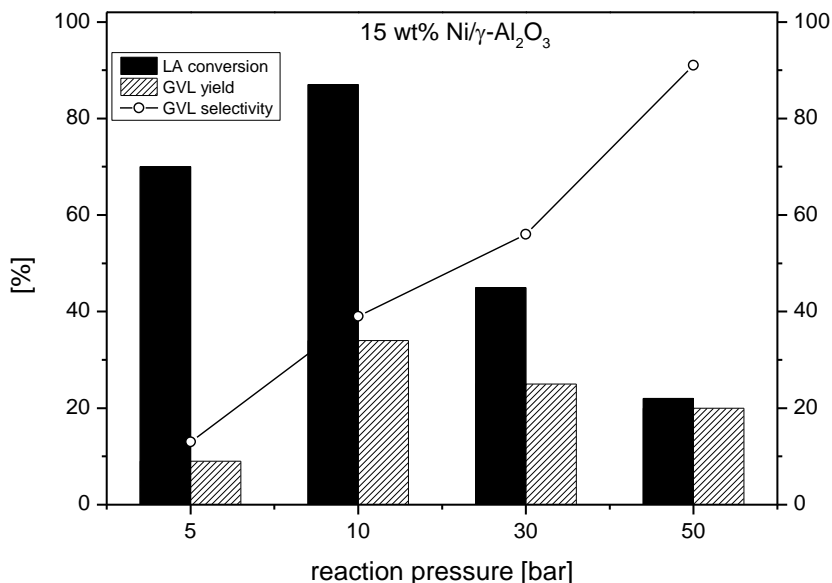


**Figure 29:** Variation of the  $H_2$  pressure with propanol as solvent and 15Ni/Al<sub>2</sub>O<sub>3</sub> catalyst; reaction conditions:  $T_{\text{reaction}}$ : 150 °C,  $t_{\text{reaction}}$ : 6 hours,  $n_{\text{Ni}}/n_{\text{LA}}$ : 0.03,  $m_{\text{catalyst}}$ : 0.1 g.

Both LA conversion and GVL yield increased from 70 % (conversion) and 9% (yield) at a  $H_2$  pressure of 5 bar to 87 % (conversion) and 34 % (yield) at a  $H_2$  pressure of 10 bar. Further increase of the pressure led to a decrease of the LA conversion as well as the GVL yield to 45 % and 25 % (at 30 bar) and to 22 % and 20 % (at 50 bar), respectively. Interestingly, the selectivity towards GVL increased over the whole pressure range. Obviously, the side reaction to the corresponding levulinic acid ester was lower at elevated hydrogen pressure.

Figure 30 depicts the LA conversion and GVL yields in water at different hydrogen pressures. Compared to the test in 2-propanol, the reactions were carried out at 200 °C with a reaction time of 4 hours and the 15Ni/Al<sub>2</sub>O<sub>3</sub> catalyst (reduced at 600 °C) was used.

## Synthesis of $\gamma$ -valerolactone in batch autoclaves over Nickel catalysts

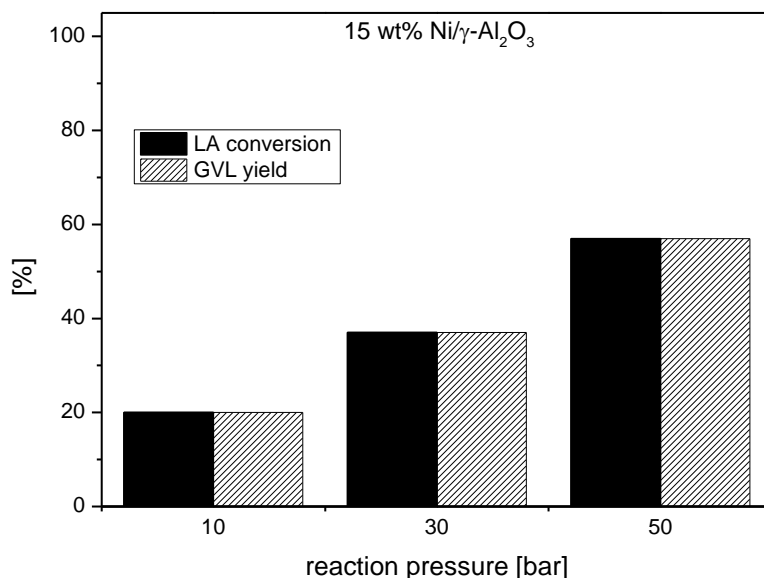


**Figure 30:** Variation of the H<sub>2</sub> pressure with water as solvent and 15Ni/Al<sub>2</sub>O<sub>3\_wi</sub> catalyst; reaction conditions: T<sub>reaction</sub>: 200 °C, t<sub>reaction</sub>: 4 hours, n<sub>Ni</sub>/n<sub>LA</sub>: 0.03, m<sub>catalyst</sub>: 0.1 g.

A higher reaction temperature of 200 °C and a reaction time of 4 hours led to an increased LA conversion (20 %) compared to 2 % LA conversion at 150 °C and a reaction time of 6 hours (cf. Figure 27). The higher reduction temperature of the Ni/Al<sub>2</sub>O<sub>3\_wi</sub> catalyst (600 °C) might also affect the catalytic activity. The GVL selectivity was 100 % at both reaction temperatures. In contrast to the tests with 2-propanol both the LA conversion and GVL yield increased with rising H<sub>2</sub> pressure when water was used as solvent. The LA conversion was increased to 37 % at 30 bar and the highest GVL yield (57 %) was obtained with a hydrogen pressure of 50 bar. With respect to the behavior in water a similar trend was found on Pd catalysts [59] and the reported LA conversions are similar to those presented in this work. Catalyst stability is a main issue, especially under hydrothermal conditions. Analysis of the 15Ni/Al<sub>2</sub>O<sub>3\_wi</sub> catalyst after the reactions in water revealed a partial phase change of the  $\gamma$ -Al<sub>2</sub>O<sub>3</sub> support to boehmite.

### 4.2.2. Solvent free conversion of LA to GVL

To prevent side reactions with alcohols to levulinic acid esters and to potentially increase the LA conversion compared to the use of water as solvent, the



## Synthesis of $\gamma$ -valerolactone in batch autoclaves over Nickel catalysts

hydrogenation of LA to GVL was additionally conducted in the absence of solvents. GVL is reported as good solvent for the LA hydrogenation to GVL.[81, 137] Therefore, the formed GVL in the solvent free hydrogenation of LA might have a positive effect on the catalytic activity. For the catalytic tests with neat LA, 10 g LA and 50 bar  $H_2$  pressure were used for all experiments. Hydrogen consumption was very high under these conditions which resulted in a significant pressure drop. Figure 31 shows LA conversion and GVL yields after a reaction time of 4 hours at different reaction temperatures. To obtain comparable data, 15Ni/Al<sub>2</sub>O<sub>3\_wi</sub> was used in all parameter optimization experiments.

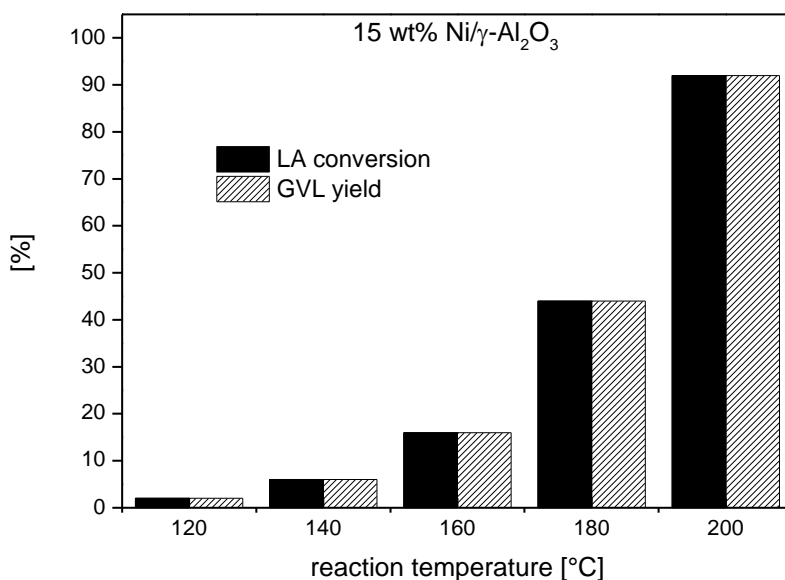


**Figure 31:** Variation of the reaction temperature in a solvent free reaction with the 15Ni/Al<sub>2</sub>O<sub>3\_wi</sub> catalyst; reaction conditions:  $t_{\text{reaction}}$ : 4 hours,  $n_{\text{Ni}}/n_{\text{LA}}$ : 0.03,  $m_{\text{catalyst}}$ : 1 g,  $p_{H_2}$ : 50 bar.

At 120 °C a LA conversion of only 2 % was obtained which increased at higher reaction temperatures. LA conversions of 44 % and 92 % were achieved at 180 °C and 200 °C, respectively. The GVL selectivity was 100 % at all temperatures.

For other transition metal catalysts or those containing Raney-nickel, reaction temperatures above 200 °C were also required to achieve LA conversions that were

## Synthesis of $\gamma$ -valerolactone in batch autoclaves over Nickel catalysts

in the same range (> 80 %) as reported for noble metal catalyst. [41, 59, 63, 66] A reaction temperature of 200 °C as reported here is still quite low for non-noble metal catalysts with a comparable catalyst/reactant ratio to obtain a LA conversion over 90 %. The influence of the catalyst amount on the LA conversion is depicted in Figure 32.

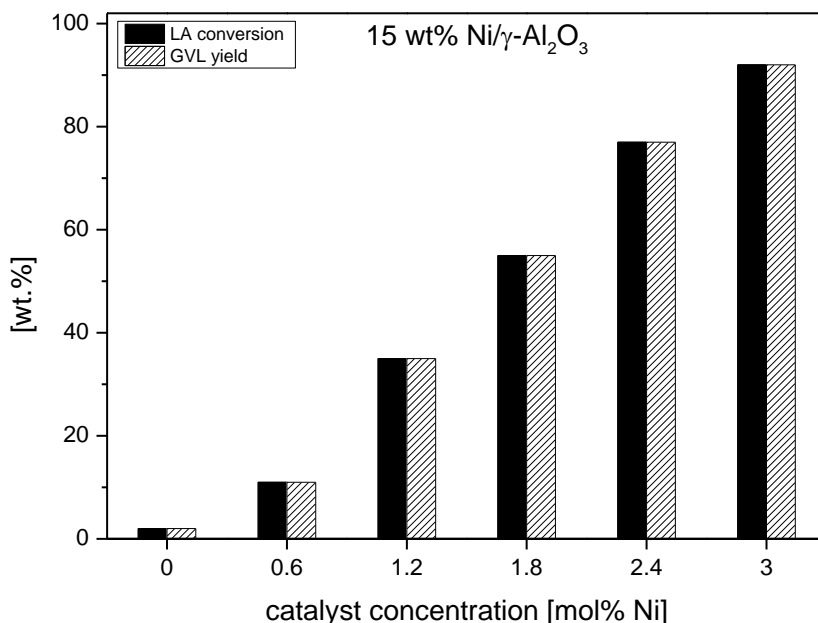


**Figure 32:** Variation of the Ni concentration in a solvent free reaction with a 15Ni/Al<sub>2</sub>O<sub>3</sub>\_wi catalyst; reaction conditions: T<sub>reaction</sub>: 200 °C, t<sub>reaction</sub>: 4 hours, p<sub>H<sub>2</sub></sub>: 50 bar, m<sub>LA</sub>: 10 g.

Without any catalyst both LA conversion and GVL yield were about 2 % (blank test). With increasing nickel content, the LA conversion and GVL yields increased from 11 % (0.6 mol % Ni) to 92 % (3.0 mol % Ni). In the literature, generally higher reaction temperatures were required to obtain comparable LA conversion and GVL yield when similar Ni concentrations (1 to 3 mol % Ni [63, 66]) were applied.

Finally, the reaction time was varied and the obtained GVL yields are depicted in Figure 33. The GVL yields increased continuously with longer reaction times. The starting point of the reaction (t = 0 h) was defined after reaching the desired

Synthesis of  $\gamma$ -valerolactone in batch autoclaves over Nickel catalysts temperature and a GVL yield of 5 % was then found. After 30 minutes and 1 hour the GVL yield increased to 20 % and 33 %, respectively, and after 4 hours 92 % GVL yield were achieved. The GVL selectivity was 100 % in all cases.

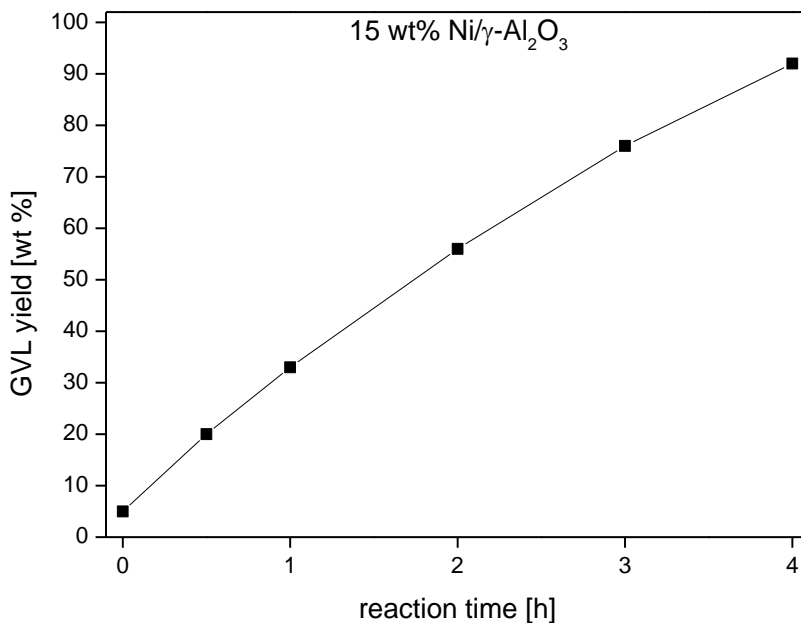


**Figure 33:** Variation of the reaction time in a solvent free reaction with a 15Ni/Al<sub>2</sub>O<sub>3</sub>\_wi catalyst; reaction conditions: T<sub>reaction</sub>: 200 °C, n<sub>Ni</sub>/n<sub>LA</sub>: 0.03, m<sub>catalyst</sub>: 1 g, p<sub>H2</sub>: 50 bar.

Although the catalyst did not show significant deactivation with increasing reaction time (Figure 33), recycling experiments revealed that the catalytic activity dropped significantly (Table 8).

## Synthesis of $\gamma$ -valerolactone in batch autoclaves over Nickel catalysts

**Table 8:** Recycling experiments with 15Ni/Al<sub>2</sub>O<sub>3</sub>\_wi; reaction conditions: Run 1: T<sub>reaction</sub>: 200 °C, n<sub>Ni</sub>/n<sub>LA</sub>: 0.03, m<sub>catalyst</sub>: 1.5 g, m<sub>LA</sub>: 15 g, p<sub>H2</sub>: 50 bar, t<sub>reaction</sub>: 4 hours, Run 2: T<sub>reaction</sub>: 200 °C, n<sub>Ni</sub>/n<sub>LA</sub>: 0.03, m<sub>catalyst</sub>: 1 g, m<sub>LA</sub>: 10 g, p<sub>H2</sub>: 50 bar, t<sub>reaction</sub>: 4 hours.

Run	Treatment after 1 <sup>st</sup> run	LA conversion [%]	GVL yield [%]
1 <sup>st</sup>	fresh reduced	68	68
2 <sup>nd</sup>	washed with acetone	4	4
2 <sup>nd</sup>	washed with acetone, calcined (550 °C), reduced (600 °C)	38	38

Washing of the catalyst with acetone prior to the second run resulted in a complete loss of activity. Washing, calcination and reduction of the catalyst prior to the second run increased the activity compared to the simple washing step. However, the LA conversion and GVL yields were still lower (38 %) compared to the 1<sup>st</sup> run with the fresh catalyst (68 %). The characterization data of the spent catalysts did not show significant changes in their structure which could explain the loss of activity. ICP-OES analysis of the catalyst after the reaction and the second run did also not show metal leaching which might explain the lower catalytic activity. Catalyst stability was studied in more detail in continuous-flow experiments in a fixed-bed reactor (cf. 5.2.2.4). This has the advantage that the catalyst is not exposed to air and / or other solvents after the reaction which may also have an influence on the reaction and activity.

The parameter screening of the hydrogenation of LA to GVL under solventless conditions using 3 mol % Ni (Ni/Al<sub>2</sub>O<sub>3</sub>\_wi) revealed that the highest LA conversion (92 %) and GVL yield (92 %) were obtained at a reaction temperature of 200 °C after 4 hours. For comparison, catalysts prepared by precipitation and flame spray pyrolysis were tested under these optimized conditions (Figure 34).

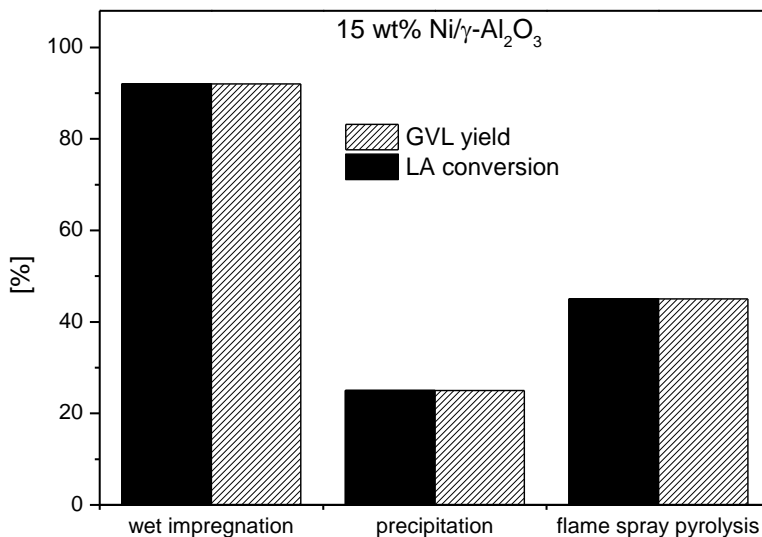


**Figure 34:** Comparison of catalysts preparation with different methods in a solvent free reaction; reaction conditions:  $T_{\text{reaction}}$ : 200 °C,  $t_{\text{reaction}}$ : 4 hours,  $n_{\text{Ni}}/n_{\text{LA}}$ : 0.03,  $m_{\text{catalyst}}$ : 1 g,  $p_{\text{H}_2}$ : 50 bar.

LA conversion and GVL yield were much lower with 15Ni/Al<sub>2</sub>O<sub>3</sub>\_p (25 %) and 15Ni/Al<sub>2</sub>O<sub>3</sub>\_fsp (45 %) compared to 15Ni/Al<sub>2</sub>O<sub>3</sub>\_wi (92 %). The lower catalytic activity of 15Ni/Al<sub>2</sub>O<sub>3</sub>\_fsp may be caused by a partial incorporation of Ni into the framework structure of the support, as evidenced by TPR and XAS (cf. section 3.1.2.2). The significantly lower LA conversion of Ni/Al<sub>2</sub>O<sub>3</sub>\_p compared to the Ni/Al<sub>2</sub>O<sub>3</sub>\_wi catalyst is surprising since it featured similar textural properties (see section 3.1). Especially the XANES analysis showed strong similarities. However, the surface area of the precipitated catalyst was slightly higher and EXAFS analysis showed significantly higher backscattering contributions for the precipitated catalyst (Figure 15). Thus also the data fitting resulted in smaller Ni-Ni coordination numbers for 15Ni/Al<sub>2</sub>O<sub>3</sub>\_wi than 15Ni/Al<sub>2</sub>O<sub>3</sub>\_p. Hence, the difference in the catalytic activity may result from Ni particles with smaller size (< 5 nm) which are invisible by XRD but detected by EXAFS. In contrast to 15Ni/Al<sub>2</sub>O<sub>3</sub>\_wi, Ni particles were not detected by XRD for 15Ni/Al<sub>2</sub>O<sub>3</sub>\_fsp. Since probably only 50 % of the Ni sites are available in the flame-made catalyst, as LC-analysis gave nearly a 1:1 ratio of Ni particles and Ni in spinel-like structures, it is remarkable that the FSP catalyst was significantly more active than the catalyst prepared by precipitation reaching almost half of the conversion of

## Synthesis of $\gamma$ -valerolactone in batch autoclaves over Nickel catalysts

the wet impregnated catalyst. The TOF and initial rates of the catalysts prepared by wet impregnation and precipitation were calculated at about 20 % LA conversion (Table 9). The Ni dispersion of these catalysts was calculated with the Ni particle size estimated using the Scherrer equation (15Ni/Al<sub>2</sub>O<sub>3</sub>\_wi (37 nm, D = 0.027 %) and 15Ni/Al<sub>2</sub>O<sub>3</sub>\_p (65 nm, D = 0.016 %)).

**Table 9:** TOF and initial rates for catalysts 15Ni/Al<sub>2</sub>O<sub>3</sub>\_wi and 15Ni/Al<sub>2</sub>O<sub>3</sub>\_p at iso-conversion.

Catalyst	LA conversion [%]	t <sub>reaction</sub> [min]	TOF [h <sup>-1</sup> ]	Initial rate [mmol/min]
15Ni/Al <sub>2</sub> O <sub>3</sub> _wi	20	30	491	0.57
15Ni/Al <sub>2</sub> O <sub>3</sub> _p	25	240	129	0.09

The TOF and initial rate of the WI catalyst are about four times and six times higher compared to those of the corresponding precipitated catalyst. This confirms that smaller Ni particles are obviously more active for the LA hydrogenation to GVL. Note that the TOF was based on the XRD-particle size, which may disregard smaller particles. The highest TON for nickel catalysts reported in literature is 4950 at 250 °C after 24 h.[63] Hence, the 15Ni/Al<sub>2</sub>O<sub>3</sub>\_wi catalyst investigated in this work shows interesting turnover rates at similar LA conversions and GVL yields (> 90 %) but at lower reaction temperatures.

This indicates that Ni particles with a size < 5nm led to an increased catalytic activity and thus to much higher LA conversions and GVL yields. The higher activity of smaller Ni particles was also reported for other hydrogenation reactions, e.g., for the hydrogenation of benzene with supported Ni catalysts, as described by Molina and Poncelet [138].

### 4.3. Conclusion

Four different 15 wt.% Ni/ $\gamma$ -Al<sub>2</sub>O<sub>3</sub> catalysts were prepared using different preparation methods that lead to different textural and catalytic properties in the hydrogenation

Synthesis of  $\gamma$ -valerolactone in batch autoclaves over Nickel catalysts of LA to GVL. In the first part of the study solvents and reactions conditions were varied to optimize the hydrogenation of LA to GVL over Ni based catalysts. For this purpose a standard IWI catalyst was used. Among all alcohols, 2-propanol gave the highest GVL yield (34 % at 87 % LA conversion). Due to side reactions to the corresponding levulinic acid esters, GVL selectivity was relatively low (40 %) at a H<sub>2</sub> pressure of 10 bar. By increasing the hydrogen pressure both LA conversion and GVL yield decreased, but the GVL selectivity increased (91 % at 50 bar). The GVL selectivity with water as solvent was 100 % but higher reaction temperatures were required. Under optimized conditions (reaction temperature: 200 °C, reaction time 4 h, p<sub>H2</sub> = 50 bar, n<sub>Ni</sub> : n<sub>LA</sub> = 0.3, reduction temperature 600 °C) GVL yields of 57 % were observed. This could be further improved by optimizing the catalyst preparation and the solvent.

The most attractive results of this work concern the hydrogenation of LA to GVL under solvent free conditions. In all cases, the GVL selectivity was 100 % and the best GVL yields (92 %) were obtained at 200 °C with 3 mol % Ni after 4 h. The catalytic activity of the GVL synthesis depended strongly on the reaction temperature. Among the different catalysts 15Ni/Al<sub>2</sub>O<sub>3</sub>\_wi showed the highest catalytic activity (GVL yield 92 %) of all applied catalysts with high reaction rates. The comparison catalysts prepared by flame spray pyrolysis and by precipitation indicated that the difference in the catalytic activity could probably be explained by differences in Ni particle size and partial incorporation of Ni into the lattice. Combined TPR, XRD and EXAFS analysis revealed that the flame made catalyst featured a fraction of Ni which was incorporated into the lattice of the support, whereas the catalyst prepared by wet impregnation contained both small particles (active, as evidenced by EXAFS and TEM, invisible for XRD) and larger particles (reduced at low temperatures in TPR and detected by XRD). Hence, small Ni particles seem to be beneficial for the hydrogenation of LA to GVL and can be considered an interesting alternative to the commonly studied and reported noble metal catalysts. However, further improvement is necessary. A continuous flow experiment would be beneficial and is described in the next section.

## **5. Continuous synthesis of $\gamma$ -valerolactone in a trickle-bed reactor**

### **5.1. Introduction**

As an alternative to noble metal catalyzed hydrogenation of levulinic acid (LA) and starting from the interesting results reported in the previous section on the discontinuous batch process for  $\gamma$ -valerolactone (GVL), various Ni based catalysts were tested in the continuous liquid phase hydrogenation of LA to GVL in a trickle-bed reactor using water as solvent. A decreased reaction temperature compared to vapour phase hydrogenation as described in literature (cf. section 1.3.1.3) in combination with cheap catalysts and a green solvent (water) would in principle provide an economic and environmental friendly process for GVL synthesis from LA.

Hence, we investigated the liquid phase hydrogenation of LA to GVL in a trickle-bed reactor over supported Ni nanoparticles using water as solvent. For this purpose, a set of Ni based catalysts was synthesised according to different preparation methods; these catalysts were characterized, in particular with respect to Ni particle size. Then they were screened in batch and continuous mode in order to gain insight on the effect of particle size. For comparison, a commercial Ru/C reference catalyst is included. Finally, the reason for some deactivation was identified and discussed.

### **5.2. Results and discussion of catalytic tests**

#### **5.2.1. Catalyst screening in batch autoclaves**

In the first series of experiments, the catalysts were tested in batch autoclaves at  $T = 200\text{ }^{\circ}\text{C}$  and  $P_{\text{H}_2} = 50\text{ bar}$  using water as a solvent. The results are displayed in Figure 35. Also a commercial 5Ru/C (Sigma-Aldrich) catalyst was tested as a benchmark. All catalysts were reduced and stored in air at room temperature prior



to reaction and therefore were re-oxidized to some extent as uncovered by XANES (cf. 3.1.2.2).

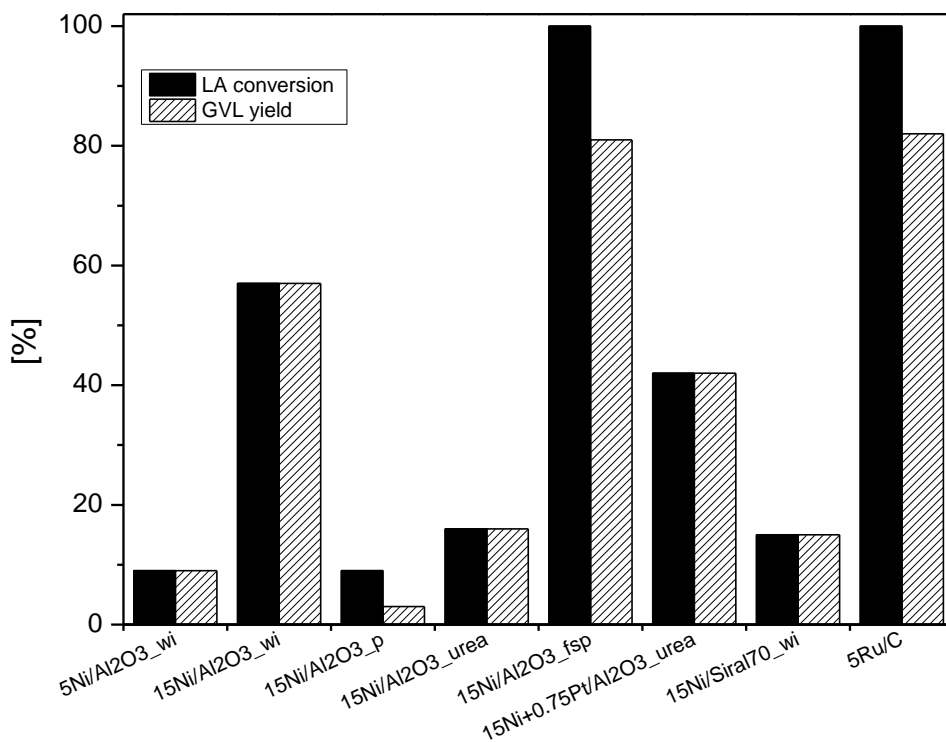


**Figure 35:**  $X_{LA}$  (closed bars) and  $Y_{GVL}$  (crossed bars) after hydrogenation of levulinic acid in a batch autoclave over various catalysts. Reaction conditions:  $T = 200\text{ }^{\circ}\text{C}$ ,  $P_{H_2} = 50\text{ bar}$ ,  $TOS = 4\text{ h}$ ,  $n_{Ni}/n_{LA} = 0.03$ ,  $m_{cat} = 0.1\text{ g}$  ( $0.01\text{ g}$  for 5Ru/C).

Most of the Ni catalysts converted LA 100 % selective to GVL. The only exceptions are 15Ni/Al<sub>2</sub>O<sub>3</sub>\_fsp that completely converted LA to GVL at a maximum yield of 82 % and some 4-hydroxyvaleric acid by-product (evidenced by NMR spectroscopy) and, whereas 15Ni/Al<sub>2</sub>O<sub>3</sub>\_p was able to convert 9% of LA with a GVL yield of just 3 %. Hence, 15Ni/Al<sub>2</sub>O<sub>3</sub>\_wi converted 57% of LA with 100% selectivity to GVL. Unfortunately, LA conversions of 15Ni/Al<sub>2</sub>O<sub>3</sub>\_urea and 15Ni+0.75Pt/Al<sub>2</sub>O<sub>3</sub>\_urea were much lower, despite fully selective. This result might have been a consequence of the fact that these catalysts contain the smallest Ni particle sizes, which are much more prone to oxidation than large ones.[125] Note that catalyst oxidation occurred prior to the reaction. Therefore, an effect of average Ni particle size and catalyst

## Continuous synthesis of $\gamma$ -valerolactone in a trickle-bed reactor

performance in these batch experiments cannot be deduced. Further, things are more complicated as the conversion of LA over 5Ni/Al<sub>2</sub>O<sub>3</sub>\_wi is lower than 15Ni/Al<sub>2</sub>O<sub>3</sub>\_urea while their average Ni particle size is rather similar. Still, we tested 15Ni/Siral70\_wi in order to study the effect of support acidity. Siral70 contains Brønsted acid sites and is therefore more acidic than  $\gamma$ -Al<sub>2</sub>O<sub>3</sub>. This might possibly open up other reaction pathways via  $\alpha$ - or  $\beta$ -angelica lactone as intermediate products.[37] Unfortunately, 15Ni/Siral70\_wi did not perform better than 15Ni/Al<sub>2</sub>O<sub>3</sub>\_urea or 15Ni+0.75Pt/Al<sub>2</sub>O<sub>3</sub>\_urea that have a comparable average Ni particle size. Thus, we did not pursue the performance of this catalyst further up in this study. On the other hand, Ru/C performed ( $X_{LA} = 100\%$ ,  $Y_{GVL} = 82\%$  with 4-hydroxyvaleric acid as by-product) very similar to 15Ni/Al<sub>2</sub>O<sub>3</sub>\_fsp. This result is similar to data on Ru-based catalysts in aqueous solution.[45]

### 5.2.2. Catalytic tests in a trickle-bed reactor

#### 5.2.2.1. Influence of reaction temperature and H<sub>2</sub> pressure

After catalyst screening in batch mode the catalysts were tested in continuous mode by performing LA hydrogenation in a trickle-bed reactor. This implies also that the catalyst was reduced *in situ* prior to the experiment (cf. section 2.3.3). In a first step, the T and P<sub>H<sub>2</sub></sub> were optimized in continuous mode over 15Ni/Al<sub>2</sub>O<sub>3</sub>\_wi as it showed a good performance in the batch mode test. The effect of temperature on  $X_{LA}$  and  $Y_{GVL}$  for this catalyst is depicted in Figure 36.

With increasing reaction temperatures, both  $X_{LA}$  (up to 100 %) and  $Y_{GVL}$  increased (up to 89 % at 220 °C and 1 h on stream (TOS)). In this temperature range, for at least 2 h on stream  $X_{LA}$  and  $Y_{GVL}$  were rather constant. Beyond that they gradually decreased. At 180 °C,  $S_{GVL}$  was nearly 100 % whereas at 200 °C and 220 °C they were rather similar (between 80 % and 90 %) and constant for at least 4 h on stream.  $S_{GVL}$  were lower at higher T because of the formation of some 4-hydroxyvaleric acid. From 180 °C to 200 °C,  $X_{LA}$  and  $Y_{GVL}$  almost doubled, whereas a further temperature raise to 220 °C only led to 15% increases in  $X_{LA}$  and  $Y_{GVL}$ . A strong increase in catalytic performance at >180 °C has also been reported earlier by our group for LA hydrogenation in batch mode using various Ni-based catalysts (cf. 4.2.2).

## Continuous synthesis of $\gamma$ -valerolactone in a trickle-bed reactor

For other non-noble metal catalysts, it required temperatures higher than 200 °C in order to reach similar levels of  $X_{LA}$  as noble metal catalysts (>80 %). [63, 66] For further reactions, we used  $T = 200$  °C (at 220 °C,  $X_{LA}$  is 100 % for 2 h on stream, this is obviously too high to elucidate the impact of other reaction parameters).

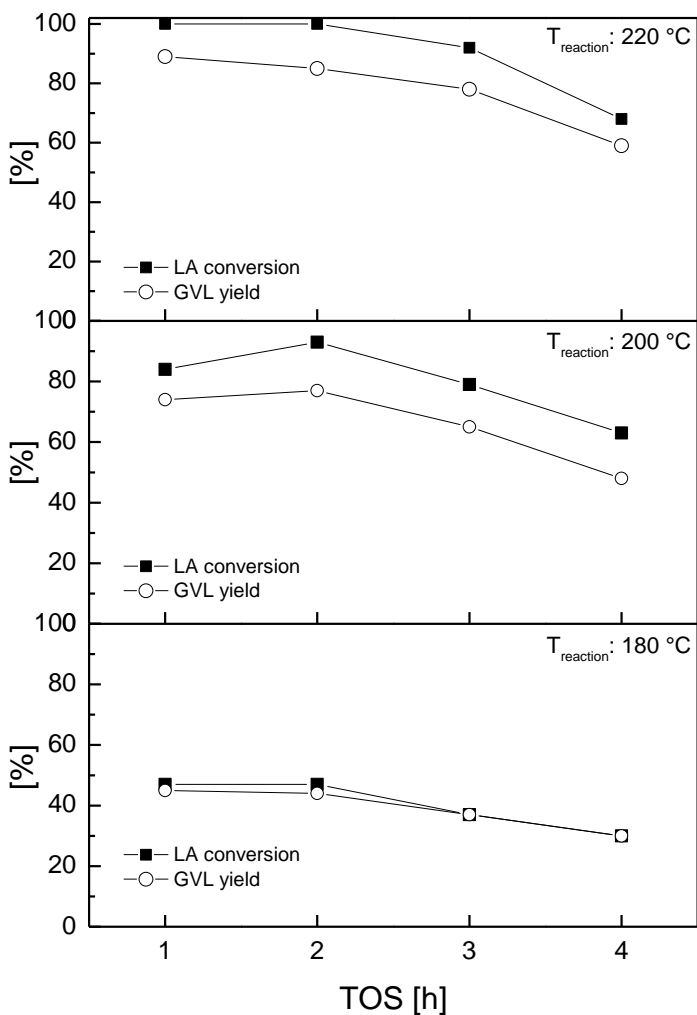


**Figure 36:**  $X_{LA}$  (closed symbols) and  $Y_{GVL}$  (open symbols) during continuous hydrogenation of levulinic acid in a trickle bed reactor over 15Ni/Al<sub>2</sub>O<sub>3</sub>\_wi at different reaction temperatures (T). Reaction conditions:  $P_{H_2} = 50$  bar,  $WHSV = 1$  h<sup>-1</sup>,  $m_{cat} = 0.5$  g,  $\dot{m}_{LA/H_2O} = 5$  g/h,  $\dot{V}_{H_2} = 50$  mL/h.

## Continuous synthesis of $\gamma$ -valerolactone in a trickle-bed reactor

In the next step,  $P_{H_2}$  was varied over 15Ni/Al<sub>2</sub>O<sub>3</sub>\_wi. At 50 bar (Figure 36),  $X_{LA}$  was similar to 30 bar for 3 h on stream and are depicted in Figure 37. The catalyst deactivated to some extent after 4 h on stream. This effect is strongly influenced by  $P_{H_2}$  *i.e.* at higher  $P_{H_2}$  the catalyst performance is more stable.  $S_{GVL}$  is also higher at higher  $P_{H_2}$ . (Figure 37). Overall, we established that  $T = 200\text{ }^\circ\text{C}$  and  $P_{H_2} = 50\text{ bar}$  are the optimal reaction conditions for further reactions.

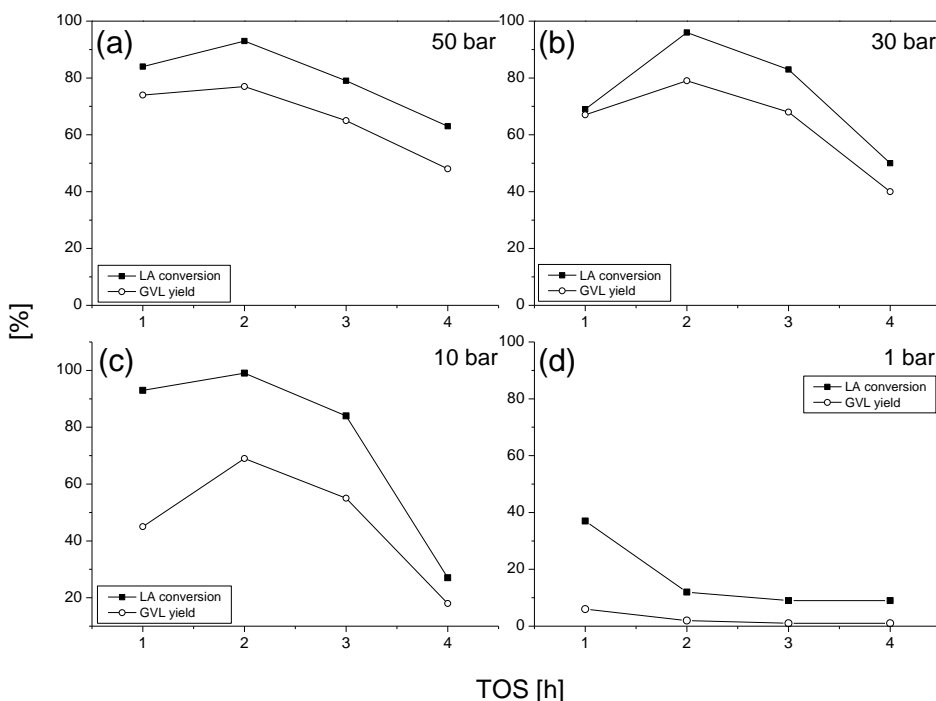


**Figure 37:** LA conversion and GVL yield using different reaction pressures and the 15Ni/Al<sub>2</sub>O<sub>3</sub>\_wi catalyst; reaction conditions: RT: 200 °C, WHSV: 1 h<sup>-1</sup>,  $m_{\text{catalyst}}$ : 0.1 g,  $\dot{m}_{LA/H_2O}$ : 5 g/h,  $\dot{V}_{H_2}$ : 50 mL/h.

### 5.2.2.2. Effect of the preparation route and Ni particle size

$X_{LA}$  and  $Y_{GVL}$  over the set of Ni catalysts (and 5Ru/C for reference) as a function of time on stream are shown in Figure 38.

Continuous synthesis of  $\gamma$ -valerolactone in a trickle-bed reactor

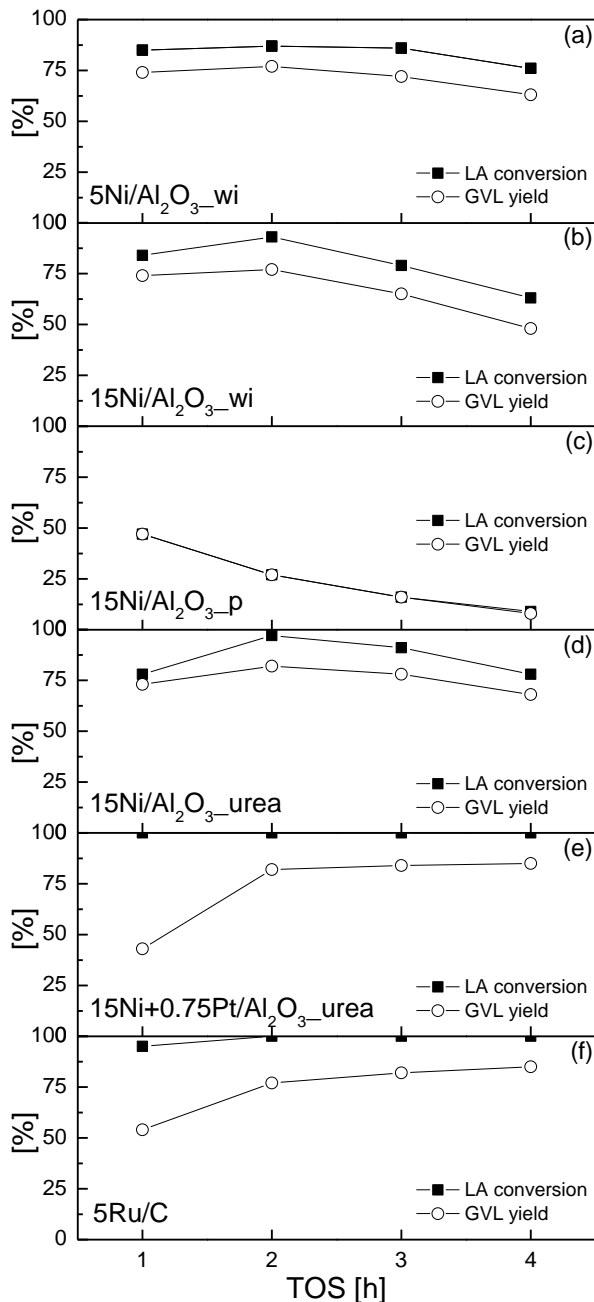


**Figure 38:**  $X_{LA}$  (closed symbols) and  $Y_{GVL}$  (open symbols) during continuous hydrogenation of levulinic acid in a trickle bed reactor over Ni catalysts and Ru/C Reaction conditions:  $T = 200\text{ }^{\circ}\text{C}$ ,  $P_{H_2} = 50\text{ bar}$ ,  $WHSV = 1\text{ h}^{-1}$ ,  $m_{cat} = 0.5\text{ g}$  ( $0.05\text{ g } 5\text{Ru/C}$ ),  $\dot{m}_{LA/H_2O} = 5\text{ g/h}$ ,  $\dot{V}_{H_2} = 50\text{ mL/h}$ .

## Continuous synthesis of $\gamma$ -valerolactone in a trickle-bed reactor

The 15Ni/Al<sub>2</sub>O<sub>3</sub>\_p catalyst with the largest Ni particles (65 nm) showed the lowest X<sub>LA</sub> and Y<sub>GVL</sub> (Figure 38c). However, this catalyst exhibited the highest GVL selectivity (100 %) of all investigated catalysts. A strong deactivation was found: The LA conversion decreased steadily from 47 % after 1 h to 9 % after 4 h TOS. The catalysts 5Ni/Al<sub>2</sub>O<sub>3</sub>\_wi, 15Ni/Al<sub>2</sub>O<sub>3</sub>\_wi and 15Ni/Al<sub>2</sub>O<sub>3</sub>\_urea showed a similar catalytic activity for LA hydrogenation (Figure 38 a, b, d). GVL selectivities were always between 80 and 95 % and the corresponding LA conversions and GVL yields were constant (or slightly increasing) during the first 2 h TOS. After 3 h and 4 h TOS both the LA conversion and GVL yields decreased. The drop in catalytic activity was more pronounced for 15Ni/Al<sub>2</sub>O<sub>3</sub>\_wi (featuring the largest Ni particle size of those 3 catalysts) compared to 5Ni/Al<sub>2</sub>O<sub>3</sub>\_wi and 15Ni/Al<sub>2</sub>O<sub>3</sub>\_urea. The Ni particle size of 5Ni/Al<sub>2</sub>O<sub>3</sub>\_wi and 15Ni/Al<sub>2</sub>O<sub>3</sub>\_urea are similar, but 5Ni/Al<sub>2</sub>O<sub>3</sub>\_wi features only small Ni particles (cf. Table 3 and Figure 25). The same amount of catalyst was used for LA hydrogenation. The catalytic activity was nearly stable over 4 h TOS using 5Ni/Al<sub>2</sub>O<sub>3</sub>\_wi. Strikingly, the 15Ni+0.75Pt/Al<sub>2</sub>O<sub>3</sub>\_urea catalyst showed the highest LA conversion (100 % for 4 h TOS) of all catalysts and, probably due to the high performance, no catalyst deactivation. Note that this catalyst exhibited the highest dispersion as derived by chemisorption (Table 3). The GVL yields were low (43 %) after 1 h TOS but increased to the level of catalysts 5Ni/Al<sub>2</sub>O<sub>3</sub>\_wi, 15Ni/Al<sub>2</sub>O<sub>3</sub>\_wi and 15Ni/Al<sub>2</sub>O<sub>3</sub>\_urea after 2 h TOS and stayed constant afterwards. According to these results smaller Ni particles showed higher catalytic activity compared to larger ones. 15Ni/Al<sub>2</sub>O<sub>3</sub>\_wi and 15Ni/Al<sub>2</sub>O<sub>3</sub>\_urea showed good catalytic performance compared to 15Ni/Al<sub>2</sub>O<sub>3</sub>\_p because low-coordinated Ni atoms are more reactive [138]. A reason for that might be the stronger interaction of small Ni particles with the support, resulting in a different particle shape (more flat) compared to large particles. However, they were less active than 15Ni+0.75Pt/Al<sub>2</sub>O<sub>3</sub>\_urea which showed both a smaller particle size and a higher dispersion according to chemisorption results (cf. Table 3). Catalysts 15Ni/Al<sub>2</sub>O<sub>3</sub>\_p, 15Ni/Al<sub>2</sub>O<sub>3</sub>\_wi and 15Ni/Al<sub>2</sub>O<sub>3</sub>\_urea are deactivating in a pronounced manner during the reaction. As leaching was hardly observed by elemental analysis after reaction, both sintering or phase transformations may account for this observation [139]. For example, the Ni content of 15Ni/Al<sub>2</sub>O<sub>3</sub> catalysts after 4 h on stream in continuous mode was just ~1 wt.% lower in comparison to their fresh counterparts. This amount of leached Ni does not

Continuous synthesis of  $\gamma$ -valerolactone in a trickle-bed reactor reflect the origin of deactivation. Although no leaching was detected for 5Ni/Al<sub>2</sub>O<sub>3</sub>\_wi. This is possibly related to the stronger interaction between small Ni particles (cf. Table 3 and Figure 36) with  $\gamma$ -Al<sub>2</sub>O<sub>3</sub> (Figure 11). Sintering was considered by recording XRD patterns of the catalysts after the continuous reaction in the trickle bed reactor (Figure 12(ii)). Significant changes are visible at comparison to the freshly reduced catalysts. Reflections corresponding to  $\gamma$ -Al<sub>2</sub>O<sub>3</sub>, boehmite (red line) and Ni are clearly visible (Figure 12 (ii)). The intensities of latter increased for several catalysts. This indicates that larger Ni particles are present, hence sintering occurred (Table 3). It could be triggered by the transformation of  $\gamma$ -Al<sub>2</sub>O<sub>3</sub> to boehmite, thus weakening the metal-support interactions under hydrothermal conditions as already described by Li et al. [139].

Interestingly, no growth of Ni particles was found for 5Ni/Al<sub>2</sub>O<sub>3</sub>\_wi. This might be due to the absence of larger Ni particles in line with conclusions by Simonsen et al. [140] on Pt/Al<sub>2</sub>O<sub>3</sub> catalysts. Nevertheless, 5Ni/Al<sub>2</sub>O<sub>3</sub>\_wi also starts slightly deactivating after 3 h TOS.

### 5.2.2.3. Comparison of Ni/Al<sub>2</sub>O<sub>3</sub> and Ru/C catalysts

The overall performance *i.e.*  $X_{LA}$  and  $Y_{GVL}$  of 5Ru/C was similar to 15Ni+0.75Pt/Al<sub>2</sub>O<sub>3</sub>\_urea. It should be mentioned though that the space velocity is ten times higher for the former catalyst. The LA conversion using Ru/C was similar to that reported for Ru/C in 1,4-dioxane [44] and the GVL yields (up to 80 %) were only slightly lower. Compared to the results with Ru/C in H<sub>2</sub>O [67] higher LA conversion and GVL yields were achieved, but our study also focussed on a higher reaction temperature. In conclusion, the results obtained with the Ru/C reference catalyst are in good agreement with literature.

Considering the low Ni content of 5Ni/Al<sub>2</sub>O<sub>3</sub>\_wi, this catalyst showed the best performance among the undoped Ni based catalysts for the hydrogenation of LA. In order to determine the reaction rate in terms of turnover frequency (TOF), the weight hour space velocity (WHSV) was increased using 5Ni/Al<sub>2</sub>O<sub>3</sub>\_wi and the TOF was calculated at low LA conversions (WHSV: 1.75 and 2.5 h<sup>-1</sup>). After 1 h on stream  $X_{LA} = 24\%$  at  $WHSV = 2.5\text{ h}^{-1}$  and  $X_{LA} = 42\%$  at  $WHSV = 1.75\text{ h}^{-1}$  which corresponds to TOFs of  $1.9 \cdot 10^{-3}\text{ s}^{-1}$  and  $2.4 \cdot 10^{-3}\text{ s}^{-1}$ , respectively (overall, TOF  $\sim 2 \cdot 10^{-3}\text{ s}^{-1}$ ).

## Continuous synthesis of $\gamma$ -valerolactone in a trickle-bed reactor

Surprisingly, the catalyst deactivation was much more pronounced at higher WHSV (see section 5.2.2.4). A comparison of this TOF value for 5Ni/Al<sub>2</sub>O<sub>3</sub>\_wi to literature revealed that the performance is pretty similar to the reported  $5 \cdot 10^{-3} \text{ s}^{-1}$  for Cu/Al<sub>2</sub>O<sub>3</sub> [68] (265 °C), but a magnitude lower than the  $5 \cdot 10^{-2}$  (lower Ni loading) and  $15 \cdot 10^{-2} \text{ s}^{-1}$  (at 250 °C) for various Ni/H-ZSM-5 [65].

### 5.2.2.4. Catalyst stability

To study the catalyst stability, we measured 5Ni/Al<sub>2</sub>O<sub>3</sub>\_wi, for longer time on stream *i.e.* 10 h (Figure 39) instead of 4 h (Figure 38).

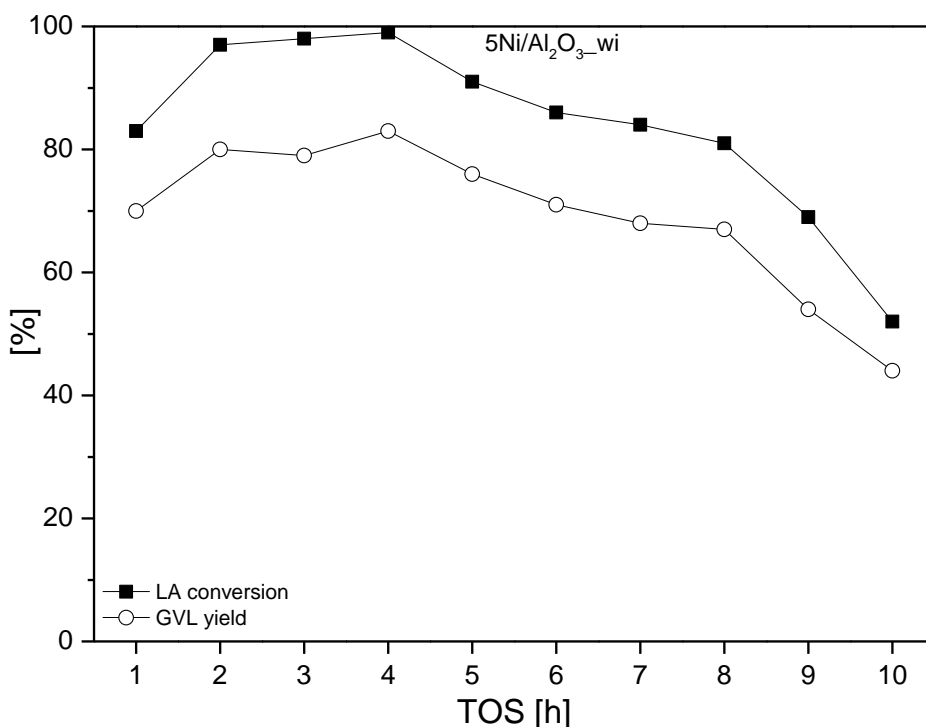


**Figure 39:**  $X_{LA}$  (closed symbols) and  $Y_{GVL}$  (open symbols) during continuous hydrogenation of levulinic acid in a trickle bed reactor over 5Ni/Al<sub>2</sub>O<sub>3</sub>\_wi. Reaction conditions:  $T = 200 \text{ }^\circ\text{C}$ ,  $P_{H_2} = 50 \text{ bar}$ ,  $WHSV = 1 \text{ h}^{-1}$ ,  $m_{cat} = 0.5 \text{ g}$ ,  $\dot{n}_{LA/H_2O} = 5 \text{ g/h}$ ,  $\dot{V}_{H_2} = 50 \text{ mL/h}$ .

$X_{LA}$  and  $Y_{GVL}$  are somewhat higher in comparison to the former test for 4 h on stream (Figure 8a). Between 5 h and 8 h TOS, LA conversions and GVL yields decreased



Continuous synthesis of  $\gamma$ -valerolactone in a trickle-bed reactor steadily to the level obtained after 1 h TOS (80 % LA conversion and 70 % GVL yield). After 9 h and 10 h TOS the deactivation of the catalyst was significantly stronger. A comparison with literature showed a similar deactivation to Cu/Al<sub>2</sub>O<sub>3</sub> [68] and Ni/H-ZSM-5 [65] catalysts with longer TOS. Interestingly the deactivation occurred also faster at high space velocities. For example, at a WHSV of 2.5 h<sup>-1</sup>, a LA conversion of 24 % after 1 h TOS was obtained, which decreased to 20 % after 2 h TOS, to 9 % after 3 h TOS and to 6 % after 4 h TOS. Also the GVL selectivities decreased steadily, from 83 % after 1 h TOS to 16 % after 4 h TOS. According to XRD data the 5Ni/Al<sub>2</sub>O<sub>3</sub>\_wi (Table 3) may have deactivated due to Ni sintering fostered by a phase change of the  $\gamma$ -Al<sub>2</sub>O<sub>3</sub> support towards boehmite (Figure 12). This change in alumina phase by water has also been observed by others.[139] In addition, the formation of boehmite could deactivate the catalyst by covering the Ni particles or Ni could be re-oxidized to some extent by water. The formation of boehmite might have triggered catalyst deactivation by some sintering and/or Ni oxidation by water (cf. section 5.2.1).

### 5.3. Conclusion

Various Ni/Al<sub>2</sub>O<sub>3</sub> catalysts with different average Ni particle sizes in the range of 6 – 65 nm were found to be differently active and stable in the continuous liquid phase hydrogenation of LA to GVL in a trickle-bed reactor. The average Ni particle size had to be determined by various techniques (XRD, STEM and chemisorption) to reveal their predominant size. For this purpose Ni particles supported on Al<sub>2</sub>O<sub>3</sub> were prepared by using a variety of synthesis methods e.g. wet impregnation, precipitation and flame spray pyrolysis. Catalysts containing smaller Ni particles (<10 nm) were most active in the continuous hydrogenation of LA carried out in water. At optimized reaction conditions (T = 200 °C and P<sub>H<sub>2</sub></sub> = 50 bar) 6 nm Ni particles (5Ni/Al<sub>2</sub>O<sub>3</sub>\_wi) performed best in terms of activity and stability. Some catalyst deactivation occurred but was traced back to sintering of Ni particles and / or due to some transformation of  $\gamma$ -Al<sub>2</sub>O<sub>3</sub> to boehmite under hydrothermal conditions, which may also promote the sintering (weaker metal support interaction).

In addition, re-oxidation of Ni particles may have a strong impact as the screening studies in batch reactors revealed significantly worse catalytic activity for those

Continuous synthesis of  $\gamma$ -valerolactone in a trickle-bed reactor

catalysts that exhibit small Ni size and were exposed to air after reduction. The studies demonstrated, that Ni based catalysts are an attractive alternative to noble metal catalysts and should be further improved in future.

## 6. Formic acid as hydrogen donor for the $\gamma$ -valerolactone synthesis

### 6.1. Introduction

The hydrogen used in the hydrogenation of levulinic acid (LA) to  $\gamma$ -valerolactone (GVL) is often fossil generated. Thus the sustainability of  $\gamma$ -valerolactone production would increase if formic acid (FA) is used as hydrogen source, especially because it is a by-product in the formation of levulinic acid from 5-hydroxymethylfurfural (Scheme 4, section 1.3.2). For this approach, FA can be decomposed giving  $H_2$  and  $CO_2$  (conventional hydrogenation using *in situ* formed  $H_2$ ) or LA could be hydrogenated via transfer hydrogenation.

For this purpose, different noble and non-noble metal catalysts were synthesized and tested in the FA decomposition. The most suitable decomposition catalysts were subsequently studied for the LA hydrogenation using external hydrogen and finally examined in the cascade reaction of LA and FA towards GVL.

Only a few different catalytic systems (Au, Ru, Cu, Ag-Ni) have been reported in literature (section 1.3.2), hence, this study focused on the identification of new metals for the LA hydrogenation with FA as hydrogen donor.

### 6.2. Results and discussion of catalytic tests

#### 6.2.1. Formic acid decomposition

##### 6.2.1.1. Blank tests

In a first series of experiments, the FA decomposition was investigated without any catalyst at different reaction temperatures. The corresponding FA conversions and  $H_2/CO_2$  selectivities are shown in Table 10. The FA conversion was calculated using the ideal gas equation and pressure difference (tests with FA, purity >95 %).

## Formic acid as hydrogen donor for the $\gamma$ -valerolactone synthesis

**Table 10:** FA conversions and H<sub>2</sub>/CO<sub>2</sub> selectivities at different reaction temperatures without catalyst; reaction conditions:  $t_{\text{reaction}} = 4 \text{ h}$ ;  $m_{\text{FA}} = 10 \text{ g}$ , N<sub>2</sub> atmosphere.

Temperature [°C]	FA conversion [%]	H <sub>2</sub> /CO <sub>2</sub> selectivity [%]
100	0	0
120	1	0
140	5	< 0.5
160	13	< 0.5
180	26	1

A higher reaction temperature led to an increased FA conversion (26 % at 180 °C), but the H<sub>2</sub>/CO<sub>2</sub> selectivity was only 1 %. Afterwards, the FA decomposition in a solution of FA in water (1/10, 1/20, 1/50) was investigated (Table 11). The dilution of FA with water should shift the equilibrium of the FA decomposition and increase the H<sub>2</sub>/CO<sub>2</sub> selectivity.[84] The FA conversion in the experiments using water as solvent was determined by HPLC.

**Table 11:** FA conversions and H<sub>2</sub>/CO<sub>2</sub> selectivities at different dilutions without catalyst; reaction conditions:  $t_{\text{reaction}} = 4 \text{ h}$ ;  $T_{\text{reaction}} = 180 \text{ °C}$ ;  $m_{\text{H}_2\text{O}} = 10 \text{ g}$ .

FA/H <sub>2</sub> O ratio	FA conversion [%]	H <sub>2</sub> /CO <sub>2</sub> selectivity [%]
pure FA	26	1
1/10	< 1	61
1/20	< 1	81
1/50	< 1	92

The H<sub>2</sub>/CO<sub>2</sub> selectivity increased significantly by diluting FA with water (up to 92 %, FA/H<sub>2</sub>O ratio = 1/50) but simultaneously the FA conversion decreased below 1 %. Increasing the reaction temperature to 200 °C resulted in a much higher FA

Formic acid as hydrogen donor for the  $\gamma$ -valerolactone synthesis conversion of 15% (FA/H<sub>2</sub>O ratio = 1/10) with a similar H<sub>2</sub>/CO<sub>2</sub> selectivity. A FA/H<sub>2</sub>O ratio of 1/10 was used for all catalyst screening experiments.

### 6.2.1.2. Catalyst screening

Different non-noble metal catalysts (5Ni/SiO<sub>2</sub>, 5Ni/ZrO<sub>2</sub>, 5Cu/SiO<sub>2</sub>, 5Co/SiO<sub>2</sub>, Fe/SiO<sub>2</sub>) were tested in the decomposition of FA ( $t_{\text{reaction}} = 4$  h,  $m_{\text{FA}} = 10$  g,  $m_{\text{Catalyst}} = 0.1$  g, N<sub>2</sub> atmosphere). No catalytic activity was observed in terms of the decomposition of FA. Moreover, the catalysts prepared by wet impregnation were not stable under the applied reaction conditions and the metals leached completely from the solid support under the given conditions. Therefore, non-noble metal based catalysts were not further investigated.

A set of different noble metal catalysts supported on SiO<sub>2</sub> (1Ru/SiO<sub>2</sub>, 1Pd/SiO<sub>2</sub>, 1Au/SiO<sub>2</sub>, Pt/SiO<sub>2</sub>, Ir/SiO<sub>2</sub>) was tested in the FA decomposition at 180 °C for 4 h (Figure 40).

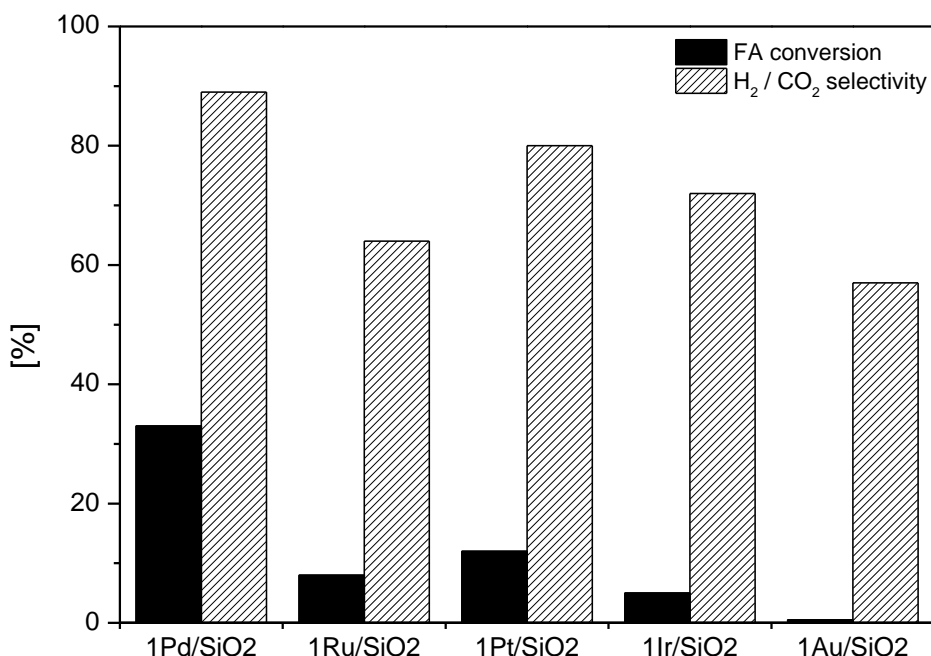


**Figure 40:** FA conversions and H<sub>2</sub> / CO<sub>2</sub> selectivities of different noble metals supported on SiO<sub>2</sub>; reaction conditions:  $T_{\text{reaction}}: 180$  °C;  $t_{\text{reaction}}: 4$  h;  $m_{\text{catalyst}}: 0.1$  g; FA/H<sub>2</sub>O: 1/10; V: 10 mL.

Formic acid as hydrogen donor for the  $\gamma$ -valerolactone synthesis

The highest FA conversion (33 %) and  $H_2/CO_2$  selectivity was obtained using 1Pd/SiO<sub>2</sub>. The FA conversion and  $H_2/CO_2$  selectivity using 1Au/SiO<sub>2</sub> was similar to the blank test, which indicates no catalytic activity of Au supported on SiO<sub>2</sub>. This fact is surprising, because Au was reported as an excellent catalyst for the hydrogenation of LA to GVL with FA as hydrogen donor.[72] However, the catalytic activity of Au is strongly dependent on the Au particle size and the wet impregnation method used for the synthesis of 1Au/SiO<sub>2</sub> may result in too large and therefore inactive Au particles. The catalyst stability was investigated by analyzing the metal content of the product mixture using ICP-OES. No noble metals could be detected with ICP-OES, which proved the stability of all noble metal catalysts under the applied conditions. Noble metal leaching was not observed in all further catalytic tests.

Whereas here, the Ru based catalysts showed a good performance on FA decomposition, in literature, Ru based catalysts were reported to give the highest catalytic activity for the LA hydrogenation to GVL [45] Also Pd based catalysts are reported in literature as active catalysts for the GVL synthesis.[59] Therefore, the focus was laid on Ru and Pd as active species for further optimization of FA decompositions catalysts with respect to support and reaction conditions.

### **6.2.1.3. Influence of catalyst support, reaction temperature and catalyst amount**

ZrO<sub>2</sub> was reported as a stable support in the presence of FA and is thus often used for the GVL production using FA as hydrogen donor.[59, 72, 75, 79] High GVL yields were also obtained using Ru supported on activated carbon.[73] Hence, 1Pd/SiO<sub>2</sub>, 1Pd/ZrO<sub>2</sub>, 1Ru/SiO<sub>2</sub>, 1Ru/ZrO<sub>2</sub>, 1Ru/C and a commercial 5Ru/C catalyst were tested in the FA decomposition reaction. In addition, 0.75Pd+15Ni/ZrO<sub>2</sub> was investigated as an interesting bifunctional catalyst for GVL synthesis considering that Pd could decompose FA and prevent Ni leaching while Ni could hydrogenate LA to GVL using the *in situ* produced hydrogen. Pd might prevent Ni leaching by decomposing FA prior to the start of leaching. In contrast to the previous experiments, the reaction temperature was increased to 200 °C and the results of the catalytic tests are depicted in Table 12.

**Table 12:** FA conversion and TON using different catalyst supports; reaction conditions:  $T_{\text{reaction}}$ : 200 °C;  $t_{\text{reaction}}$ : 4 h;  $m_{\text{catalyst}}$ : 0.1 g; FA/H<sub>2</sub>O: 1/10; V: 10 mL.

Catalyst	FA conversion [%]	TON
1Pd/SiO <sub>2</sub>	68	1576
1Pd/ZrO <sub>2</sub>	100	2312
1Ru/SiO <sub>2</sub>	30	668
1Ru/ZrO <sub>2</sub>	33	1012
1Ru/C	86	1840
5Ru/C	37	732
0.75Pd+15Ni/ZrO <sub>2</sub>	88	72

The turnover number (TON) was calculated using the theoretical metal content of the catalysts in mol.

A higher FA conversion was obtained with ZrO<sub>2</sub> as catalyst support compared to SiO<sub>2</sub> and the positive catalytic effect was more pronounced for Pd. 1Ru/C showed the highest FA conversion of all Ru based catalysts (86 %). Surprisingly, the obtained FA conversion and TON of the commercial 5Ru/C catalyst decreased more than 50 % compared to 1Ru/C. Especially the high FA conversion (100 %) and high TON (2312) of 1Pd/ZrO<sub>2</sub> are promising in terms of further application in LA hydrogenation. The H<sub>2</sub>/CO<sub>2</sub> selectivity was > 90 % for all Pd based catalysts (95 %, 1Pd/ZrO<sub>2</sub>) and > 80 % for all Ru based catalysts. Also 0.75Pd+15Ni/ZrO<sub>2</sub> showed a high FA conversion (88 %), but Ni was not stabilized by Pd and leached under reaction conditions.

The 1Pd/ZrO<sub>2</sub> catalyst showed a high activity for the dehydrogenation of FA (high FA conversion and H<sub>2</sub>/CO<sub>2</sub> selectivity). Therefore, 1Pd/ZrO<sub>2</sub> was tested using different reaction temperatures, reaction times and catalyst amounts.

FA conversion at different reaction temperatures using 1Pd/ZrO<sub>2</sub> is shown in Figure 41.

## Formic acid as hydrogen donor for the $\gamma$ -valerolactone synthesis

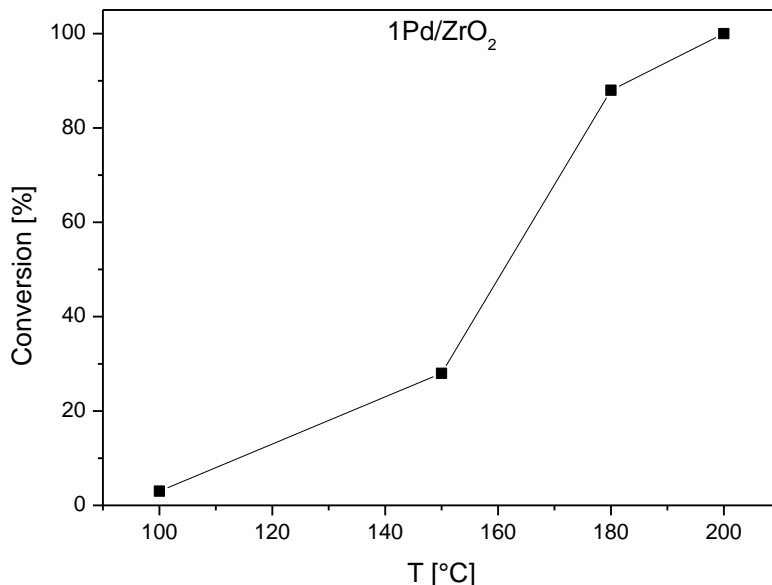


**Figure 41:** FA conversion using 1Pd/ZrO<sub>2</sub> at different reaction temperatures; reaction conditions:  $t_{\text{reaction}}$ : 4 h;  $m_{\text{catalyst}}$ : 0.1 g; FA/H<sub>2</sub>O: 1/10; V: 10 mL.

At 100 °C, a FA conversion of only 3 % was obtained which increased further at higher temperatures. FA conversions of 28 % and 88 % were achieved at 150 °C and 180 °C, respectively and full FA conversion was reached at 200 °C.

The ratio of FA/ $m_{\text{catalyst}}$  was increased by decreasing the amount of catalyst to 0.05 g and 0.01 g, respectively (Table 13).

**Table 13:** FA conversions and TOFs using different catalyst amounts; reaction conditions:  $t_{\text{reaction}}$ : 4 h;  $T_{\text{reaction}}$ : 200 °C; FA/H<sub>2</sub>O: 1/10; V: 10 mL.

Catalyst mass [g]	FA conversion [%]	TOF [sec <sup>-1</sup> ]
0.1	100	0.16 <sup>a</sup>
0.05	99	0.7 <sup>a</sup>
0.01	77	2.5

a = smaller TOF due to full conversion

Still 99 % FA were converted after 4 h at 200 °C which corresponds to a TOF of 0.7 sec<sup>-1</sup> using 0.05 g 1Pd/ZrO<sub>2</sub>. The FA conversion decreased to 77 % if only 0.1 g



Formic acid as hydrogen donor for the  $\gamma$ -valerolactone synthesis 1Pd/ZrO<sub>2</sub> were used but the TOF increased to 2.5 sec<sup>-1</sup>. The obtained TOF is one of the highest compared to reports in literature for the decomposition of FA. However, one should take into account that the reaction temperature of 200 °C is quite high for the FA decomposition and higher than temperatures that are applied in literature studies usually. The high temperature was chosen to get information on FA decomposition at temperatures similar to that used for LA hydrogenation.

#### 6.2.1.4. Catalyst stability

The reaction time was varied and the FA conversion, TON and FA decomposition rate are depicted in Table 14.

**Table 14:** Influence of reaction temperature on FA conversion, TON, FA decomposition rate using 1Pd/ZrO<sub>2</sub>; reaction conditions: T<sub>reaction</sub>: 200 °C; ; m<sub>catalyst</sub>: 0.1 g; FA/H<sub>2</sub>O: 1/10; V: 10 mL.

Reaction time [h]	FA conversion [%]	TON	Decomposition rate [min <sup>-1</sup> ]
1	88	2027	0.37
2	94	2182	0.2
3	100	2312	0.14
4	100	2312	0.11

After 1 h, a FA conversion of already 88 % was obtained, which increased to 94 % after 2 h. Full FA conversion was achieved after 3 and 4 h, respectively. The TON increased until 100 % FA conversion was reached (2312) but the rate of decomposition decreased steadily due to the high conversion after 1 h (FA decomposition rate = 0.37 min<sup>-1</sup>). The small increase in FA conversion after 2 h hints at a deactivation of 1Pd/ZrO<sub>2</sub> with longer reaction time. Therefore, recycling experiments using 1Pd/ZrO<sub>2</sub> were performed and no loss in catalytic activity was observed after four runs (100 % FA decomposition after 4 h at 200 °C). To further prove the catalyst stability, tests with less than 100 % FA conversion are required. Note that the catalyst was washed with acetone and dried at air prior to the next catalytic run.

## **6.2.2. Hydrogenation of levulinic acid to $\gamma$ -valerolactone using formic acid as hydrogen donor**

### **6.2.2.1. Screening of noble metal catalysts using external hydrogen**

The most active catalysts for the FA decomposition (1Pd/ZrO<sub>2</sub>, 0.75Pd+15Ni/ZrO<sub>2</sub>, 1Ru/C) were tested in the hydrogenation of LA to GVL in water using external hydrogen. Optimized reaction conditions were used (cf. section 4.2.1) and the resulting LA conversion and GVL selectivity can be found in Figure 42. The obtained LA conversion and GVL yields with 1Pd+15Ni/ZrO<sub>2</sub> were higher compared to the results obtained with 15Ni/Al<sub>2</sub>O<sub>3</sub>\_wi (57 %, cf. Figure 30). This indicates a positive effect of both, Pd doping and the use of ZrO<sub>2</sub> as support, on the catalytic activity in LA hydrogenation. The LA conversion (73 %) and GVL yields (47 %) achieved with 1Ru/C were lower than the values reported in literature [49] (comparison of reaction rate) and the GVL selectivity, especially in water, was surprisingly low. With respect to further hydrogenation of LA using FA, LA conversions and GVL yields obtained using 1Pd/ZrO<sub>2</sub> were too low. Yan *et al.* [59] reported an increased LA conversion using a higher Pd loading (5Pd/ZrO<sub>2</sub>). Furthermore, bimetallic Au-Pd catalysts [55] and Au supported on Pd [141] were reported as active catalysts for the LA hydrogenation using molecular hydrogen. Therefore 5Pd/ZrO<sub>2</sub> and 2.5Pd+2.5Au/ZrO<sub>2</sub>, were prepared according to Edwards *et al.* [142] and tested in the LA hydrogenation. Almost quantitative LA conversion to GVL was obtained with both catalysts (Figure 42). Note that a hydrogen pressure of 50 bar corresponds to 12 equivalents of hydrogen and should therefore promote the GVL synthesis. Moreover, a higher amount of Pd supported on ZrO<sub>2</sub> as well as a bi-metallic Au-Pd system should have a positive effect on FA decomposition.

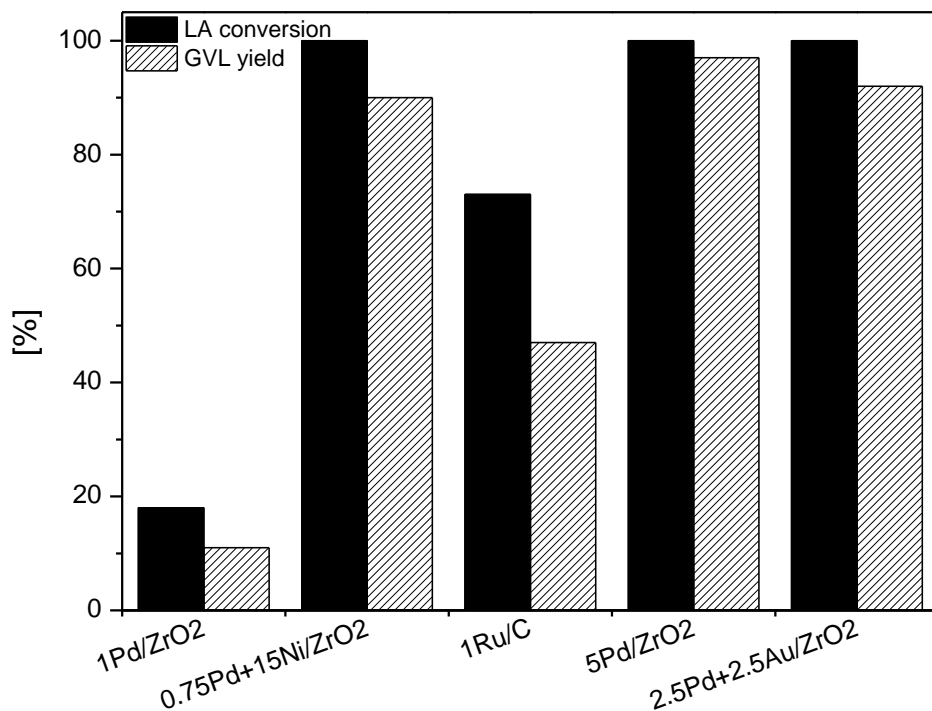


**Figure 42:** LA conversions and GVL yields during the LA hydrogenation using external hydrogen and FA decomposition catalysts; reaction conditions:  $T_{\text{reaction}}$ : 200 °C;  $t_{\text{reaction}}$ : 4 h;  $m_{\text{catalyst}}$ : 0.1 g; LA/H<sub>2</sub>O: 1/10; V: 10 mL; 50 bar H<sub>2</sub>.

#### 6.2.2.2. Catalytic tests using formic acid as H<sub>2</sub> donor

All noble metal catalysts screened in the LA hydrogenation using molecular hydrogen were subsequently tested in the LA hydrogenation to GVL using FA as hydrogen donor. In addition a reference 1mol% Au/ZrO<sub>2</sub> catalyst prepared according to Du et al. [72] was synthesized and tested. The results of the catalytic tests using one equivalent FA are depicted in Table 15. In a blank test, 22 % FA conversion, 2 % LA conversion and 2 % GVL yield were obtained. All other catalysts (except the 1mol% Au/ZrO<sub>2</sub> reference catalyst) showed a GVL yield similar to the blank test or even no GVL yield. However, an almost quantitative FA conversion (always > 87 %) was achieved in all catalytic tests.

## Formic acid as hydrogen donor for the $\gamma$ -valerolactone synthesis

**Table 15:** FA conversion, LA conversion, GVL yields and amount of metal using different noble metal catalysts for the LA hydrogenation with FA as hydrogen donor; reaction conditions:  $T_{\text{reaction}}$ : 200 °C;  $t_{\text{reaction}}$ : 4 h;  $m_{\text{catalyst}}$ : 0.1 g; LA/H<sub>2</sub>O: 1/10; V: 10 mL; 1 equivalent FA.

Catalyst	FA conversion [%]	LA conversion [%]	GVL yields [%]	$n_{\text{metal}}$ [mmol]
no (blank test)	22	2	2	0
1Pd/ZrO <sub>2</sub>	100	1	1	0.0094
1Pd+15Ni/ZrO <sub>2</sub>	99	1.5	1.5	/
1Ru/C	87	2	2	0.01
1Pd/ZrO <sub>2</sub> + 1Ru/C	97	1	1	0,01
5PdZrO <sub>2</sub>	100	0	0	0.047
2.5Pd+2.5Au/ZrO <sub>2</sub>	100	0	0	0.024(Pd) 0.013(Au)
1 mol % Au/ZrO <sub>2</sub> <sup>a</sup>	100	46	46	0.005
1 mol % Au/ZrO <sub>2</sub> <sup>a,b</sup>	100	53	53	0.018

a = reference catalyst prepared according to Du *et al.* [72]; b = reaction conditions according to Du *et al.* [72];  $T_{\text{reaction}}$ : 150 °C;  $t_{\text{reaction}}$ : 6 h;  $m_{\text{catalyst}}$ : 0.3417 g; LA/H<sub>2</sub>O: 1/20; V: 40 mL; 1 equivalent FA.

One reason for the inactivity of the catalysts during the test using formic acid as hydrogen donor may be poisoning of Pd or Ru by CO. CO may block the active sites of the metal particles and as a consequence, they are not accessible for LA anymore. CO is formed by dehydration of FA during the decomposition (5 – 10 %). Another explanation for the low LA conversions and GVL yields might be the low H<sub>2</sub> pressure during the reaction. The decomposition of FA resulted in an elevated pressure of only 3 – 5 bar compared to the screening experiments at 50 bar H<sub>2</sub>.

The following reaction parameters were varied to obtain an enhanced catalytic activity towards GVL using 1Pd/ZrO<sub>2</sub>. 1Pd/ZrO<sub>2</sub> was used for optimization reactions towards GVL since most of the FA decomposition experiments were carried out using this catalyst. The dilution of LA and FA in water was increased (1/20 and 1/100) to enhance the H<sub>2</sub>/CO<sub>2</sub> selectivity of the FA decomposition (cf. Table 11) but no GVL

Formic acid as hydrogen donor for the  $\gamma$ -valerolactone synthesis was obtained after 4 h of reaction time. Furthermore, NaOH was added to the reaction mixture, since bases lead to a higher  $H_2/CO_2$  selectivity and faster FA decomposition.[143] No GVL was obtained in the product mixture. The amount of FA was increased from one equivalent to five equivalents to increase the  $H_2$  pressure during the reaction. Again, no GVL was obtained.

In order to obtain an enhanced catalytic activity towards GVL, several reaction parameters were varied with  $2.5Pd+2.5Au/ZrO_2$  as catalyst. The reactor was pressurized with 5 bar  $H_2$  prior to the reaction. These conditions usually lead to 10 % LA conversion to GVL. However, no GVL was produced, which indicates poisoning of Pd by FA or its decomposition products like CO. Afterwards, the reactor was pressurized with 50 bar  $H_2$  prior to the reaction whereby 100 % LA conversion and 95 % GVL yield were obtained without FA insight the reactor. A GVL yield of 4 % was obtained, which also indicates poisoning of Pd by CO or other formic acid derivatives. To further gain insight into the catalyst poisoning, the reactor was charged with 5 %  $CO/H_2$  (50 bar) in addition to LA in water (1/10). After 4 h at 200 °C, no GVL was obtained.

Besides the FA decomposition mechanism proposed for Au catalysts, two other possible mechanisms that might cause the formation of CO-species on the metal surfaces are shown in Scheme 6 (cf. 1.3.2.1). The catalyst poisoning by CO indicates, that Pd or Ru based catalysts applied in this work may decompose FA over either one of these mechanisms. The desorption of CO is very slow at the applied reaction temperature (200 °C) due to the high CO binding energies of those metals and may cause catalyst poisoning. Note that the binding energy of CO is strongly dependent on the metal particle size, the catalyst support and the reaction temperature. Therefore, a higher reaction temperature (volcano plot, section 1.3.2.1), the formation of metal alloys, changes in metal particle size as well as different catalyst supports could decrease the binding energies of CO on Pd and/or Ru and increase the catalytic activity.

Moreover, spectroscopic methods like attenuated total reflection infrared spectroscopy (ATR-IR) (cf. section 7) should be executed to confirm the anticipated catalyst poisoning by CO. In addition, a better understanding of the FA

Formic acid as hydrogen donor for the  $\gamma$ -valerolactone synthesis

decomposition mechanism over different metals could be provided using *in operando* spectroscopy.

Using 1 mol % Au/ZrO<sub>2</sub> as reference catalyst, LA conversions and GVL yields of 46 % and 53 % (reaction conditions in accordance to Du *et al.* [72]), respectively were achieved. This demonstrates that the reaction system used in this study is suitable for the GVL synthesis with FA as hydrogen donor and some catalyst poisoning is responsible for a lack of catalytic activity regarding GVL production.

### 6.3. Conclusion

Various noble metal catalysts were tested in the FA decomposition and hydrogenation of LA to GVL using FA as hydrogen donor. The selectivity of the FA decomposition (FA dehydrogenation) towards H<sub>2</sub>/CO<sub>2</sub> was increased by a higher dilution of FA with water. Noble metals supported on ZrO<sub>2</sub> increased both, the conversion of FA and the H<sub>2</sub>/CO<sub>2</sub> selectivity compared to SiO<sub>2</sub> as catalyst support. The most active catalyst for the FA decomposition was 1Pd/ZrO<sub>2</sub> with 100 % FA conversion and 95 % H<sub>2</sub>/CO<sub>2</sub> selectivity under optimized reaction conditions (200 °C, 4 h). No deactivation of 1Pd/ZrO<sub>2</sub> was observed after four re-uses.

5Pd/ZrO<sub>2</sub> and 2.5Pd+2.5Au/ZrO<sub>2</sub> were the most active FA decomposition catalysts in the LA hydrogenation using external hydrogen (100 % LA conversion and > 90 % GVL yields). Unfortunately, no catalytic activity towards GVL was observed when FA was used as hydrogen donor. Small amounts of CO, which were formed during the FA decomposition, were identified as possible catalyst poison. Tests with 5 % CO/H<sub>2</sub> as external hydrogen source revealed, that CO indeed blocks the catalytic sites and thus deactivates the catalysts.

## 7. Final remarks and outlook

This thesis shows that Ni catalysts represent an attractive alternative to expensive noble metal based systems for the synthesis of GVL using molecular hydrogen. In the case of non-noble metal catalysts stability is one of the most important issues. Deactivation of the Ni catalysts was observed after tests both in batch autoclaves and in the trickle-bed reactor. A decrease in activity during recycling experiments of LA hydrogenation using batch autoclaves may originate from re-oxidation of the Ni particles (4.2.2), whereas catalyst deactivation in the trickle-bed reactor probably results from sintering of Ni due to a phase change of  $\gamma$ -Al<sub>2</sub>O<sub>3</sub> to boehmite (5.2.2.4). Due to the required high reduction temperatures of Ni, it was difficult to avoid its re-oxidation, since *in situ* reduction was not possible with the batch autoclaves used in this work. Therefore, continuous LA hydrogenation is advantageous compared to GVL synthesis in batch autoclaves, also with regard to industrial applications. The phase change of the  $\gamma$ -Al<sub>2</sub>O<sub>3</sub> support to boehmite was observed in all experiments using water as solvent. Obviation of this phase change was only possible by changing the solvent. Alternatively, other supports could be used or the temperature may be decreased to a minimum (< 100 °C). However, a high reaction temperature was required to obtain reasonable LA conversions and GVL yields over Ni catalysts and water as green solvent was considered important for the sustainability of the GVL process. The catalytic tests in batch autoclaves using 15Ni+0.75Pd/ZrO<sub>2</sub> in the LA hydrogenation (cf. section 6.2.2.1) showed higher LA conversion and GVL yields compared to 15Ni/Al<sub>2</sub>O<sub>3</sub>\_wi (cf. section 4.2.1). Hence, the ZrO<sub>2</sub> based Ni catalyst should be applied in future studies on the continuous LA hydrogenation to GVL, since it may not deactivate with longer TOS.

The catalytic activity of the investigated Ni catalysts was strongly dependent on the Ni particle size and smaller particles featured an increased activity in LA hydrogenation. The increased number of active sites is responsible for this increase

## Final remarks and outlook

in catalytic activity. Also the shape of the smaller Ni particles could be different compared to the large Ni particles which may be beneficial for LA hydrogenation.

The correlation between catalytic activity and Ni particle size was similar for the GVL process in batch autoclaves and in the continuous trickle-bed reactor. Slow precipitation of Nickel on  $\gamma$ -Al<sub>2</sub>O<sub>3</sub> using urea resulted in smaller Ni particles compared to precipitation with NaOH or wet impregnation of Ni. In addition, a lower Ni content as well as doping with Pt further increased the Ni dispersion. Therefore, a 5 wt.% Ni/ $\gamma$ -Al<sub>2</sub>O<sub>3</sub> catalysts doped with 0.5 wt.% Pt prepared with urea precipitation might be of interest for future studies of LA hydrogenation in continuous mode. Smaller Ni particles should be formed thus increasing the catalytic activity. In case of the FSP catalyst incorporation of Ni into the Al<sub>2</sub>O<sub>3</sub> support including spinel formation was observed resulting in an incomplete reduction at 600 °C. Noble metal doping could enhance the reducibility of the flame derived catalysts and furthermore increase the metal dispersion. [144] Therefore, noble metal doped Ni based catalysts prepared by FSP are also interesting for the LA hydrogenation. In addition, the preparation method for 15Ni+0.75Pd/ZrO<sub>2</sub> which should be stable in the continuous liquid phase hydrogenation of LA in water (no phase change of the support), could be improved using precipitation with urea or flame spray pyrolysis.

During LA hydrogenation using different monovalent alcohols as solvent formation of LA esters was observed. The GVL selectivity was increased by increasing the hydrogen pressure leading to a decrease in LA conversion. However, high GVL selectivities and LA conversion can be obtained via transfer hydrogenation in alcohols over Meerwein-Ponndorf-Verley reduction under mild reaction conditions. The sustainability of the GVL process could be improved at lower reaction temperatures and ambient pressure. The unexpectedly low LA conversion and formation of LA esters as side products using alcohols as solvent might be due to the large Ni particle size in the 15Ni/Al<sub>2</sub>O<sub>3</sub>\_iwi catalyst and the high hydrogen pressure (cf. section 4.2.1). ZrO<sub>2</sub> is reported as an active catalyst for the Meerwein-Ponndorf-Verley reduction and impregnation with Ni could further enhance the catalytic activity. Precipitation of Ni using urea should decrease the Ni particle size, thus being beneficial for the activity with respect to previous characterization results compared to 15Ni/Al<sub>2</sub>O<sub>3</sub>\_iwi. Hence, 15Ni+0.75Pt/ZrO<sub>2</sub> would be a promising



catalyst for the hydrogenation of LA to GVL using iso-propanol as hydrogen donor under mild reaction conditions.

In the LA hydrogenation using FA as hydrogen donor poisoning of Pd with CO (5Pd/ZrO<sub>2</sub> and 2.5Pd+2.5Au/ZrO<sub>2</sub>) was observed resulting in insignificant catalytic activity. Further investigation of Pd poisoning by catalytic experiments and spectroscopic methods is required. Furthermore, the synthesis of 2.5Pd+2.5Au/ZrO<sub>2</sub> can still be optimized (e.g. precipitation method). The 1mol% Au/ZrO<sub>2</sub> reference catalyst was prepared using precipitation with ammonia and the Au particles might be decreased (in size) compared to Au particles on catalysts prepared by wet impregnation. Smaller Au particles showed high catalytic activity in LA hydrogenation using FA as hydrogen source. A 2.5Pd+2.5Au/ZrO<sub>2</sub> alloy catalyst with small Au (and Pd) particles should have a higher activity and Au could prevent Pd poisoning by a different decomposition mechanism (cf. Scheme 6). This was not the case for 2.5Pd+2.5Au/ZrO<sub>2</sub> prepared by wet impregnation.

Attenuated total reflection infrared spectroscopy (ATR-IR) might be a useful method to study the CO poisoning of Pd based catalysts *in situ*. Powdered catalyst layers of several micrometers thickness can be deposited on the reflecting crystal, allowing the identification and characterization of surface intermediates during LA hydrogenation using FA as hydrogen donor. Such a system should be suitable to detect absorbed CO species at the active sites, thus confirming the assumed CO poisoning of the catalyst. An ATR-IR cell, which can be operated at high reaction temperature and pressure, was built during this PhD work based on the concept applied in [145]. A schematic drawing of the ATR-IR cell is shown in Figure 43 (focus on the ATR part).

In addition, screening of other metals and metal alloys in the LA hydrogenation using FA as hydrogen donor would be interesting and may result in more active catalysts. For a rational catalyst design, the binding energies of CO and hydrogen to those metals or alloys should be in a range between the binding energies of Pd and Au (volcano plot, cf. 1.3.2.1).

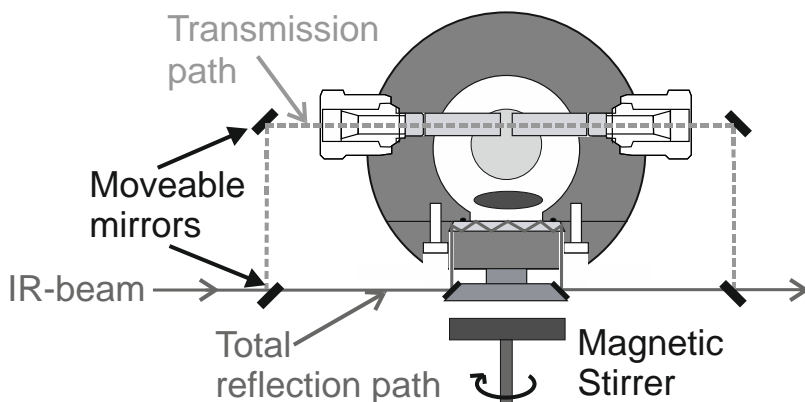


**Figure 43:** Scheme of a high pressure cell (designed to work up to 150 bar) for combined ATR-IT (bottom of the cell) and transmission IR (middle of the cell); adapted from [145].

Finally, FA as hydrogen donor in a continuous reaction mode might be beneficial compared to reactions in batch autoclaves. The  $\text{H}_2/\text{CO}_2$  selectivity of the FA decomposition might be higher (1.3.2.1) and poisoning of Pd may not occur. Also testing of non-noble metal catalysts in a continuous set-up is considered as an attractive approach since their stability could be higher and metal leaching could be avoided due to lower actual FA concentrations. Another option might be the use of two catalyst beds, the first containing a (noble metal based) FA decomposition catalyst and the second containing a (non-noble metal based e.g. Ni) hydrogenation catalyst.

## Literature

- [1] S. Lee, Preface, in: S. Lee, J.G. Speight, S.K. Loyal (Eds.), *Handbook of Alternative Fuel Technologies*, Second Edition, CRC Press, 2014, pp. i-xviii.
- [2] D.L. Klass, Chapter 1 - Energy Consumption, Reserves, Depletion, and Environmental Issues, in: D.L. Klass (Ed.), *Biomass for Renewable Energy, Fuels, and Chemicals*, Academic Press, San Diego, 1998, pp. 1-27.
- [3] BP Statistical Review of World Energy 2014, 2014, [www.bp.com](http://www.bp.com), 29. May 2015
- [4] Bundesministerium für Wirtschaft und Technologie, *Energiestatistiken*, 2015, [www.bmwi.de](http://www.bmwi.de), 29. May 2015
- [5] T. Patterson, R. Dinsdale, S. Esteves, Review of Energy Balances and Emissions Associated with Biomass-Based Transport Fuels Relevant to the United Kingdom Context, *Energy Fuels*. 22 (2008) 3506-3512.
- [6] B.G. Miller, 1 - Coal as Fuel: Past, Present, and Future, in: B.G. Miller (Ed.), *Clean Coal Engineering Technology*, Butterworth-Heinemann, Boston, 2011, pp. 1-51.
- [7] *Liquid Transportation Fuels from Coal and Biomass: Technological Status, Costs, and Environmental Impacts*, The National Academies Press, Washington, DC, 2009.
- [8] M. Asaro, R.M. Smith, Gas to Liquid Technologies, in: R. Malhotra (Ed.), *Fossil Energy*, Springer New York, 2013, pp. 247-310.
- [9] G.W. Huber, A. Corma, Synergien zwischen Bio- und Ölraffinerien bei der Herstellung von Biomassetreibstoffen, *Angew. Chem.* 119 (2007) 7320-7338.
- [10] Verband der Chemischen Industrie e.V., *Rohstoffbasis der chemischen Industrie*, 2015, [www.vci.de](http://www.vci.de), 29. May 2015
- [11] G.W. Huber, S. Iborra, A. Corma, Synthesis of Transportation Fuels from Biomass: Chemistry, Catalysts, and Engineering, *Chem. Rev.* 106 (2006) 4044-4098.
- [12] B. Kamm, Production of platform chemicals and synthesis gas from biomass, *Angew. Chem. Int. Ed.* 46 (2007) 5056-5058.
- [13] J.N. Chheda, G.W. Huber, J.A. Dumesic, Liquid-phase catalytic processing of biomass-derived oxygenated hydrocarbons to fuels and chemicals, *Angew. Chem. Int. Ed.* 46 (2007) 7164-7183.
- [14] F. Schuth, Chemical Compounds for Energy Storage, *Chem. Ing. Tech.* 83 (2011) 1984-1993.
- [15] N. Dahmen, E. Dinjus, E. Henrich, Synthesekraftstoffe aus Biomasse, in: T. Bührke, R. Wengenmayr (Eds.), *Erneuerbare Energie*, WILEY-VCH Verlag GmbH & Co. KGaA, Weinheim, 2007, pp. 59-63.

- [16] Chemrec AB, Processes for energy and chemicals recovery from black liquor in pulp mills, 2005, [www.chemrec.se](http://www.chemrec.se), 29. May 2015
- [17] Andritz AG, Renewable gasoline from wood 2014, <http://www.spectrum.andritz.com/>, 29. May 2015
- [18] B. Kamm, M. Kamm, Das Konzept der Bioraffinerie – Produktion von Plattformchemikalien und Finalprodukten, *Chem. Ing. Tech.* 79 (2007) 592-603.
- [19] R. Rinaldi, P. Engel, J. Büchs, A.C. Spiess, F. Schüth, An Integrated Catalytic Approach to Fermentable Sugars from Cellulose, *ChemSusChem*. 3 (2010) 1151-1153.
- [20] K. Hengst, M. Schubert, W. Kleist, J.-D. Grunwaldt, Hydrodeoxygenation of Lignocellulose-Derived Platform Molecules, in: R. Rinaldi (Ed.), *Catalytic Hydrogenation for Biomass Valorization*, Royal Society of Chemistry, 2015, pp. 125-150.
- [21] A.V. Bridgwater, S. Czernik, J. Diebold, D. Meier, A. Oasmaa, C. Peacocke, J. Piskorz, D. Radlein, *Fast Pyrolysis of Biomass: A Handbook*, CPL Press, Newbury, 1999.
- [22] P.M. Mortensen, J.D. Grunwaldt, P.A. Jensen, K.G. Knudsen, A.D. Jensen, A review of catalytic upgrading of bio-oil to engine fuels, *Appl. Catal. A*. 407 (2011) 1-19.
- [23] RWTH Aachen, <http://www.fuelcenter.rwth-aachen.de>, 29. May 2015
- [24] Netherlands Institute for Catalysis Research (NIOK), [www.catchbio.com](http://www.catchbio.com), 29. May 2015
- [25] Technical University of Denmark, [www.case.dtu.dk](http://www.case.dtu.dk), 29. May 2015
- [26] G.P. T. Werpy, J. Holladay, J. White, A. Manheim, M. Gerber, K.Ibsen, L. Lumberg, S.Kelley, U.S. Department of Energy, 2004.
- [27] F. Schuth, Hydrogen: Economics and its Role in Biorefining, in: R. Rinaldi (Ed.), *Catalytic Hydrogenation for Biomass Valorization*, The Royal Society of Chemistry, 2015, pp. 1-21.
- [28] A.R. Ardiyanti, R.H. Venderbosch, W. Yin, H.J. Heeres, Catalytic Hydrotreatment of Fast Pyrolysis Oils Using Supported Metal Catalysts, in: R. Rinaldi (Ed.), *Catalytic Hydrogenation for Biomass Valorization*, The Royal Society of Chemistry, 2015, pp. 151-173.
- [29] A. Kruse, A. Gawlik, Biomass Conversion in Water at 330–410 °C and 30–50 MPa. Identification of Key Compounds for Indicating Different Chemical Reaction Pathways, *Ind. Eng. Chem. Res.* 42 (2003) 267-279.
- [30] X.L. Tong, Y. Ma, Y.D. Li, Biomass into chemicals: Conversion of sugars to furan derivatives by catalytic processes, *Appl. Catal. A*. 385 (2010) 1-13.
- [31] P.N.R. Vennestrom, C.M. Osmundsen, C.H. Christensen, E. Taarning, Beyond Petrochemicals: The Renewable Chemicals Industry, *Angew. Chem. Int. Ed.* 50 (2011) 10502-10509.

- [32] C. Jaimes, R. Dobрева-Schué, O. Giani-Beaune, F. Schué, W. Amass, A. Amass, Ring-opening homopolymerization and copolymerization of lactones. Part 2. enzymatic degradability of poly( $\beta$ -hydroxybutyrate) stereoisomers and copolymers of  $\beta$ -butyrolactone with  $\epsilon$ -caprolactone and  $\delta$ -valerolactone, *Polym. Int.* 48 (1999) 23-32.
- [33] D. Fegyverneki, L. Orha, G. Lang, I.T. Horvath, Gamma-valerolactone-based solvents, *Tetrahedron.* 66 (2010) 1078-1081.
- [34] D.M. Alonso, S.G. Wettstein, J.A. Dumesic, Gamma-valerolactone, a sustainable platform molecule derived from lignocellulosic biomass, *Green Chem.* 15 (2013) 584-595.
- [35] X. Tang, X. Zeng, Z. Li, L. Hu, Y. Sun, S. Liu, T. Lei, L. Lin, Production of  $\gamma$ -valerolactone from lignocellulosic biomass for sustainable fuels and chemicals supply, *Renewable Sustainable Energy Rev.* 40 (2014) 608-620.
- [36] J.Q. Bond, D.M. Alonso, D. Wang, R.M. West, J.A. Dumesic, Integrated Catalytic Conversion of gamma-Valerolactone to Liquid Alkenes for Transportation Fuels, *Science.* 327 (2010) 1110-1114.
- [37] Z.P. Yan, L. Lin, S.J. Liu, Synthesis of gamma-Valerolactone by Hydrogenation of Biomass-derived Levulinic Acid over Ru/C Catalyst, *Energy Fuels.* 23 (2009) 3853-3858.
- [38] M. Chia, J.A. Dumesic, Liquid-phase catalytic transfer hydrogenation and cyclization of levulinic acid and its esters to [gamma]-valerolactone over metal oxide catalysts, *Chem. Commun.* 47 (2011) 12233-12235.
- [39] A.M. Hengne, C.V. Rode, Cu-ZrO<sub>2</sub> nanocomposite catalyst for selective hydrogenation of levulinic acid and its ester to [gamma]-valerolactone, *Green Chem.* 14 (2012) 1064-1072.
- [40] P. Sabatier, A. Mailhe, *Ann. Chin. Physi.* 8 (1909).
- [41] R.V. Christian, H.D. Brown, R.M. Hixon, Derivatives of gamma-Valerolactone, 1,4-Pentanediol and 1,4-di-(beta-cyanoethoxy)-pentane, *J. Am. Chem. Soc.* 69 (1947) 1961-1963.
- [42] H. A. Schuette, R.W. Thomas, Normal Valerolactone, III. Its preparation by the catalytic reduction of levulinic acid with hydrogen in the presence of Platinum oxide, *J. Am. Chem. Soc.* 52 (1930) 3010 - 30121.
- [43] L.E. Manzer, Catalytic synthesis of alpha-methylene-gamma-valerolactone: a biomass-derived acrylic monomer, *Appl. Catal. A.* 272 (2004) 249-256.
- [44] P.P. Upare, J.M. Lee, D.W. Hwang, S.B. Halligudi, Y.K. Hwang, J.S. Chang, Selective hydrogenation of levulinic acid to gamma-valerolactone over carbon-supported noble metal catalysts, *J. Ind. Eng. Chem.* 17 (2011) 287-292.
- [45] M.G. Al-Shaal, W.R.H. Wright, R. Palkovits, Exploring the ruthenium catalysed synthesis of gamma-valerolactone in alcohols and utilisation of mild solvent-free reaction conditions, *Green Chem.* 14 (2012) 1260-1263.

- [46] W. Luo, U. Deka, A.M. Beale, E.R.H. van Eck, P.C.A. Bruijninx, B.M. Weckhuysen, Ruthenium-catalyzed hydrogenation of levulinic acid: Influence of the support and solvent on catalyst selectivity and stability, *J. Catal.* 301 (2013) 175-186.
- [47] A.M.R. Galletti, C. Antonetti, V. De Luise, M. Martinelli, A sustainable process for the production of  $\gamma$ -valerolactone by hydrogenation of biomass-derived levulinic acid, *Green Chem.* 14 (2012) 688-694.
- [48] S. Cao, J.R. Monnier, C.T. Williams, W. Diao, J.R. Regalbuto, Rational nanoparticle synthesis to determine the effects of size, support, and K dopant on Ru activity for levulinic acid hydrogenation to  $\gamma$ -valerolactone, *J. Catal.* 326 (2015) 69-81.
- [49] C. Ortiz-Cervantes, J.J. García, Hydrogenation of levulinic acid to  $\gamma$ -valerolactone using ruthenium nanoparticles, *Inorg. Chim. Acta.* 397 (2013) 124-128.
- [50] M. Sudhakar, M. Lakshmi Kantam, V. Swarna Jaya, R. Kishore, K.V. Ramanujachary, A. Venugopal, Hydroxyapatite as a novel support for Ru in the hydrogenation of levulinic acid to  $\gamma$ -valerolactone, *Catal. Commun.* 50 (2014) 101-104.
- [51] Y. Yao, Z. Wang, S. Zhao, D. Wang, Z. Wu, M. Zhang, A stable and effective Ru/polyethersulfone catalyst for levulinic acid hydrogenation to  $\gamma$ -valerolactone in aqueous solution, *Catal. Today.* 234 (2014) 245-250.
- [52] D. Ding, J. Wang, J. Xi, X. Liu, G. Lu, Y. Wang, High-yield production of levulinic acid from cellulose and its upgrading to  $\gamma$ -valerolactone, *Green Chem.* 16 (2014) 3846-3853.
- [53] S.G. Wettstein, J.Q. Bond, D.M. Alonso, H.N. Pham, A.K. Datye, J.A. Dumesic, RuSn bimetallic catalysts for selective hydrogenation of levulinic acid to  $\gamma$ -valerolactone, *Appl. Catal. B.* 117-118 (2012) 321-329.
- [54] Y. Yang, G. Gao, X. Zhang, F. Li, Facile Fabrication of Composition-Tuned Ru-Ni Bimetallics in Ordered Mesoporous Carbon for Levulinic Acid Hydrogenation, *ACS Catal.* 4 (2014) 1419-1425.
- [55] W. Luo, M. Sankar, A.M. Beale, Q. He, C.J. Kiely, P.C.A. Bruijninx, B.M. Weckhuysen, High performing and stable supported nano-alloys for the catalytic hydrogenation of levulinic acid to  $\gamma$ -valerolactone, *Nat Commun.* 6 (2015).
- [56] L. Corbel-Demilly, B.-K. Ly, D.-P. Minh, B. Tapin, C. Especel, F. Epron, A. Cabiac, E. Guillon, M. Besson, C. Pinel, Heterogeneous Catalytic Hydrogenation of Biobased Levulinic and Succinic Acids in Aqueous Solutions, *ChemSusChem.* 6 (2013) 2388-2395.
- [57] J.C. Serrano-Ruiz, R.M. West, J.A. Dumesic, Catalytic Conversion of Renewable Biomass Resources to Fuels and Chemicals, in: J.M. Prausnitz, M.F. Doherty, R.A. Segalman (Eds.), *Annual Review of Chemical and Biomolecular Engineering*, Vol 1, Annual Reviews, Palo Alto, 2010, pp. 79-100.

- [58] K. Yan, C. Jarvis, T. Lafleur, Y. Qiao, X. Xie, Novel synthesis of Pd nanoparticles for hydrogenation of biomass-derived platform chemicals showing enhanced catalytic performance, *RSC Adv.* 3 (2013) 25865-25871.
- [59] K. Yan, T. Lafleur, G. Wu, J. Liao, C. Ceng, X. Xie, Highly selective production of value-added  $\gamma$ -valerolactone from biomass-derived levulinic acid using the robust Pd nanoparticles, *Appl. Catal. A.* 468 (2013) 52-58.
- [60] L.E. Manzer, K.W. Hutcherson, (E. I. Du Pont De Nemours & Co., USA), Production of 5-methyl-dihydro-furan-2-one from Levulinic Acid in Supercritical Media, US 20040254384 (2004)
- [61] R.A. Bourne, J.G. Stevens, J. Ke, M. Poliakoff, Maximising opportunities in supercritical chemistry: the continuous conversion of levulinic acid to  $\gamma$ -valerolactone in CO<sub>2</sub>, *Chem. Commun.* (2007) 4632-4634.
- [62] Z. Yang, Y.-B. Huang, Q.-X. Guo, Y. Fu, RANEY® Ni catalyzed transfer hydrogenation of levulinate esters to  $\gamma$ -valerolactone at room temperature, *Chem. Commun.* 49 (2013) 5328-5330.
- [63] K.-I. Shimizu, S. Kanno, K. Kon, Hydrogenation of levulinic acid to  $\gamma$ -valerolactone by Ni and MoO<sub>x</sub> co-loaded carbon catalysts, *Green Chem.* 16 (2014) 3899-3903.
- [64] V. Mohan, V. Venkateshwarlu, C.V. Pramod, B.D. Raju, K.S.R. Rao, Vapour phase hydrocyclisation of levulinic acid to  $\gamma$ -valerolactone over supported Ni catalysts, *Catal. Sci. Tech.* 4 (2014) 1253-1259.
- [65] V. Mohan, C. Raghavendra, C.V. Pramod, B.D. Raju, K.S. Rama Rao, Ni/H-ZSM-5 as a promising catalyst for vapour phase hydrogenation of levulinic acid at atmospheric pressure, *RSC Adv.* 4 (2014) 9660-9668.
- [66] I. Obregón, E. Corro, U. Izquierdo, J. Requies, P.L. Arias, Levulinic acid hydrogenolysis on Al<sub>2</sub>O<sub>3</sub>-based Ni-Cu bimetallic catalysts, *Chinese J. Catal.* 35 (2014) 656-662.
- [67] J.M. Tukacs, R.V. Jones, F. Darvas, G. Dibo, G. Lezsak, L.T. Mika, Synthesis of  $\gamma$ -valerolactone using a continuous-flow reactor, *RSC Adv.* 3 (2013) 16283-16287.
- [68] B. Putrakumar, N. Nagaraju, V.P. Kumar, K.V.R. Chary, Hydrogenation of levulinic acid to  $\gamma$ -valerolactone over copper catalysts supported on  $\gamma$ -Al<sub>2</sub>O<sub>3</sub>, *Catal. Today.*
- [69] A. P. Dunlop, J.W. Madden, (Quaker Oats Co.), Process of Preparing  $\gamma$ -Valerolactone, US 2786852 (1957)
- [70] W.R.H. Wright, R. Palkovits, Development of Heterogeneous Catalysts for the Conversion of Levulinic Acid to  $\gamma$ -Valerolactone, *ChemSusChem.* 5 (2012) 1657-1667.
- [71] J. Horvat, B. Klaić, B. Metelko, V. Šunjić, Mechanism of levulinic acid formation, *Tetrahedron Lett.* 26 (1985) 2111-2114.

- [72] X.L. Du, L. He, S. Zhao, Y.M. Liu, Y. Cao, H.Y. He, K.N. Fan, Hydrogen-Independent Reductive Transformation of Carbohydrate Biomass into  $\gamma$ -Valerolactone and Pyrrolidone Derivatives with Supported Gold Catalysts, *Angew. Chem. Int. Ed.* 50 (2011) 7815-7819.
- [73] P.A. Son, S. Nishimura, K. Ebitani, Production of  $\gamma$ -valerolactone from biomass-derived compounds using formic acid as a hydrogen source over supported metal catalysts in water solvent, *RSC Adv.* 4 (2014) 10525-10530.
- [74] X. Du, Y. Liu, J. Wang, Y. Cao, K. Fan, Catalytic conversion of biomass-derived levulinic acid into  $\gamma$ -valerolactone using iridium nanoparticles supported on carbon nanotubes, *Chinese J. Catal.* 34 (2013) 993-1001.
- [75] A.M. Hengne, A.V. Malawadkar, N.S. Biradar, C.V. Rode, Surface synergism of an Ag-Ni/ZrO<sub>2</sub> nanocomposite for the catalytic transfer hydrogenation of bio-derived platform molecules, *RSC Adv.* 4 (2014) 9730-9736.
- [76] D. Kopetzki, M. Antonietti, Transfer hydrogenation of levulinic acid under hydrothermal conditions catalyzed by sulfate as a temperature-switchable base, *Green Chem.* 12 (2010) 656-660.
- [77] V. Fábos, L.T. Mika, I.T. Horváth, Selective Conversion of Levulinic and Formic Acids to  $\gamma$ -Valerolactone with the Shvo Catalyst, *Organometallics.* 33 (2014) 181-187.
- [78] L. Deng, J. Li, D.M. Lai, Y. Fu, Q.X. Guo, Catalytic Conversion of Biomass-Derived Carbohydrates into  $\gamma$ -Valerolactone without Using an External H-2 Supply, *Angew. Chem. Int. Ed.* 48 (2009) 6529-6532.
- [79] J. Yuan, S.-S. Li, L. Yu, Y.-M. Liu, Y. Cao, H.-Y. He, K.-N. Fan, Copper-based catalysts for the efficient conversion of carbohydrate biomass into  $\gamma$ -valerolactone in the absence of externally added hydrogen, *Energy Environ. Sci.* 6 (2013) 3308-3313.
- [80] D.J. Braden, C.A. Henao, J. Heltzel, C.T. Maravelias, J.A. Dumesic, Production of liquid hydrocarbon fuels by catalytic conversion of biomass-derived levulinic acid, *Green Chem.* 13 (2011) 1755-1765.
- [81] L. Qi, I.T. Horvath, Catalytic Conversion of Fructose to  $\gamma$ -Valerolactone in  $\gamma$ -Valerolactone, *ACS Catal.* 2 (2012) 2247-2249.
- [82] A.M.R. Galletti, C. Antonetti, E. Ribechini, M.P. Colombini, N.N.O. Di Nasso, E. Bonari, From giant reed to levulinic acid and  $\gamma$ -valerolactone: A high yield catalytic route to valeric biofuels, *Appl. Energy.* 102 (2013) 157-162.
- [83] H. Heeres, R. Handana, D. Chunai, C. Borromeus Rasrendra, B. Girisuta, H. Jan Heeres, Combined dehydration/(transfer)-hydrogenation of C6-sugars (D-glucose and D-fructose) to  $\gamma$ -valerolactone using ruthenium catalysts, *Green Chem.* 11 (2009) 1247-1255.
- [84] F. Solymosi, Á. Koós, N. Liliom, I. Ugrai, Production of CO-free H<sub>2</sub> from formic acid. A comparative study of the catalytic behavior of Pt metals on a carbon support, *J. Catal.* 279 (2011) 213-219.



- [85] S. Ha, R. Larsen, R.I. Masel, Performance characterization of Pd/C nanocatalyst for direct formic acid fuel cells, *J. Power Sources*. 144 (2005) 28-34.
- [86] S. Singh, S. Li, R. Carrasquillo-Flores, A.C. Alba-Rubio, J.A. Dumesic, M. Mavrikakis, Formic acid decomposition on Au catalysts: DFT, microkinetic modeling, and reaction kinetics experiments, *AIChE Journal*. 60 (2014) 1303-1319.
- [87] B. Loges, A. Boddien, H. Junge, M. Beller, Controlled Generation of Hydrogen from Formic Acid Amine Adducts at Room Temperature and Application in H<sub>2</sub>/O<sub>2</sub> Fuel Cells, *Angew. Chem. Int. Ed.* 47 (2008) 3962-3965.
- [88] A. Boddien, B. Loges, F. Gärtner, C. Torborg, K. Fumino, H. Junge, R. Ludwig, M. Beller, Iron-Catalyzed Hydrogen Production from Formic Acid, *J. Am. Chem. Soc.* 132 (2010) 8924-8934.
- [89] C. Fellay, P.J. Dyson, G. Laurenczy, A Viable Hydrogen-Storage System Based On Selective Formic Acid Decomposition with a Ruthenium Catalyst, *Angew. Chem. Int. Ed.* 47 (2008) 3966-3968.
- [90] A. Gazsi, T. Bánsági, F. Solymosi, Decomposition and Reforming of Formic Acid on Supported Au Catalysts: Production of CO-Free H<sub>2</sub>, *J. Phys. Chem. C*. 115 (2011) 15459-15466.
- [91] R.S. Jayashree, J.S. Spendelow, J. Yeom, C. Rastogi, M.A. Shannon, P.J.A. Kenis, Characterization and application of electrodeposited Pt, Pt/Pd, and Pd catalyst structures for direct formic acid micro fuel cells, *Electrochimica Acta*. 50 (2005) 4674-4682.
- [92] D.A. Bulushev, L. Jia, S. Beloshapkin, J.R.H. Ross, Improved hydrogen production from formic acid on a Pd/C catalyst doped by potassium, *Chem. Commun.* 48 (2012) 4184-4186.
- [93] D.A. Bulushev, S. Beloshapkin, P.E. Plyusnin, Y.V. Shubin, V.I. Bukhtiyarov, S.V. Korenev, J.R.H. Ross, Vapour phase formic acid decomposition over PdAu/ $\gamma$ -Al<sub>2</sub>O<sub>3</sub> catalysts: Effect of composition of metallic particles, *J. Catal.* 299 (2013) 171-180.
- [94] D.A. Bulushev, S. Beloshapkin, J.R.H. Ross, Hydrogen from formic acid decomposition over Pd and Au catalysts, *Catal. Today*. 154 (2010) 7-12.
- [95] M. Ojeda, E. Iglesia, Formic Acid Dehydrogenation on Au-Based Catalysts at Near-Ambient Temperatures, *Angew. Chem. Int. Ed.* 48 (2009) 4800-4803.
- [96] M. Yadav, A.K. Singh, N. Tsumori, Q. Xu, Palladium silica nanosphere-catalyzed decomposition of formic acid for chemical hydrogen storage, *J. Mater. Chem.* 22 (2012) 19146-19150.
- [97] C. Hu, S.-W. Ting, J. Tsui, K.-Y. Chan, Formic acid dehydrogenation over PtRuBiOx/C catalyst for generation of CO-free hydrogen in a continuous-flow reactor, *Int. J. Hydrogen Energy*. 37 (2012) 6372-6380.
- [98] X. Zhou, Y. Huang, W. Xing, C. Liu, J. Liao, T. Lu, High-quality hydrogen from the catalyzed decomposition of formic acid by Pd-Au/C and Pd-Ag/C, *Chem. Commun.* (2008) 3540-3542.

- [99] X. Gu, Z.-H. Lu, H.-L. Jiang, T. Akita, Q. Xu, Synergistic Catalysis of Metal–Organic Framework-Immobilized Au–Pd Nanoparticles in Dehydrogenation of Formic Acid for Chemical Hydrogen Storage, *J. Am. Chem. Soc.* 133 (2011) 11822–11825.
- [100] Y. Huang, X. Zhou, M. Yin, C. Liu, W. Xing, Novel PdAu@Au/C Core–Shell Catalyst: Superior Activity and Selectivity in Formic Acid Decomposition for Hydrogen Generation, *Chem. Mater.* 22 (2010) 5122–5128.
- [101] Z.-L. Wang, Y. Ping, J.-M. Yan, H.-L. Wang, Q. Jiang, Hydrogen generation from formic acid decomposition at room temperature using a NiAuPd alloy nanocatalyst, *Int. J. Hydrogen Energy.* 39 (2014) 4850–4856.
- [102] S. Zhang, Ö. Metin, D. Su, S. Sun, Monodisperse AgPd Alloy Nanoparticles and Their Superior Catalysis for the Dehydrogenation of Formic Acid, *Angew. Chem. Int. Ed.* 52 (2013) 3681–3684.
- [103] W.J.M. Rootsaert, W.M.H. Sachtler, Interaction of Formic Acid Vapour with Tungsten, *Z. Phys. Chem. Neue Fol.* 26 (1960) 16–26.
- [104] J. Yu, P.E. Savage, Decomposition of Formic Acid under Hydrothermal Conditions, *Ind. Eng. Chem. Res.* 37 (1998) 2–10.
- [105] C. Hu, S.-W. Ting, K.-Y. Chan, W. Huang, Reaction pathways derived from DFT for understanding catalytic decomposition of formic acid into hydrogen on noble metals, *Int. J. Hydrogen Energy.* 37 (2012) 15956–15965.
- [106] S.-C. Huang, C.-H. Lin, J.H. Wang, Trends of Water Gas Shift Reaction on Close-Packed Transition Metal Surfaces, *J. Phys. Chem. C.* 114 (2010) 9826–9834.
- [107] N. Schumacher, A. Boisen, S. Dahl, A.A. Gokhale, S. Kandoi, L.C. Grabow, J.A. Dumesic, M. Mavrikakis, I. Chorkendorff, Trends in low-temperature water–gas shift reactivity on transition metals, *J. Catal.* 229 (2005) 265–275.
- [108] X. Tang, H. Chen, L. Hu, W. Hao, Y. Sun, X. Zeng, L. Lin, S. Liu, Conversion of biomass to  $\gamma$ -valerolactone by catalytic transfer hydrogenation of ethyl levulinate over metal hydroxides, *Appl. Catal. B.* 147 (2014) 827–834.
- [109] J. Wang, S. Jaenicke, G.-K. Chuah, Zirconium-Beta zeolite as a robust catalyst for the transformation of levulinic acid to  $[\gamma]$ -valerolactone via Meerwein-Ponndorf-Verley reduction, *RSC Adv.* 4 (2014) 13481–13489.
- [110] R. Strobel, S.E. Pratsinis, Flame aerosol synthesis of smart nanostructured materials, *J. Mater. Chem.* 17 (2007) 4743–4756.
- [111] W.Y. Teoh, R. Amal, L. Madler, Flame spray pyrolysis: An enabling technology for nanoparticles design and fabrication, *Nanoscale.* 2 (2010) 1324–1347.
- [112] R. Strobel, A. Alfons, S.E. Pratsinis, Aerosol flame synthesis of catalysts, *Advanced Powder Technology.* 17 (2006) 457–480.
- [113] M. Høj, K. Linde, T.K. Hansen, M. Brorson, A.D. Jensen, J.-D. Grunwaldt, Flame spray synthesis of CoMo/Al<sub>2</sub>O<sub>3</sub> hydrotreating catalysts, *Appl. Catal. A.* 397 (2011) 201–208.

- [114] A.L. Patterson, The Scherrer Formula for X-Ray Particle Size Determination, *Phys. Rev.* 56 (1939) 978-982.
- [115] C.H. Bartholomew, R.B. Pannell, The stoichiometry of hydrogen and carbon monoxide chemisorption on alumina- and silica-supported nickel, *J. Catal.* 65 (1980) 390-401.
- [116] C. Karakaya, O. Deutschmann, A simple method for CO chemisorption studies under continuous flow: Adsorption and desorption behavior of Pt/Al<sub>2</sub>O<sub>3</sub> catalysts, *Appl. Catal. A.* 445–446 (2012) 221-230.
- [117] A.T. Gremminger, H.W. Pereira de Carvalho, R. Popescu, J.-D. Grunwaldt, O. Deutschmann, Influence of gas composition on activity and durability of bimetallic Pd-Pt/Al<sub>2</sub>O<sub>3</sub> catalysts for total oxidation of methane, *Catal. Today.*
- [118] J.D. Grunwaldt, M. Caravati, S. Hannemann, A. Baiker, X-ray absorption spectroscopy under reaction conditions: suitability of different reaction cells for combined catalyst characterization and time-resolved studies, *Phys. Chem. Chem. Phys.* 6 (2004) 3037-3047.
- [119] J.-D. Grunwaldt, N.v. Vegten, A. Baiker, Insight into the structure of supported palladium catalysts during the total oxidation of methane, *Chem. Commun.* (2007) 4635-4637.
- [120] B. Ravel, M. Newville, ATHENA, ARTEMIS, HEPHAESTUS: data analysis for X-ray absorption spectroscopy using IFEFFIT, *J. Synchrotron Radiat.* 12 (2005) 537-541.
- [121] J.J. Rehr, R.C. Albers, Theoretical Approaches to X-ray Absorption Fine Structure, *Rev. Mod. Phys.* 72 (2000) 621.
- [122] J.J. Rehr, J.J. Kas, M.P. Prange, A.P. Sorini, Y. Takimoto, F.D. Vila, Ab initio theory and calculations of X-ray spectra, *C. R. Phys.* 10 (2009) 548-559.
- [123] S. Calvin, E.E. Carpenter, B. Ravel, V.G. Harris, S.A. Morrison, Multiedge refinement of extended x-ray-absorption fine structure of manganese zinc ferrite nanoparticles, *Phys. Rev.* 66 (2002) 224405.
- [124] Z. Boukha, C. Jiménez-González, B. de Rivas, J.R. González-Velasco, J.I. Gutiérrez-Ortiz, R. López-Fonseca, Synthesis, characterisation and performance evaluation of spinel-derived Ni/Al<sub>2</sub>O<sub>3</sub> catalysts for various methane reforming reactions, *Appl. Catal. B.* 158–159 (2014) 190-201.
- [125] D.A.J.M. Ligthart, J.A.Z. Pieterse, E.J.M. Hensen, The role of promoters for Ni catalysts in low temperature (membrane) steam methane reforming, *Appl. Catal. A.* 405 (2011) 108-119.
- [126] N. Salhi, A. Boulahouache, C. Petit, A. Kiennemann, C. Rabia, Steam reforming of methane to syngas over NiAl<sub>2</sub>O<sub>4</sub> spinel catalysts, *Int. J. Hydrogen Energy.* 36 (2011) 11433-11439.
- [127] R. López-Fonseca, C. Jiménez-González, B. de Rivas, J.I. Gutiérrez-Ortiz, Partial oxidation of methane to syngas on bulk NiAl<sub>2</sub>O<sub>4</sub> catalyst. Comparison with alumina supported nickel, platinum and rhodium catalysts, *Appl. Catal. A.* 437–438 (2012) 53-62.

- [128] J.-D. Grunwaldt, B. Kimmeler, S. Hannemann, A. Baiker, P. Boye, C.G. Schroer, Parallel structural screening of solid materials, *J. Mater. Chem.* 17 (2007) 2603-2606.
- [129] R.W.G. Wyckoff, *Crystal Structures*, Interscience, New York, 1964.
- [130] M. Meng, P. Lin, Y. Fu, XAFS characterization on the active sites of Ni/ $\gamma$ -Al<sub>2</sub>O<sub>3</sub> catalysts for NO-SCR by propene, *Spectrosc. Lett.* 34 (2001) 83-92.
- [131] A. Guerrero-Ruiz, A. Maroto-Valiente, M. Cerro-Alarcón, B. Bachiller-Baeza, I. Rodríguez-Ramos, Surface Properties of Supported Metallic Clusters as Determined by Microcalorimetry of CO Chemisorption, *Top. Catal.* 19 (2002) 303-311.
- [132] K. Nomura, K. Noro, Y. Nakamura, H. Yoshida, A. Satsuma, T. Hattori, Combustion of a trace amount of CH<sub>4</sub> in the presence of water vapor over ZrO<sub>2</sub>-supported Pd catalysts, *Catal. Lett.* 58 (1999) 127-130.
- [133] K. Kon, W. Onodera, K.-I. Shimizu, Selective hydrogenation of levulinic acid to valeric acid and valeric biofuels by a Pt/HMF1 catalyst, *Catal. Sci. Tech.* 4 (2014) 3227-3234.
- [134] J. Geboers, X. Wang, A.B. de Carvalho, R. Rinaldi, Densification of biorefinery schemes by H-transfer with Raney Ni and 2-propanol: A case study of a potential avenue for valorization of alkyl levulinates to alkyl  $\gamma$ -hydroxypentanoates and  $\gamma$ -valerolactone, *J. Mol. Catal. A: Chem.* 388–389 (2014) 106-115.
- [135] J.T. Scanlon, D.E. Willis, Calculation of Flame Ionization Detector Relative Response Factors Using the Effective Carbon Number Concept, *J. Chromatogr. Sci.* 23 (1985) 333-340.
- [136] M. Kállai, Z. Veres, J. Balla, Response of flame ionization detectors to different homologous series, *Chromatographia.* 54 (2001) 511-517.
- [137] S.G. Wettstein, D.M. Alonso, Y.X. Chong, J.A. Dumesic, Production of levulinic acid and gamma-valerolactone (GVL) from cellulose using GVL as a solvent in biphasic systems, *Energy Environ. Sci.* 5 (2012) 8199-8203.
- [138] R. Molina, G. Poncelet, Hydrogenation of Benzene over Alumina-Supported Nickel Catalysts Prepared from Ni(II) Acetylacetonate, *J. Catal.* 199 (2001) 162-170.
- [139] H. Li, Y. Xu, C. Gao, Y. Zhao, Structural and textural evolution of Ni/ $\gamma$ -Al<sub>2</sub>O<sub>3</sub> catalyst under hydrothermal conditions, *Catal. Today.* 158 (2010) 475-480.
- [140] S.B. Simonsen, I. Chorkendorff, S. Dahl, M. Skoglundh, K. Meinander, T.N. Jensen, J.V. Lauritsen, S. Helveg, Effect of Particle Morphology on the Ripening of Supported Pt Nanoparticles, *J. Phys. Chem. C.* 116 (2012) 5646-5653.
- [141] M.L. Testa, L. Corbel-Demilly, V. La Parola, A.M. Venezia, C. Pinel, Effect of Au on Pd supported over HMS and Ti doped HMS as catalysts for the hydrogenation of levulinic acid to  $\gamma$ -valerolactone, *Catal. Today.*
- [142] J.K. Edwards, E. Ntainjua N, A.F. Carley, A.A. Herzing, C.J. Kiely, G.J. Hutchings, Direct Synthesis of H<sub>2</sub>O<sub>2</sub> from H<sub>2</sub> and O<sub>2</sub> over Gold, Palladium, and

Gold–Palladium Catalysts Supported on Acid-Pretreated TiO<sub>2</sub>, *Angew. Chem. Int. Ed.* 48 (2009) 8512-8515.

[143] S. Fukuzumi, T. Kobayashi, T. Suenobu, Unusually Large Tunneling Effect on Highly Efficient Generation of Hydrogen and Hydrogen Isotopes in pH-Selective Decomposition of Formic Acid Catalyzed by a Heterodinuclear Iridium–Ruthenium Complex in Water, *J. Am. Chem. Soc.* 132 (2010) 1496-1497.

[144] W.Y. Teoh, D.E. Doronkin, G.K. Beh, J.A.H. Dreyer, J.-D. Grunwaldt, Methanation of carbon monoxide over promoted flame-synthesized cobalt clusters stabilized in zirconia matrix, *J. Catal.* 326 (2015) 182-193.

[145] J.-D. Grunwaldt, A. Baiker, In situ spectroscopic investigation of heterogeneous catalysts and reaction media at high pressure, *Phys. Chem. Chem. Phys.* 7 (2005) 3526-3539.



## List of Abbreviations

2,5DMF	2,5-dimethylfuran
a.u.	arbitrary unit
acac	acetylacetonate
ANKA	Angströmquelle Karlsruhe
ATR-IR	attenuated total reflection infrared spectroscopy
BET	Brunauer Emmett Teller
BHMF	2,5-bis-(hydroxymethyl)furfural
BTX	benzene, toluene, xylene
C	activated carbon
CCDC	Cambridge Crystallographic Data Center
cf.	compare / confer
CSD	Cambridge Structural Database
CtL	coal-to-liquid
DFT	density functional theory
DMF	dimethylformamide
DMTHF	2,5-dimethyltetrahydrofuran
ECN	effective carbon number
EG	ethylene glycol
EO	ethylene oxide
EXAFS	extended X-ray absorption fine structure
FA	formic acid
FSP	flame spray pyrolysis
FT	Fourier transform
gc	gas chromatography
GtL	gas-to-liquid
GVL	$\gamma$ -valerolactone
HDO	hydrodeoxygenation
HMF	5-hydroxymethylfurfural
HPLC	high performance liquid chromatography

ICDD	International Centre for Diffraction Data
ICP-OES	inductively coupled plasma optical emission spectrometry
IR	infrared spectroscopy
iwi	incipient wetness impregnation
LA	levulinic acid
LA ester	levulinic acid ester
LCA	linear combination analysis
MOC	mean oxidation number of organic carbon
MPV	Meerwein-Ponndorf-Verley
MTHF	2-methyltetrahydrofuran
NMR	nuclear magnetic resonance spectroscopy
NREL	National Renewable Energy Laboratory
p	precipitation with NaOH
PE	polyethylene
PG	propylene glycol
PP	polypropylene
PPh <sub>3</sub>	triphenylphosphine
scCO <sub>2</sub>	supercritical CO <sub>2</sub>
STEM	scanning transmission electron microscopy
TCD	thermal conductivity detector
TD	tetradecane
TEM	transmission electron microscopy
TFA	trifluoroacetic acid
TOF	turnover frequency
TON	turnover number
TPD	temperature-programmed desorption
TPPTS	3,3',3''-Phosphanetriyltris(benzenesulfonic acid) trisodium salt
TPR	temperature-programmed reduction
urea	precipitation with urea
WGS	water-gas shift
WHSV	weight hourly space velocity
wi	wet impregnation



wt. %	weight percentage
XANES	X-ray absorption near edge structure
XAS	X-ray absorption spectroscopy
XRD	X-ray diffraction

## List of Symbols

Å	Ångström
d	diameter
E	energy
eV	electron Volt
I	intensity
m	mass
p	pressure
T	temperature
t	time
UV	ultraviolet
$\theta$	angle of incidence of the X-rays

# Curriculum Vitae

## Konstantin Hengst

born 24. 03. 1985 in Münster (Westfalen)

Marital status: Married, 1 daughter

Nationality: German

## Education

05/2012-present **PhD-program** of KIC InnoEnergy; Knowledge & Innovation Community of the European Institute of Innovation and Technology (EIT)

12/2011-present **PhD-student / research assistant**  
Karlsruhe Institute of Technology (KIT), Institute for Chemical Technology and Polymer Chemistry, supervisor: Prof. Jan-Dierk Grunwaldt

01/2014-07/2014 **International exchange / Guest PhD-student**  
Technical University of Eindhoven (Tu/e), Netherlands, Department of Chemical Engineering and Chemistry, supervisor: Prof. Emiel J.M. Hensen

03/2011-07/2011 **Diploma thesis**  
Rheinisch Westfälische Technische Hochschule Aachen (RWTH), Department of Chemical Technology and Heterogeneous Catalysis, supervisor: Prof. Wolfgang F. Hölderich  
Topic: "Production of 2<sup>nd</sup> generation biofuel"  
(in cooperation with ADM Research GmbH)

10/2005-07/2011 **Chemistry (Dipl.-Chem.)**  
Specialization in Chemical Technology, RWTH Aachen

08/1997-06/2004 **University admission certificate (Abitur)**  
Humboldt Oberschule, Berlin

## Practical Experience

10/2004-06/2005 **Military** - 3. Airborne-battalion, Varel

07/2004-08/2004 **Internship in pharmacokinetics**  
Schering AG, Berlin

## List of Publications

### Publications related to this thesis

#### **Synthesis of $\gamma$ -Valerolactone by Hydrogenation of Levulinic Acid over Supported Nickel Catalysts**

K. Hengst, M. Schubert, H. W. P. Carvalho, C. Lu, W. Kleist, J.-D. Grunwaldt, *Applied Catalysis A*, 2015

Results from this publication are presented in chapter 1, 2, 3 and 4, reprinted with permission from Elsevier.

#### **Continuous Synthesis of $\gamma$ -Valerolactone in a Trickle-bed Reactor over Supported Nickel Catalysts**

K. Hengst, D. A. J. M. Ligthart, D. E. Doronkin, W. Kleist, E. J. M. Hensen, J.-D. Grunwaldt, to be submitted.

Results from this publication are presented in chapter 1, 2, 3 and 5.

#### **Hydrodeoxygenation of Lignocellulose-Derived Platform Molecules**

K. Hengst, M. Schubert, W. Kleist, J.-D. Grunwaldt, in *Catalytic Hydrogenation for Biomass Valorization*, R. Rinaldi (Editor), RSC, 2015

Results from this book chapter are presented in chapter 1, reproduced by permission of The Royal Society of Chemistry.

### Other publications

#### **Deoxygenation and cracking of Free Fatty Acids over Acidic Catalysts by Single Step Conversion for the Production of Diesel Fuel and Fuel Blends**

K. Hengst, M. Arend, R. Pfützenreuter, W. F. Hölderich, *Applied Catalysis B*, 2015

#### **Herstellung von Dieselkraftstoff durch einstufige Umwandlung von freien Fettsäuren**

K. Hengst, M. Arend, W. F. Hölderich, DE 102012019759 A1, 2012

#### **Decorating the lanthanide terminus of heterodinuclear lanthanum(III)/gallium(III) helicates**

M. Albrecht, I. Latorre, G. Mehmeti, K. Hengst, I. M. Oppel, *Dalton Trans.*, 2011

## Oral presentations

### **New Catalysts for Biodiesel Production of First and Second Generation**

W. F. Hölderich, M. Arend, K. Hengst, Oral presentation 23rd NAM, 2013

## Poster presentations

### **Sustainable Synthesis of $\gamma$ -Valerolactone**

K. Hengst, M. Schubert, W. Kleist, J.-D. Grunwaldt  
ProcessNet-Jahrestagung 2014, Aachen, 30. Sep.-02. Oct. 2014

### **Hydrodesoxygenation of Levulinic Acid to $\gamma$ -Valerolactone over Heterogeneous Non-noble Metal Catalysts**

K. Hengst, C. Lu, W. Kleist, J.-D. Grunwaldt  
Workshop der AG Chemie und Energie der GDCH, Karlsruhe, 15.-16. Nov. 2012

### **Hydrodesoxygenation of Levulinic Acid to $\gamma$ -Valerolactone over Heterogeneous Non-noble Metal Catalysts**

K. Hengst, C. Lu, W. Kleist, J.-D. Grunwaldt  
KIC InnoEnergy Scientist Conference, Leuven (Belgium), 04.-09. Oct. 2012

### **Hydrodesoxygenierung von Lävulinsäure zu $\gamma$ -Valerolacton an heterogenen Übergangsmetall-Katalysatoren**

K. Hengst, C. Lu, W. Kleist, J.-D. Grunwaldt  
ProcessNet-Jahrestagung und 30. DECHEMA-Jahrestagung der Biotechnologen, Karlsruhe, 11.-13. Sep. 2012  
(Chem. Ing. Tech., 84 (8) (2012) 1247.)

## Eidesstattliche Erklärung

Hiermit erkläre ich, Konstantin Hengst, an Eides statt, dass ich die vorliegende Dissertation selbstständig verfasst und keine anderen als die angegebenen Quellen und Hilfsmittel verwendet habe. Darüber hinaus versichere ich, dass ich die Regeln zur Sicherung guter wissenschaftlicher Praxis im Karlsruher Institut für Technologie (KIT) in der gültigen Fassung beachtet habe. Die Arbeit wurde in gleicher oder anderer Form keiner anderen Prüfungsbehörde zur Erlangung eines akademischen Grades vorgelegt.

Karlsruhe, den

---

Datum und Unterschrift